PBAT biocomposite with banana pseudo-stem fibers

Rita Maria Nobre Serôdio

Thesis to obtain the Master Science Degree in

Chemistry

Supervisor: Prof. Dr. Ana C. Marques

Examination Committee

Chairperson: Prof. Dr. Carlos Baleizão

Supervisor: Prof. Dr. Ana C. Marques

Member of the Committee: Prof. Dr. Rui Galhano and Prof. Dr. Célio Pina

November 2022

Index

Acknowledgments iii

Resumo iv

Abstract v

List of Tables vi

List of Figures vii

List of Graphics x

List of Acronyms and Symbols xi

Motivation 1

Chapter 1: Introduction 2

1.1. PBAT 3

1.2. Synthesis of PBAT 3

1.3. Biodegradation of PBAT 3

1.4. PBAT composites 4

1.5. Starch-PBAT based blends 6

1.6. PLA-PBAT based blends 9

1.7. Banana fiber composites 11

Chapter 2: Materials and methods 18

2.1. Materials 18

2.2. Methods 20

2.2.1. Tree segmentation and fiber extraction 20

2.2.1.1. Manual extraction of fibers 20

2.2.1.2. Chemical extraction of fibers 20

2.2.2. Fiber powder preparation 20

2.2.3. Fiber powder alkali treatment 20

2.2.4. Composite preparation and extrusion 21

2.3. Characterization techniques 21

2.3.1. Fourier transform infrared (FTIR) spectroscopy 22

2.3.2. Scanning electron microscopy (SEM) 22

2.3.3. Mechanical test 22

2.3.4. Dynamic mechanical analysis (DMA) 23

2.3.5. Thermogravimetric and derivative thermogravimetric analysis (TGA/DTG) ... 23
2.3.6. Water absorption ... 23
2.3.7. 3D printing ... 24
Chapter 3: Results and Discussion ... 25
3.1. Fiber and fiber powder ... 25
3.1.1. Fiber powder preparation ... 27
3.1.2. Chemical and morphological structure ... 28
3.1.3. Thermal behavior analysis ... 35
3.2. PBAT/Banana powder composites ... 38
3.2.1. Composite extrusion ... 38
3.2.2. Chemical and morphological structure ... 43
3.2.3. Thermal behavior analysis and thermo-mechanical behavior ... 47
3.2.4. Mechanical tests ... 58
3.2.5. Water absorption ... 61
3.2.6. 3D printing of extrudates ... 63
4. **Concluding remarks** ... 65
5. **Considerations for future work** ... 67
6. **References** ... 68
Appendix A - Comprehensive list of the varied PBAT blends ... 79
Appendix B –SPEX SamplePrep 6770 Freezer/Mills apparatus and 3Devo® composer 450 desktop apparatus ... 87
Appendix C – Sample sizes for DMA and water absorption tests ... 89
Appendix D – FTIR spectra and Thermogravimetric analysis (TGA) and Differential thermogravimetric analysis (DTG) thermogarms ... 90
Appendix E - EDS data and SEM images ... 93

Acknowledgments

First and foremost, I would like to thank my supervisor Prof. Dr. Ana Clara Marques for accepting and enabling this project to go forward, and for all the support, enriching discussions, suggestions, availability, and extremely valuable contributions throughout its development.

I am also extremely grateful to all the current members of CERENA who are present at the IST laboratories for the support provided during all stages of this work and willingness to give a hand when requested.

A note of appreciation to all my neighbours for providing the essential materials, that is, the banana pseudo-stems, which allowed this project to proceed and move forward. A special thanks to Prof. Dr. Susete Martins and Dr. Renata Alexandra Ferreira for granting the opportunity of using the cryogenic impact mill, and for the lively and pleasant company provided during this arduous task.

To Prof. Rui Galhano, Master student António Mariquito, PhD student Sofia Moreira Fernandes, Postdoc researcher Tânia Frade Costa and childhood friend Miguel Vasconcelos a particular note of gratitude and recognition for the tireless dedication, informed guidance and fruitful discussions that were essential in the development of this work.

Last but not least, I extend my thanks to my family, childhood friends and master colleagues for the unconditional patience and unlimited support, provided during this challenging journey. In particular I would like to thank my father for all the time spent together scrapping the fibers, without whom I would not have managed to finish this project on time.

To all, my deepest gratitude and esteem.

Resumo

Devido ao aumento dos problemas ambientais, em parte resultantes da poluição causada pelos plásticos, têm surgido novas tendências para lidar com esta crise. Uma delas tira proveito do uso de bioplásticos como possíveis substitutos de polímeros sintéticos, em que, a utilização de compósitos de PBAT tem apresentado resultados promissores. A inovação apresentada neste projeto consiste no reaproveitamento das fibras do tronco da bananeira, provenientes de resíduos agrícolas, para o reforço destas misturas. Estas são boas candidatas devido ao seu alto conteúdo de celulose, elevada resistência à tração e flexão, rigidez e baixo angulo microfibrilar (11 º). Para o fabrico dos compósitos as fibras foram extraídas de três secções do tronco, secas, moídas, sujeita a um tratamento químico, e misturadas por extrusão com PBAT para obter filamentos com 2, 5 e 8 wt% em pó de fibra. Os compósitos foram caracterizados por SEM, espetroscopia de FTIR, TGA, absorção de água, DMA e ensaios mecânicos. Os compósitos com pós de fibra tratados, provenientes das camadas intermédias apresentaram uma interação fibra-matriz polimérica, contudo esta adição levou a má dispersão do reforço, uma menor estabilidade térmica, menor resistência à tração e maior tendência para absorver água. O compósito reforçado por pós de fibra tratados, provenientes das camadas exteriores, foi o único que apresentou uma melhoria ao nível das propriedades mecânicas, termo-mecânicas e redução na absorção de água. Assim, estes pós são bons reforços para o PBAT e permitem diminuir o custo geral do material, sem comprometer as propriedades e comportamentos originais deste polímero biodegradável.

Palavras-chave: PBAT, fibra da bananeira, extrusão, impressão 3D, moinho criogénico de impacto, produto de valor acrescentado

Abstract

With increasing environmental problems presented today due in part to plastic pollution, new trends are emerging to deal with this crises. One approach takes advantage of bioplastics to substitute synthetic polymers where PBAT blends are a promising candidate. Natural fibers, as agricultural waste, have been previously used as reinforcements for bioplastic blends, but the novelty of this project lies in repurposing banana pseudo-stem fibers. These fibers were ellected as excellent candidates due to their high cellulose content, high tensile and flexural strength, high stiffness and low microfibrillar angle (11°). In order to produce the composites the fibers were extracted from three regions of the trunk, dried, grinded and subject to carefully designed treatments, and blended, by extrusion, with PBAT pellets to obtain filaments with 2, 5 and 8 wt% in fiber powder. Composites were characterized by SEM, FTIR spectroscopy, TGA, water adsorption, DMA and tensile tests. Composites reinforced with grinded fibers from the middle sheaths presented an interaction between the fillers and the polymer matrix, however, the addition of powders lead to composites with improper dispersive mixing, lower thermal stability, lower tensile strength and higher water absorption tendencies. Composites reinforced with grinded fibers from the exterior sheaths were the only ones that presented enhanced mechanical, thermo-mechanical properties and water absorption capacity. Therefore, these powders are a good reinforcement/fillers for PBAT that allow to reduce the cost of the materials without compromising its original properties and behavior of this biodegradable polymer.

Key words: PBAT, banana fiber, extrusion, 3D printing, cryogenic impact mill, high value product

List of Tables

Table 1 – Comprehensive list of mechanical properties and chemical composition of banana fiber found in the literature ... 14

Table 2 - List of most important equipment used in the laboratory work ... 19

Table 3 – Composites of PBAT and its respective fiber percentage and origin ... 21

Table 4 – FTIR spectra peak list of raw banana fiber with absorption, assignment and references from the literature for comparison ... 29

Table 5 - Thermal stability of untreated and treated powders compared with the literature ... 36

Table 6 - First and second extrusion processing parameters and diameter control measurements for PBAT/banana fiber powder treated and untreated composites ... 40

Table 7– FTIR spectra peak list of neat PBAT with absorption, assignment and references from the literature for comparison ... 43

Table 8 - SEM images and optical microscopy photographs (at 4.5x for a;c;f;h;k;m;p) of PBAT/treated and untreated middle fiber powder composites with 2, 5 and 8 wt% and neat PBAT (1500x, scale bar 20 μm – b;d;g;i;l;n;q; 8400x, scale bar 3 μm – e;j;o) ... 46

Table 9 – Thermal decomposition parameters of PBAT and PBAT/powder blends ... 49

Table 10– Thermal behavior of either banana fiber, LDPE or PBAT blends from the literature ... 51

Table 11– Storage modulus G' (at -45 ºC and 35 ºC), glass transition temperature Tg and loss modulus G″ of neat PBAT and PBAT/powder blends. ... 53

Table 12– Tensile strength and elongation at break of PBAT and PBAT/powder blends ... 58

Table 13 – Mechanical properties of LDPE or PBAT blends with banana fibers or other natural fibers and fillers from the literature ... 61

Table 14– Water absorption values along with standard deviation for 2, 5 and 8 days for PBAT and PBAT/powder blends ... 63

Table 15 – Comprehensive list of the varied PBAT/additive composites found in the literature, along with the corresponding mechanical properties, water absorption, rheological and thermal behaviour ... 79

Table 16 – Comprehensive list of the varied PBAT/TPS composites found in the literature, along with the corresponding mechanical properties, water absorption, rheological and thermal behaviour 81

Table 17 – Comprehensive list of the varied PBAT/PLA composites found in the literature, along with the corresponding mechanical properties, water absorption, rheological and thermal behaviour 83

Table 18 – Comprehensive list of the varied Banana fiber/LDPE composites found in the literature, along with the corresponding mechanical properties, water absorption, rheological and thermal behaviour ... 85

Table 19 – Sample dimensions of DMA testing ... 89

Table 20 – Sample dimensions of water absorption testing ... 89

List of Figures

Figure 1 - Circular material economy framework. Adapted from Hong and Chen [4] ... 2

Figure 2 - Schematic diagram of the synthesis of PBAT with adipic acid (AA), 1,4-butanediol (BDO) and terephthalic acid (TPA) by polycondensation [6] ... 3

Figure 3 - Proposed hydrolytic mechanism of PBAT [13] ... 4

Figure 4 – Munguba fiber on the right and babassu epicarp fiber on the left [34,26] ... 5

Figure 5 – Starch molecules: A) scheme amylose structure; B) scheme amylopectin structure [48] ... 6

Figure 6 – Grafting reaction of maleic anhydride onto PBAT with a free radical initiator and a schematic overview of the compatibilizer. Adapted from Wu [33] and Wu [24] ... 7

Figure 7 – PLA chemical structure [70] ... 9

Figure 8– Graphic representation of the effect of chain extenders. Adapted from Pan et al. [84] ... 10

Figure 9 – Schematic representation of hydrogen bonding in natural fibers. Adapted from A. K. Mohanty, Misra, and Drzal [103] ... 11

Figure 10– Structural organization of the three major constituents in the fiber cell wall [20,102] ... 12

Figure 11 – Diagrammatic representation of A) banana plant; B) cross-sectional view of banana pseudo-stem [42] ... 13

Figure 12 - Schematic overview of chemical treatments and hypothetical models of interface of banana fiber [101,103,106,119] ... 15

Figure 13 – Schematic representation of the structure of raw and alkali treated natural fiber. Adapted from Kabir et al. [102], A. K. Mohanty, Misra, and Drzal [103] ... 16

Figure 14 - Pseudo-stem from (a) Barrocalvo, Leiria and (b) from Sobreiro, Mafra ... 18

Figure 15 - Overview diagram of the processes and materials for the experimental phase ... 19

Figure 16 – Mechanical decorticator that extracts banana fiber and its apparatus. Adapted from Mukhopadhyay et al. [116] ... 26

Figure 17 – Steps for the manual extraction of fibers and a schematic representation of the cross section sheath and morphology ... 27

Figure 18- Schematic representation of the steps followed to transform fiber to fiber powder [125,126] ... 28

Figure 19- FTIR spectra of (a) raw manually extracted fiber and (b) the absorbance peaks of interest for banana fiber ... 29

Figure 20 - FTIR spectra of (a) raw, manually extracted treated (15% NaOH for 1 h) and chemically extracted fibers (15% NaOH for 48 h); (b) alkali treated fibers (15% NaOH for 1 h; 15% NaOH for 2 h; 25% NaOH for 1h) ... 31

Figure 21 – SEM images of (a: 2000x, scale bar 80 μm; b: 12000x, scale bar 10 μm) raw fiber; (c: 2000x, scale bar 80 μm – d: 12000x, scale bar 10 μm) alkali treated fiber (15% NaOH for 1 h); (e: 2000x, scale bar 80 μm – f: 12000x, scale bar 10 μm) chemically extracted fiber (15% NaOH for 48 h) 32

Figure 22 – Optical microscopy photographs of (a: 2.5x – b: 4.5x) raw fiber; (c: 2.5x – d: 4.5x) alkali treated fiber (15% NaOH for 1 hour); (e: 2.5x – f: 4.5x) chemically extracted fiber (15% NaOH for 48h) ... 33

Figure 23- FTIR spectra of (a) interior, middle and exterior fiber powder; (b) interior treated and untreated fiber powder; (c) middle treated and untreated fiber powder; (b) exterior treated and untreated fiber powdes 34

Figure 24– (a) Thermogravimetric analysis (TGA) of untreated and treated middle fiber powder (b) Differential thermogravimetric analysis (DTG) of untreated and treated middle fiber powder 35

Figure 25 – (a) Untreated middle powder; (b) Treated middle powder; (c) PBAT/untreated middle powder at 2 wt%; (d) PBAT/ treated middle powder at 2 wt%; (e) neat PBAT and composites of PBAT with 2, 5 and 8 wt% treated middle powder (f) neat PBAT and composites of PBAT with 2, 5 and 8 wt% untreated middle powder 39

Figure 26 - Summary chart of potential causes and corrective actions when the (a) output is too low or tin and (b) the filament extruded presents bumps and particles [143] 42

Figure 27 – FTIR spectra of (a) neat PBAT and (b) the absorbance peaks of interest of PBAT 43

Figure 28 – FTIR spectra of (a) neat PBAT and PBAT/middle fiber powder composites (b) neat PBAT and PBAT/middle treated fiber powder composites (c) neat PBAT and PBAT/interior treated and untreated fiber powder (d) neat PBAT and PBAT/exterior treated and untreated fiber powder composites........ 44

Figure 29 - (a -b) Thermogravimetric analysis (TGA) of untreated and treated middle fiber powder composites (b) Differential thermogravimetric analysis (DTG) of untreated and treated middle fiber powder composites........ 48

Figure 30 - Effect of powder loading and alkali treatment with temperature on the storage modulus of neat PBAT and PBAT composites for (c) interior, (a-b) middle and (d) exterior fiber powders in the temperature range of -45 ºC to 35 ºC........ 54

Figure 31 - Effect of fiber loading and alkali treatment with temperature on the loss modulus of neat PBAT and PBAT composites for (c) interior, (a-b) middle and (d) exterior fiber powders in the temperature range of -45 ºC to 35 ºC........ 56

Figure 32- Effect of fiber loading and alkali treatment with temperature on the tan δ peaks of neat PBAT and PBAT composites for (c) interior, (a-b) middle and (d) exterior fiber powders in the temperature range of -45 ºC to 35 ºC 57

Figure 33 - Representative stress-strain curves for exterior untreated and treated composites 59

Figure 34 – Water absorption behavior of neat PBAT and (a) untreated middle composites, (b) treated middle composites, (c) untreated and treated interior composites, (d) untreated and treated exterior composites........ 62

Figure 35 – 3D printed bunnies with PBAT extruded filament 64

Figure 36 - SPEX SamplePrep 6770 Freezer/Mills apparatus (a) from the front (b) from the back 87

Figure 37- 3Devo® composer 450 desktop extruder and its apparatus (a) right side of the model (b) front of the extruder with open panel. Adapted from 3Devo - Filament Makers [153] 88

Figure 38– FTIR spectra of (a) interior fibers and (b) exterior fibers from banana pseudo-steam trunks from trees A and B from figure 14 (c) bark and exterior fiber (d) alkali treated exterior bark for concentrations of sodium hydroxide of 0.25, 0.5, 1, 3 and 5 % 90

Figure 39 – FTIR spectra of respectively zoomed section between 4000 – 2000 cm^{-1} and 1710 cm^{-1} for (a –b) neat PBAT and PBAT/treated and untreated interior composites; (c - d) neat PBAT and PBAT/ untreated middle composites; (e - f) neat PBAT and PBAT/treated middle composites; (g - h) neat PBAT and PBAT/treated and untreated exterior composites 91

Figure 40 - Thermogravimetric analysis (TGA) zoomed at the T_{onset} for (a) neat PBAT and PBAT/treated middle composite and (b) neat PBAT and PBAT/untreated middle composite 92

Figure 41 – Thermogravimetric analysis (TGA) of (a) neat PBAT and PBAT/treated and untreated interior composites and (c) neat PBAT and PBAT/treated and untreated exterior composites. Differential thermogravimetric analysis (DTG) of (b) neat PBAT and PBAT/treated a and untreated interior composites and (d) neat PBAT and PBAT/treated and untreated exterior composites 92

Figure 42 - SEM image (2000x, scale bar 80 µm) and EDS data for alkali treated fiber with 15% NaOH for 1 h at 90 ºC 93

Figure 43 - SEM image and EDS data for (a) PBAT/ 8 wt% treated middle composite (600x, scale bar 50 µm); (b) PBAT/ 8 wt% treated middle composite (600x, scale bar 50 µm); (c) PBAT/ 5 wt% treated middle composite (1150x, scale bar 30 µm); (d) PBAT/ 5 wt% treated middle composite (1150x, scale bar 30 µm) 94

Figure 44 - Optical microscopy photographs at 4.5x for (a –b) PBAT/ 2 wt% untreated exterior composites and (c – d) PBAT/ 2 wt% treated exterior composites 94

List of Graphics

Graphic 1 - Thermogravimetric and derivative thermogravimetric analysis of PBAT and PBAT powder composites 49
Graphic 2 - Storage modulus G' (at -45 ºC and 35 ºC), glass transition temperature Tg and loss modulus G″ of neat PBAT and PBAT/powder blends 53
Graphic 3 - Tensile strength (MPa) and Elongation at break (%) for PBAT and PBAT/powder blends 59

List of Acronyms and Symbols

BaF	Banana Fiber
BC	Biochar
BETT	1,3-bis(2,3-epoxypropyl)-s-triazine-2,4,6-trione
BIBP	Bis(tert-butyl dioxy isopropyl) Benzene
BP	Benzoyle Peroxide
BT	Bentonite
C15A	Cloisite 15A
C30B	Cloisite 30B
CA	Citric Acid
CLA	Cellulose Acetate
CNC	Cellulose Nanocrystal
CNF	Cellulose Nanofillers
CNT	Carbon Nanotube
CSS	Coffee Silverskin
DCP	Dicumyl Peroxide
EFG	Epoxy Functionalized Graphene
EMA-GMA	Ethylene-methyl acrylate-glycidyl methacrylate
EPS	Expanded Polystyrene
Gly	Glycerol
GMA	Glycidyl Methacrylate
GNP	Graphene Nanoplatelets
HDPE	High Density Polyethylene
HNT	Halloysite Clay Nanotubes
JF	Jute Fiber
KL	Kraft Lignin
LDPE	Low Density Polyethylene
MA	Malic acid
MAH	Maleic Anhydride
MCC	Microcrystalline Cellulose
MDI	4,40-methylene diphenyl diisocyanate
MMT	organically Modified Montmorillonite
MTPS	Maleated Thermoplastic Starch
NC	Nano Chitin
PBAT	Poly-butylene adipate-co-terephthalate
PET	Polyethylene terephthalate
PH	Peanut Husks
PHA	Polyhydroxyalkanoates
PLA	Poly(lactic acid)
PP	Polypropylene
PS	Polystyrene
PU	Polyurethane
PVC	Poly(vinyl chloride)
RH	Rice Husks
RHS	Rice Husk Silica
SCG	Spent Coffee Grounds
SO	Soybean Oil
TA	Tartaric Acid
TDI	Toluene Diisocyanate
TEC	Triethyl Citrate
T-GMA	Random terpolymer of ethylene, acrylic ester and GMA
TPRH	Thermoplastic Rice Husk
TPS	Thermoplastic Starch
WVP	Water Vapor Permeability
σ	Stress (MPa),
P	Load (N)
A_0	Initial cross section area (m^2)
ε.	Strain (no dimension)
L_0	Initial length of the sample (mm),
L	Distance between gage marks at any time (mm)
δ	Displacement (mm)
E	Young's modulus
$D_{Extrudate}$	Diameter of the extrudate
D_{die}	Diameter of the die

Motivation

The goal of the project consists in developing and characterizing a high end value product with PBAT, a biodegradable polymer reinforced with agro-food waste left over from the banana production. This biocomposite presents a potential bioplastic alternative for the widely used commodity fossil derived PE plastics. As such this dissertation may contribute to the substitution of single use plastics as it tackles issues regarding a miss use of these polymers, and gives use to once considered agro-waste from banana production, enabling its upcycling. This will produce further income for local farmers and decrease greenhouse gas emissions from the disposal of the pseudo-stems. Furthermore, the specific objectives are to evaluate the effect of:

- Alkali treatments in fiber structure;
- Fiber content on extruded filaments;
- 3D printed part quality.

In order to fulfill these objectives, the fibers were extracted from three different regions of the trunk (interior, middle and exterior), dried, grinded and subject to carefully designed treatments (15% NaOH, 1h, 90 ºC), and blended, by extrusion, with PBAT pellets to obtain filaments with 2, 5 and 8 wt% in fiber powder. Fibers and fiber powders were characterized before and after treatment by scanning electron microscopy (SEM), optic microscopy, Fourier transform infrared (FTIR) spectroscopy and thermogravimetric and derivative thermogravimetric analysis (TGA/DTG) to analyze the chemical, morphological and thermal changes. The extrusion profile was optimized (parameters: heating temperatures, screw speed, spooling and wending velocities) to obtain filaments that were further evaluated by scanning electron microscopy (SEM), Fourier transform infrared (FTIR) spectroscopy, thermogravimetric and derivative thermogravimetric analysis (TGA/DTG), water adsorption, dynamic mechanical analysis (DMA) and tensile tests. Samples were prepared to be tested by these two latter techniques. Extruded PBAT was used for 3D printing, as a proof of concept.

Chapter 1: Introduction

The 21st century is thriving with tremendous economic growth but at the same time facing irrecoverable ecological damage, in part due to plastic pollution.[1] The world of today substantially relies on synthetic polymers due to their versatility, large-scale production, low cost, lightweight, durability, geometric conformability and water resistance capacity.[2] Thus, they are put to use in a wide variety of fields such as aerospace, aeronautical, automotive, medical, etc. Within synthetic polymers, commodity plastics are the most widely produced and used and these include HDPE, LDPE, PP, PS, EPS, PVC, PU and PET. [2,3,4]

Unfortunately, current processes of production and disposal of synthetic polymers follow a linear-economy model, defined as 'fossil, take, make, use, dispose' joined with an extremely ineffective practice of recycling where only ~5% of material values are recovered for subsequent use.[4] In order to shift from the traditional and unsustainable model, a combination of measures should be put in place by upcycling waste into high end value products with integrated chemical recyclability, minimizing and recycling plastics and manufacturing sustainable polymers (SPs) such as bioplastics.[1,4,5] *Figure 1* summarizes these advances. These changes will take a 'whole-society' approach, requiring effort and collaboration from all relevant stakeholders.[1,5]

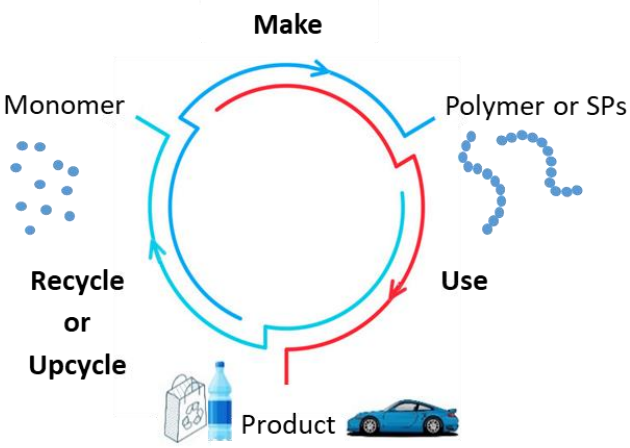

Figure 1 - Circular material economy framework. Adapted from *Hong and Chen* [4]

Bioplastics include bio-based and biodegradable plastics. Bio-based plastics are made fully or partially from biological resources, and may not necessarily be biodegradable.[5] Meanwhile, biodegradable plastics undergo decomposition due to the action of microorganisms, such as enzymes [6], forming small molecules that are metabolized by natural organisms. The latter ones can be classified into two categories: natural polymers, obtained directly from nature, and synthetic polymers.[2] Following their manufacture, comes the assessment of end-of-life management. Just like conventional plastics, bioplastics also need a specific procedure of disposal according to differences in properties and processing conditions. The most favored option to manage bioplastic waste is recycling, which includes mechanical, chemical/catalytic and organic, if it is biodegradable.[1,7] However, some challenges still remain related with the heterogeneity, low market volumes and waste contamination of samples, along with the specifically controlled conditions required for the biodegradation of bioplastics.[1,4,8] For this study, the bioplastic of interest is poly-butylene adipate-co-terephthalate (PBAT).

1.1. PBAT

PBAT is a synthetic thermoplastic aliphatic-aromatic co-polyester, that can be 50% bio-based, but most of the times derived from fossil resources. It is 100% biodegradable, very flexible, has high elongation at break, high elasticity, toughness and thermal stability, like LDPE.[2,9–16] The aliphatic regions of the polymer confer good biodegradable properties, while the aromatic regions give good physical properties.[6] This polymer has been mainly used for packaging materials, hygiene products, biomedical fields, industrial composting, and other applications.

1.2. Synthesis of PBAT

Polyesters, in general, are synthesized by polycondensation of diols and dicarboxylic acids. PBAT, specifically, can be obtained by polycondensation of 1,4-butanediol with adipic and terephthalic acids, as shown in *Figure 2* , using conventional polyester manufacturing technology and equipment. The synthesis of PBAT can be divided into pre-mixing, pre-polymerization and final-polymerization process. Its preparation requires long reaction time, high vacuum, and temperature usually higher than 190 ºC, in order to favor condensation reactions and remove lighter molecules, like water, as products.[2,6]

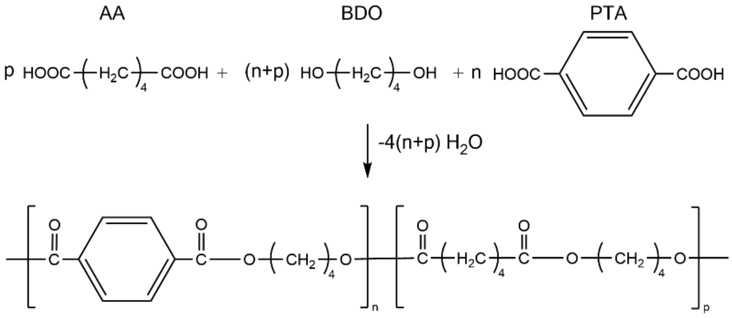

Figure 2 - Schematic diagram of the synthesis of PBAT with adipic acid (AA), 1,4-butanediol (BDO) and terephthalic acid (TPA) by polycondensation [6]

1.3. Biodegradation of PBAT

The biodegradable bioplastics are supposed to undergo biodegradation in a short period of time, around 180 days, under favorable conditions of temperature, pH, humidity, etc. The decomposition is accompanied by the formation of water, methane and/or CO_2 and biomass depending on the environmental conditions, if it is aerobic or anaerobic.[8,9]

The biodegradation can occur through the enzymatic action of microorganisms such as bacteria, fungi, and algae present in the natural environment. A number of features are listed as playing a significant role in the enzymatic degradation of PBAT, such as the degradation temperature and media, chemical structure, the presence of fillers and so on. In other cases, biodegradation occurs via the combined depolymerization process, where the polymer chain breaks down by non-enzymatic reaction, with metabolization of the intermediates by microorganisms. Several variables affect the rate of non-enzymatic degradation such as crystallinity, morphology, water concentration, temperature, presence of fillers and others.[2,7,9] Specifically, PBAT undergoes hydrolytic degradation owing to the cleavage of ester linkages, which requires the presence of water, and photo-degradation.[13,17] The figure below exemplifies the hydrolytic degradation of PBAT.

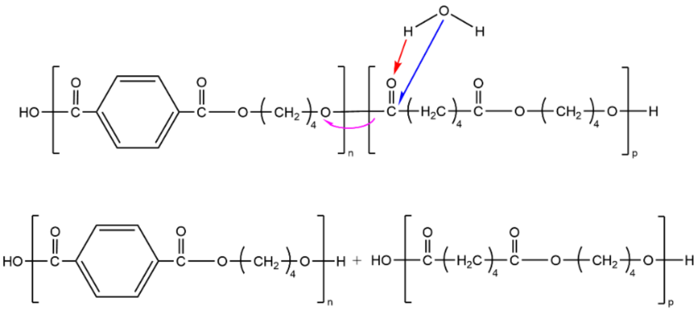

Figure 3 - Proposed hydrolytic mechanism of PBAT [13]

1.4. PBAT composites

PBAT possesses some shortcomings such as a high production cost when compared with conventional plastics and lower elastic modulus and tensile strength than LDPE.[17,18] Therefore, in order to develop blends with a desirable combination of properties PBAT composites are produced with additives and polymers like thermoplastics starch (TPS) and PLA.[19] Composites offer the possibility of adjusting the cost-performance balance and fulfill the specific properties of applications.[20,21] This section will discuss the additives used, while further sections will look more closely into blends of TPS/PBAT and PLA/PBAT.

Fillers are a type of additives that are either solid organic or inorganic materials. They can be used to reinforce polymers and enhance their mechanical performance (functional fillers) or reduce the amount of resin needed to produce a part (extenders).[22,23] While several approaches have been stated in the literature, the most important ones for this work include: agro-food/industrial waste [10,24–34] and nanofillers [12,35–40]. These fillers can decrease the production cost while still maintaining the inherant biodegradability [34] of the blend.[41]

Agro-food waste presents profitable opportunities due to its great world-wide availability to fabricate high-value added products. Peanut husks (PH) [24] and rice husks (RH) [25,27] have been tested as they are abundant, inexpensive, renewable and fully biodegradable.[24] Meanwhile, within rice husks, rice husk silica (RHS), known to improve thermal and mechanical properties and increase gas barrier properties [27], and blends of thermoplastic rice husk (TPRH), prepared by treating rice husks with glycerol [25], have been studied. Other waste used include shell waste from crustaceans that predominantly contain chitin (NC), a biodegradable polymer.[10] Additionaly, in the coffee industry a major source of residues comes from defective beans, coffee silverskin (CSS), and spent coffee grounds (SCG). Both residues were added to a 65% PBAT-35% PHBV blend. Coffee silverskin are the by-product of the coffee roasting process and consists of the innermost layer of the coffee bean, while spent coffee grounds are the residue of the brewing process.[28,29] Moreover, a by-product of pulping processes is kraft lignin (KL), a derivative of native lignin.[30] Lignin mainly comes from biomass like plant fibers and is a cross-linked nontoxic polyphenolic compound that exhibits high impact strength, good heat-resistance and is a promising bio-based flame retardant.[31] Furthermore, biochar (BC) is waste produced by the pyrolysis of forestry and agricultural industries that presents high thermal and chemical stability along with a good photo-oxidative resistance.[32]

Agro-waste residues also include natural fibers which are eco-friendly alternate to synthetic polymers.[42] They are non-toxic, biodegradable, have reinforcement properties and come from renewable natural resources. Several types of natural fibers have been tested such as munguba [34], cellulose acetate (CLA) which is a derivative of natural cellulose fiber [33] and babassu [26] (*Figure 4*). Munguba fiber are extracted from the stem of the tree and are strong and flexible while babassu fibers come from the fruit.[34] When babassu fibers are joined with PBAT they greatly enhance the degradation tendency of the matrix.[26]

Figure 4 – Munguba fiber on the right and babassu epicarp fiber on the left [34,26]

Nanofillers are effective and simple means to improve the mechanical properties of polymers. However, properties of nanocomposites are generally highly dependent on the dispersion of the particles in the polymer matrix, i.e. on the efficiency of the dispersive and distributive mixing processes employed to prepare them, as well as on the interaction between both, the viscosity ratio, interfacial tension and processing conditions in general.[35,43] It should be stressed that nano-sized particles tend to form agglomerates, making their dispersion more difficult than micron-sized particles, therefore they should be disintegrated to achieve proper reinforcing effects.[23,44] An effort should be placed to promote an effective breaking of the agglomerates (size reduction) and achieve a proper dispersive mixing, together with the use of adequate mixing equipment that promotes elongational flow and high extension and shear stresses at the surface of the particles. Cellulose particles are ideal candidates and they can come in micro or nano scale. Microcrystalline cellulose (MCC) is a crystalline micrometric powder well-known for its biocompatibility, biodegradability, and high mechanical strength.[36] Meanwhile, nanocrystal cellulose (CNC) is of particular interest due to its low weight, biodegradability, high stiffness, large specific surface area, almost perfect crystalline structure and axial elastic modulus up to 150 GPa.[37,38] Furthermore, carbon nanotube (CNT) and organoclay have also drawn some attention owing to their potential in imposing synergistically improved properties for polymer matrices.[40] On the other hand, graphene nanoplatelets (GNP) can replace carbon nanotubes in many applications due to their lower production cost. They are graphitic nanoparticles with layered structures composed of stacked 2D graphene sheets bonded together with weak Van der Waals forces and high surface area, exhibiting excellent physical properties. When joined with PBAT they enhance viscoelastic properties behaving as a solid with high filler content and liquid-like at low concentrations.[12] Meanwhile, other examples include organically modified layered silicate such as montmorillonite (MMT), which are crystalline 2:1 layered clay mineral with a central alumina octahedral layer sandwiched between two silica tetrahedral layers with a hydrophilic character.[39] When successfully compounded they have been known to enhance gas barrier properties, toughness, mechanical strength, thermo-mechanical strength, and reduced flammability with only a small amount of organoclay compared to the traditional inorganic composites.[35]

Table 15 in appendix A list some PBAT/additive composites found in the literature along with the corresponding mechanical properties, water absorption, rheological and thermal behaviour.

The following two sections will look more closely into blends of TPS/PBAT and PLA/PBAT as they were extensively mentioned in the literature.

1.5. Starch-PBAT based blends

Starch is a semi-crystalline polymer, bio synthesized by numerous plants and it consists of two types of molecules, the linear amylose and the branched amylopectin, as shown in *Figure 5*. It is an inexpensive, biodegradable, readily available, low density, non-abrasive material, that enables a wide-possibility of formulation to meet the marked requirement.[5,7,45–47]

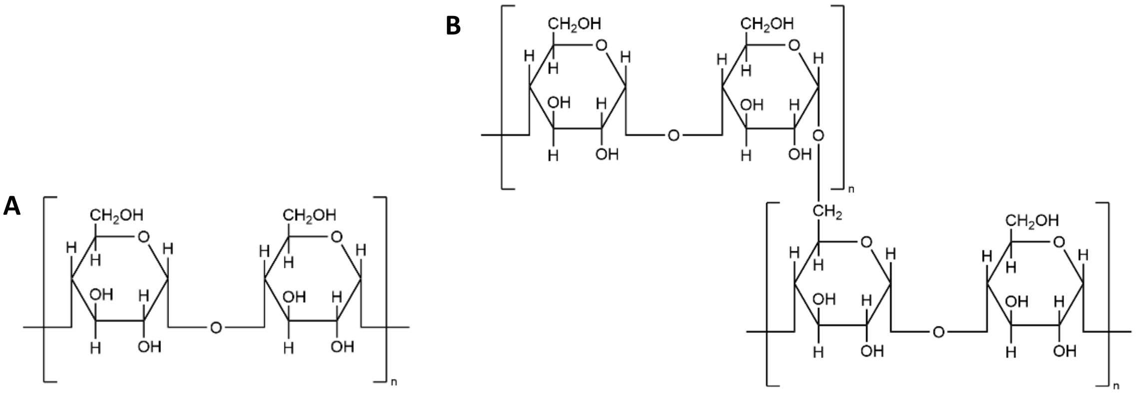

Figure 5 – Starch molecules: A) scheme amylose structure; B) scheme amylopectin structure [48]

However, native starch exists in granular form due to strong intermolecular association via hydrogen bonding of the hydroxyl groups between the starch macromolecules, exhibiting hydrophilic properties. The hydrophilicity and thermal sensitivity render the starch molecule unsuitable for thermoplastic applications.[46,49] Therefore, it can be converted into thermoplastic starch (TPS) through the use of plasticizer that destructurize granular starch by breaking hydrogen bonds accompanying with a partial depolymerization, under the combined conditions of temperature and shear.[50] The most commonly employed plasticizers are water, glycerol (Gly) and ureia.[51] Furthermore, due to its poor water resistance, high hygroscopicity [52], low strength, crystallization and plasticisation by water adsorption [45], starch is often blended with other polymers to achieve needed mechanical properties, such as PBAT.[5] But still there is a lack of miscibility between the hydrophilic starch and hydrophobic polyester matrix that induces phase separation and poor stress transfer between the two phases.[47]

Typically to increase the content of thermoplastic starch without severely imparting the mechanical properties, a reactive melt blending is carried out in the presence of a compatibilizer, which covalently links the components and strongly enhances the interfacial adhesion.[53] These compatibilizers include maleated PBAT [49], maleated TPS (MTPS) [50,54], soybean oil (SO) [55], tween 80 [55], organic acids [45,56–59], nanomaterials [44,46,52,60–62] and natural fibers [63,64] to name a few.

The maleation of PBAT and thermoplastic starch is done by reactive extrusion in the presence of maleic anhydride (MAH) as a esterification agent and mainly glycerol as a plasticizer. *Figure 6* shows the grafting reaction of maleic anhydride onto PBAT. The radical grafting of maleic anhydride onto PBAT blends through extrusion, proved to be efficient in promoting strong interfacial adhesion and improved resilience (from 84% to 95%) and hydrophobic properties in terms of lower weight gains on moisture sorption.[49] *Fourati et al.* demonstrated that the inclusion of 2 wt% of PBAT-g-MAH strongly enhanced the strain at break with a continuous PBAT phase.[56] Meanwhile, grafting of maleic anhydride onto the starch backbone replaces hydroxyl groups and introduces ester bonds that become available for covalent bonding with PBAT as well as free carboxylic acid groups that promote interfacial transesterification reactions with PBAT.[54] In addition, it was demonstrated that the preferential esterification is located in the C6 backbone alongside some hydrolysis and glucosidation reactions. Thus, there is a reduction of the melt-viscosity, and, therefore, of the relative molecular weight of maleated thermoplastic starch, improving its processability.[50] Furthermore, *Hablot et al.* established that the presence of 2 wt% MAH significantly increased the extent of glycerol grafting on the starch backbone, which enhanced the extent of grafting of MTPS onto PBAT (83% vs 26% TPS/PBAT) through transesterification reaction, with a well dispersed starch phase in the continuous PBAT matrix.[65] Moreover, a multilayer film TPS, its maleated counterpart and PBAT was studied.[54]

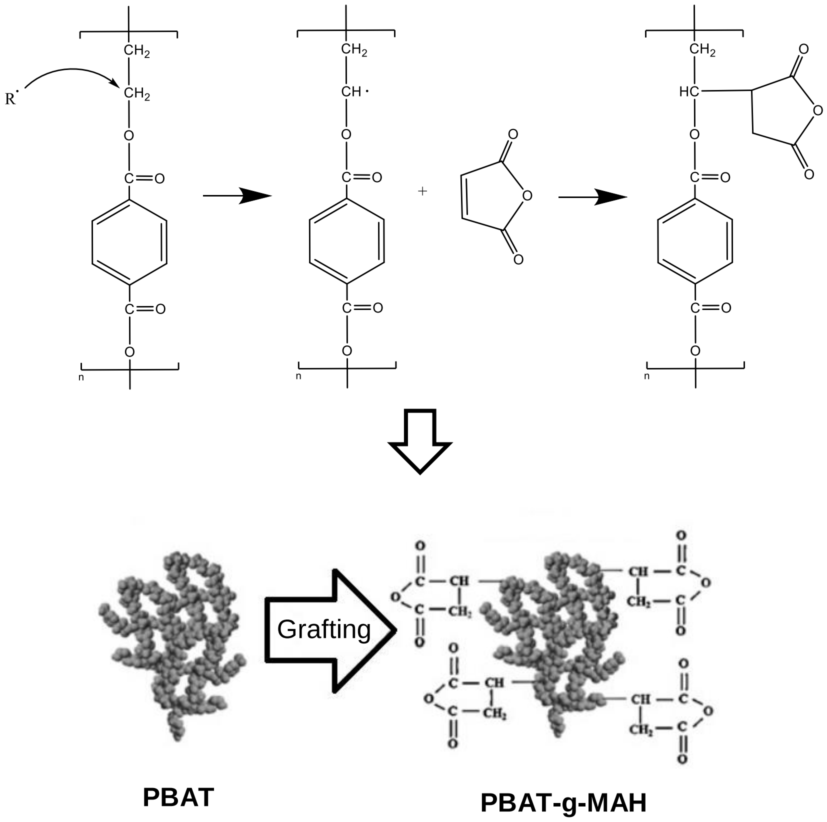

Figure 6 – Grafting reaction of maleic anhydride onto PBAT with a free radical initiator and a schematic overview of the compatibilizer. Adapted from *Wu* [33] and *Wu* [24]

Another category of compatibilizers are the organic acids. They are non-toxic, non-volatile, are naturally present in fruits and vegetables and are synthesized by microorganisms during the fermentation process.[45,58,59] Citric, malic and tartaric acids (CA, MA and TA, respectively) have been studied as they promote esterification (grafting) and transesterification reactions (cross-linking) between polymers, improving their compatibility, which will add to the plasticizing effect and acid hydrolysis of starch.[16,45,58] Although improved interfacial adhesion has been shown for PBAT/TPS blends, the unreacted organic acids must be completely removed as they tend to accelerate the degradation of PBAT.[66] Also, organic acids with low molecular weight do not interact continuously with PBAT, resulting in limited compatibility. Therefore, it is essential to seek an effective compatibilizer, which can not only interact with the hydrophilic TPS but also with the hydrophobic PBAT.[67]

Besides the use of organic acids, the addition of lipids and surfactants, such as soybean oil (SO) and Tween 80 surfactant, to starch films can reduce the film water vapor permeability (WVP), thus making the films more hydrophobic. Tween 80 is a surfactant with a high hydrophilic/lipophilic balance value (>10) allowing for a greater association of their hydrophilic fraction with the hydrophilic film matrix, therefore reducing the amount of water binding sites while the hydrophobic fraction may act as a WVP barrier.[55] Soybean oil is an abundant and renewable raw material that features a mixture of triglycerides in its chemical composition producing homogenous films with greater elongation, resistence and less moisture.[68]

Additionally, other common methods include the use of nanofillers to improve the biodegradable polymer matrix properties due to their availability, versatility, and eco-friendlyness.[60,62] One study used sepiolite nanoclays that possess a needle-like morphology with a theoretical unit cell formula $Mg_8Si_{12}O_{30}(OH)_4 \cdot (H_2O)_4 \cdot 8H_2O$ and an alternating of blocks and channels that grow up in the fiber direction. Sepiolite are easily dispersed due to their small interface surface, which leads to a higher mechanical reinforcement.[52] The silanol groups (Si-OH) of the sepiolites interacted with the hydroxyl groups of starch through hydrogen bonds and have a good dispersion in the TPS matrix. Contrary to the needle-like shape of sepiolite nanoclay, hollow-shaped halloysite clay nanotubes were also studied since geometry and structural parameters, like shape and size of the nanoclays do influence the morphologies and properties of the corresponding composites. Halloysite clay nanotubes (HNTs) belong to a subgroup of kaolin clay that are non-toxicity, biocompatible and environmentaly friendly.[62] Meanwhile, bentonite (BT) and organically modified montmorillonite (MMT) were also incorporated into TPS.[44] Furthermore, *Fourati et al*. developed the only known work on cellulose nanofibrils in PBAT/TPS/CNFs by extrusion (50/50). CNF was well dispersed and proved to be a good compatibilizer. When its content reached 8 wt%.[47]

Another way to improve the mechanical properties of TPS blends is by joining natural fibers since they possess a good set of mechanical properties and have chemical similarity to starch, providing good compatibility. Biocomposites with babassu mesocarp [63] and jute fiber [64] (JF) were studied.

Table 16 in appendix A list some PBAT/TPS composites found in the literature along with the corresponding mechanical properties, water absorption, rheological and thermal behaviour.

1.6. PLA-PBAT based blends

PLA is a linear aliphatic biodegradable thermoplastic polyester, synthesized by ring-opening polymerization of lactides which are cyclic dimers of lactic acids and are typically derived from corn starch or sugarcane fermentation, therefore produced from renewable resources.[69] *Figure 7* shows PLA chemical structure.

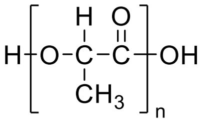

$$\mathrm{H}\left[\mathrm{O}-\underset{\mathrm{CH_3}}{\overset{\mathrm{H}}{\mathrm{C}}}-\overset{\mathrm{O}}{\overset{\|}{\mathrm{C}}}\right]_n\mathrm{OH}$$

Figure 7 – PLA chemical structure [70]

PLA presents interesting mechanical and physical properties, like high modulus (2–16 GPa) and high tensile strength (14–117 MPa), has excellent transparency, good optical properties, barrier properties and is non-toxic.[69,71,72] Generally, it is processed by injection molding and extrusion.[73] However, it also presents an inherent brittleness (strain at break 3.8%), poor thermal stability (low glass transition temperature – about 60 ºC), physical aging, slow crystallization rate and low resistance to UV radiation which restricts its use.[69,74–76] Therefore, an effective and economical method to modify its properties is by incorporating other polymers while tailoring the ratio of PLA in the blend and controlling the blend morphology.[77,78] PBAT can toughen PLA, improve its elongation, crystallization rate, nucleation density, UV resistance, processability and increase melt elasticity and viscosity while maintaining its biodegradability.[69,75,79,80] Nonetheless, the mixture of these two polymers has been described, in many cases, as immiscible.[79] Strategies for decreasing interfacial tension between the blending components, such as forming block polymers through reactive compatibilization and in-situ reactive blending, are considered effective in improving the compatibility and mechanical properties of the blend.[78,81]

Ma et al. did a reactive blending/in-situ compatibilized PLA/PBAT blend prepared with a free radical initiator dicumyl peroxide (DCP). They were able to improve the compatibility and enhance the interfacial adhesion between PLA and PBAT, and improve the mechanical properties of PLA.[82] Meanwhile, another peroxide free radical crosslinking agent that has similar properties to DCP is bis(tert-butyl dioxy isopropyl) benzene (BIBP). Due to its non-toxicity and lack of odors after decomposition it is a worthy environmental-friendly candidate to replace DCP, being an excellent crosslinking agent and improving the mechanical properties of the PLA/PBAT films.[83]

Nevertheless, according to some studies the state of a PBAT/PLA blend can vary from immiscible to partially miscible [84–87], depending on the processing and storage temperature and the molecular weights and weight ratio of both polymers at a constant temperature.[88,89] Generally, the higher the molecular weights, the lower the predicted probability of the blend miscibility, while the higher the temperature, the higher the probability of the blend miscibility.[88] One of these systems treated a blend of 50/50 PLA/PBAT in a melt mixer attached to an ultrasonic device, which increased the adhesion between the matrix and the dispersed phase by reducing the size of the dispersed phase.[85] Another had PLA/PBAT joined with T-GMA which is a random terpolymer of ethylene, acrylic ester and glycidyl methacrylate (GMA) by extrusion, toughening the blend.[87] Besides T-GMA, ethylene-methyl acrylate-glycidyl methacrylate copolymer (EMA-GMA) has also been used.[90]

Furthermore, compatibilizers can be used to enhance the interfacial adhesion and obtain thermo-dynamically stable structure. Some examples include: toluene diisocyanate (TDI) [75], 1,3-bis(2,3-epoxypropyl)-s-triazine-2,4,6-trione (BETT) [78] and tri block copolymer of PLA-PBAT-PLA [91]. BETT is an epoxy functionalized *N*-halamine precursor with good antibacterial activity against both Gram-positive and Gram-negative bacteria and promotes a co-continuous structure of the blend.[78]

On the other hand, another way to improve flexibility, processability or foamability and mechanical and thermal properties of polymeric materials is by using plasticizers that endorse interfacial adhesion and increase compatibility between polymers and plasticizer.[23,73,92] Plasticizers used include: triethyl citrate (TEC) [75], adipate, adipic acid, glycerol ester, and adipic acid ester.[92]

Additives such as chain extenders (MDI [84] and a styrene-acrylic multi-functional oligomeric agent - Joncryl ADR-4368 [93]) counteract the thermal degradation of PLA. Its main mechanisms are random main-chain scission and unzipping depolymerization reaction.[84] *Figure 8* presents a graphic representation of the effect of chain extenders. They are generally poly-functional, thermally stable and easily available, and in polyester blends they generally contain epoxy groups that react with the OH and COO groups of the polyester end groups.[93,94] They allow to form higher molecular weight and branched polymers while, at the same time, improving the properties of immiscible blends by enhancing interfacial adhesion and phase dispersion, and also the melt strength and thermal stability. MDI contains two isocyanate groups and is highly reactive to carboxyl and hydroxyl groups while ADR contains many epoxy groups with high reactivity.[84,95]

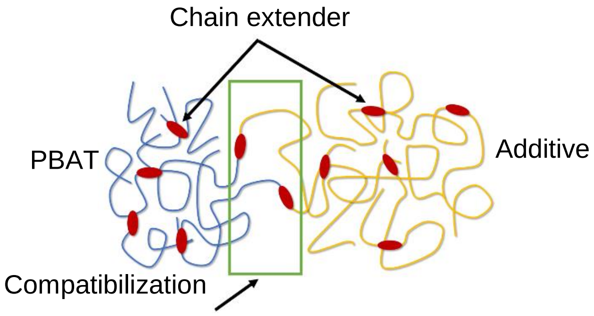

Figure 8– Graphic representation of the effect of chain extenders. Adapted from *Pan et al.* [84]

Furthermore, several researches showed that the addition of fillers or nanofillers, are one of the best ways to improve the compatibility of polymer blends.[96] Ideally when the viscosity ratio between the matrix and dispersed phases is closer and superior to one, and the interfacial tension of the blend components is low, a finer droplet morphology is expected. Alternatively, some studies have examined the combined effect of epoxy functionalized graphene (EFG) and organo-montmorillonites in PLA/PBAT blends containing 20 wt% PBAT.[96] Furthermore, graphene nanoplatelets (GNP) are expected to enhance PLA barrier properties. When comparing MMT with GNP at identical filler amount in PLA/PBAT blends, GNPs enhanced thermal stability and water vapor barrier property while decreased light transmittance by tuning the GNP loading content (0.1-1 phr). However, GNPs only worked against particular micro-organisms making MMT a nanofiller with superior antimicrobial activity.[97]

Table 17 in appendix A list some PBAT/PLA composites found in the literature along with the corresponding mechanical properties, water absorption, rheological and thermal behaviour.

1.7. Banana fiber composites

In nature, a wide variety of plants synthesize extra-cellular high-performance skeletal biocomposites that contain a matrix reinforced and held together by fibrous biopolymers that deposit in a continuous manner.[98,99] These lignocellulosic natural fibers can come from any part of the plant such as stem, root, fruit, leaves and seed and they are composed of hollow cellulose, a matrix of hemicelluloses, lignin, pectin and small amounts of organic (extractives) and inorganic (ash) components.[20,100–103]

Cellulose is the world's most abundant natural renewable biodegradable semicrystalline polymer and it is responsible for high strength, stiffness and structural stability of natural fibers.[20,101,102] Because of its chemical structure, cellulose makes intramolecular hydrogen bonds inside the cellulose macromolecule and intermolecular hydrogen bonds among other cellulose macromolecules as well as with hydroxyl groups from the air, as shown in *Figure 9*.[102,103] Meanwhile, hemicellulose is a fully amorphous branched polymer while lignin is amorphous with an aromatic structure and pectin contains complex polysaccharides.[101,102] Furthermore, organic extractives are responsible for color, odor and decay resistance whereas inorganic constituents enhance the abrasive nature of the fiber.[102]

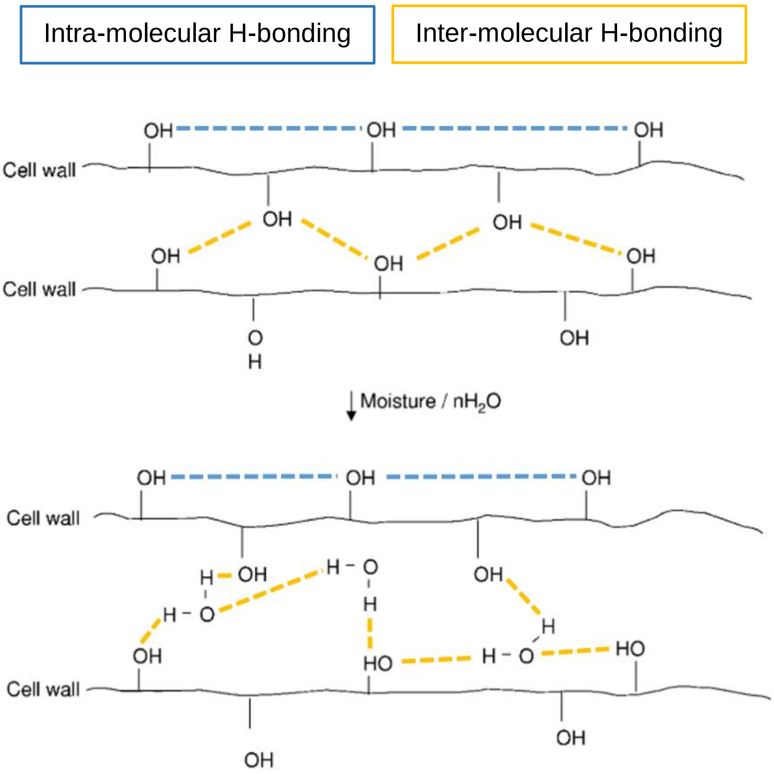

Figure 9 – Schematic representation of hydrogen bonding in natural fibers. Adapted from *A. K. Mohanty, Misra, and Drzal* [103]

The chemical constituents of natural fibers can vary in quantity according to origin (fiber type and location on plant), growth conditions, age and retting (mode of extraction of fiber from the source) process adopted. These variations in composition can influence some properties of the natural fibers. [102,103,104] *Figure 10* illustrates a schematic representation of the structure of the natural fiber along with the structural organization of the fiber cell wall.

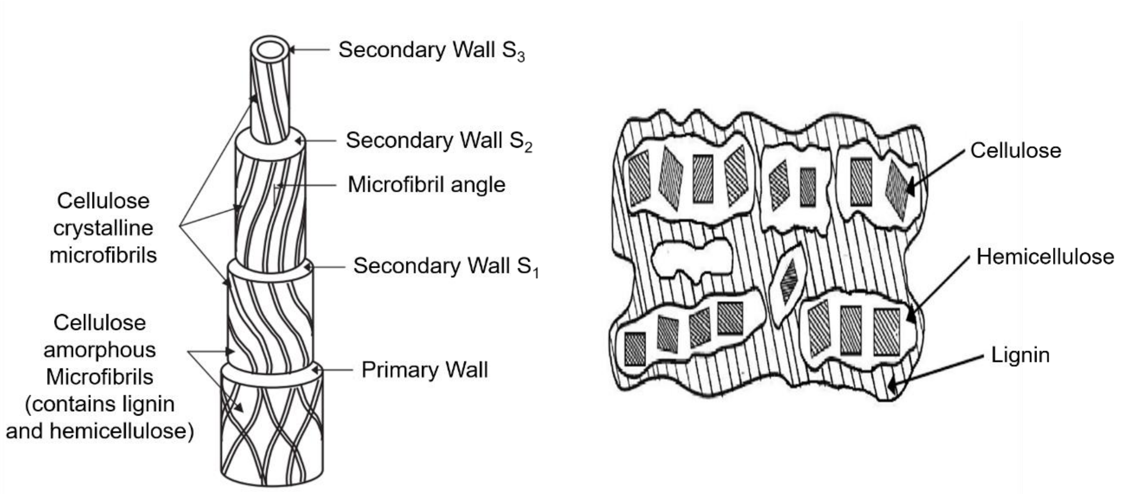

Figure 10– Structural organization of the three major constituents in the fiber cell wall [20,102]

Each fiber cell wall is comprised of a primary and three secondary layers.[102] Cellulose, the main component, and hemicellulose are laid down first and bonded through hydrogen bonds, followed by lignin and pectin that link with cellulose-hemicellulose chains and promote strength properties to the fiber by holding and cementing everything together.[20,102,103] Normally, the higher the content of cellulose and the lower the microfibrillar angle (defined as the angle between the fiber axis and cellulose microfibrils), the better strength properties presented by the fiber.[102]

Biocomposites can be composed of biodegradable polymer matrices reinforced with bio-fibers.[103] Therefore, natural fibers are a low cost environmentally friendly new generation of reinforcement/fillers for biocomposites.[103–105] They also provide additional features of eco-friendliness, renewability/recyclability, flammability, flexibility during processing, lightweight, low density, good mechanical properties and biodegradability or recovered calorific value at the end of the life cycle, making them more desired than synthetic fiber materials.[42,20,99–101,103,104,106,107] Overall, they can substitute man-made fibers like aramid fiber, or inorganic fibers such as carbon and glass fiber composites that are non-biodegradable and non-recyclable.[105,108]

Regarding natural fibers, banana fibers are of particular interest as they are the world's oldest and fourth most important food crop after rice, wheat, and maize. Traditionally, they have been used for handicrafts, ropes, doormats, in textile sector, paper making and most recently as reinforcements in polymer composite materials. [100,104,107,107] As models of banana fiber as reinforcement in PBAT composites were not found during the literature review, this project will address these blends to produce substitutional materials for PE derived plastics.

The banana plant is herbaceous and perennial belonging to the Musaceae family.[42,104,109] There are approximately 300 species, but only 20 varieties are used for human consumption.[104] It is essentially produced in subtropical and tropical countries where there is constant heat and a high degree of humidity in order for the tree to exhibit proper growth and production.[42,104,105] The banana plant consists of leaf, pseudo-stem, root and banana fruits.[107] However, even with its high availability all year round the banana trunk or pseudo-stem bears fruits only once in its lifetime, before being replaced and becoming the major portion of biomass waste, along with leaf, roots and rotten banana. It is estimated that for each hectare of banana plantation the biomass waste reaches about 220 tons, being either burned or dumped in lakes, rivers or shallow areas, causing serious environmental threats. Therefore, if reutilized and given a second life they can provide additional income to local communities and farmers while mitigating waste disposal and reducing environmental problems. [99,107,109–111] Some of these residues like banana stem juice, banana pith and banana peel have already been used in waste water treatment as absorbents, or as livestock feed and heavy metal bio-absorbents, dyes, and to eliminate phenolic compounds. Meanwhile, the waste banana stem has been used in the production of bioenergy such as biogas, and the banana fruit and residues have served as feedstock for ethanol production and as cost effective compost feedstock which reduces the use of chemical fertilizers and irrigation of crops.[105,107]

The pseudo-stem is formed of about 14 to 18 leaf sheaths wrapped around a soft central core, producing nearly 600 kg/ha of banana fiber. Bast or stem fibers are usually located adjacent to the outer surface of the leaf sheath and when cleaned and brushed might yield 80-85 % long [4-6 mm], slender [mean width 17-21 μm] fibers.[100,104] They can be extracted manually, mechanically, chemically or biologically and have different quality according to the extracted layer: (a) course fiber (outermost 2–3 sheaths) that break easily, (b) soft lustrous fiber (middle sheaths) and (c) very soft fiber (some middle and inner sheaths excluding innermost sheaths that contain pulpy matter).[42,107] *Figure 11* illustrates a schematic representation of the banana plant and the cross-section view of the pseudo-stem.

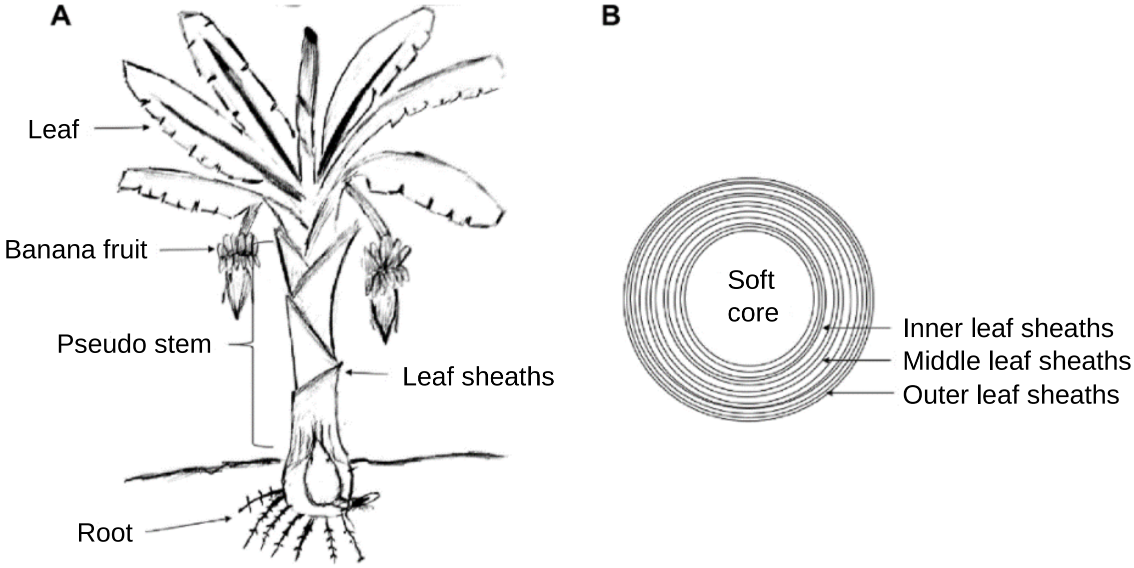

Figure 11 – Diagrammatic representation of A) banana plant; B) cross-sectional view of banana pseudo-stem [42]

Banana pseudo-stem fibers possess higher contents of cellulose, followed by hemicellulose and lignin.[106,107] Like other natural fibers, they are comparable to traditional reinforcements, owning higher values of tensile strength, flexural strength and stiffness than bamboo, sisal or coir leaf fibers.[42] Thereby, they are excellent candidates as reinforcement/fillers for biocomposites due to their high cellulose content and low microfibrillar angle (11°).[21,112–114] *Table 1* comprises a list of various data found in the literature regarding the mechanical properties and chemical composition of these fibers.

Table 1 – Comprehensive list of mechanical properties and chemical composition of banana fiber found in the literature

Density (g/cm^3)	Specific modulus (GPa)	Specific strength (MPa)	Young′s Modulus (GPa)	Elongation (%)	Tensile strength (MPa)	Initial Modulus (GPa)	
1.35	3.6-27.3	444	4.0-32.7	2.4-3.5	711-789	-	[20] a
-	-	-	27-32	3	529-914	-	[104] b
1.35	-	-	-	10.35	54-754*	7.7-20.0	[106] b
-	-	-	29–32	2-4	600–750	-	[107] b
1.35	-	-	20	5–6	550	-	[113] c

Cellulose (%)	Hemicellulose (%)	Lignin (%)	Pectin (%)	Ash (%)	Extractives (%)	Moisture (%)	
62.5	12.5	7.5	4	-	-	-	[104] b
24.19–38.34	11.00–18.96	13.78–16.36	-	8.45–8.84	4.24–4.67	6.96–12.52	[115] d
31.27	14.98	15.07	-	8.65	4.46	9.74	[116] e
60-85	6-8	5-10	2.5-4	7-21	-	-	[117] b
63–64	-	5	-	-	-	-	[113] c

*Ultimate tensile strength; a - Fiber collected from the fruits; b - Origin and section of extraction non specified; c - *Musa sepentium,* India; d - *Musa acuminata*, Guadeloupe, fiber collected from the pseudo-stem core; e - Fiber collected from the pseudo-stem

The fiber-matrix interface is a reaction zone where two phases are chemically and/or mechanically combined and it dictates whether the composites possesses adequate mechanical properties.[20,102] However, when natural fibers are joined with polymeric matrices there is a lack of proper adhesion/coupling that stem from the differences in hydrophilicity/hydrophobicity and can cause ineffective stress transfer.[20,102,103] The inherent hydrophilicity of the fibers comes from high amounts of hydroxyl groups and high moisture absorption credited to the lignocellulosic content.[101,108] Furthermore, they also possess a great variations of properties, lower durability, poor wettability and thermal instability (generally natural fibers tend to degrade at about 240ºC).[21,102,104,106] Even so, some authors reported a slight increase in the degree of crystallinity and elongation at break of the LDPE-based biocomposites with untreated fibers. Meanwhile, higher values of tensile strength and Young´s modulus were obtained with untreated fibers and LDPE-g-MAH.[118] Furthermore, in an attempt to upcycle LDPE and banana fiber into affordable eco-friendly building product, no treatments or compatibilizers were used. When lengthening fibers to 20 cm and increasing its content to strengthen and stiffen the material, a better dispersion was attained along with an increase in tensile strength.[111]

Yet, in order to enhance interfacial bonding with a polymer matrix and reduce moisture uptake, fibers can be surface treated using physical or chemical treatment techniques with the addition of compatibilizers like maleic anhydride-grafted polymer and reactive fillers, thus improving strength and hydrophobicity of the materials.[106,110] [20,21,105] The chemical treatment method involves modification of the fiber surface by exposing more reactive groups through the activating of hydroxyl groups or introducing new moieties, and also removing materials responsible for the incompatibility. Thereby, it provides an efficient coupling with the matrix maximizing the interfacial strength, the stress transferability in the composites and thermal stability.[20,101,102] Such methods include silanization, alkalization (mercerization), acetylation, benzoylation, acrylation and acrylonitrile grafting, etc.[20] However when scaling these treatments to industrial applications it is always important to consider the cost as well as the disposal of the used chemical products. The following figure schematizes a summary of some of the most used chemical treatments stated in the literature.

Figure 12 - Schematic overview of chemical treatments and hypothetical models of interface of banana fiber [101,103,106,119]

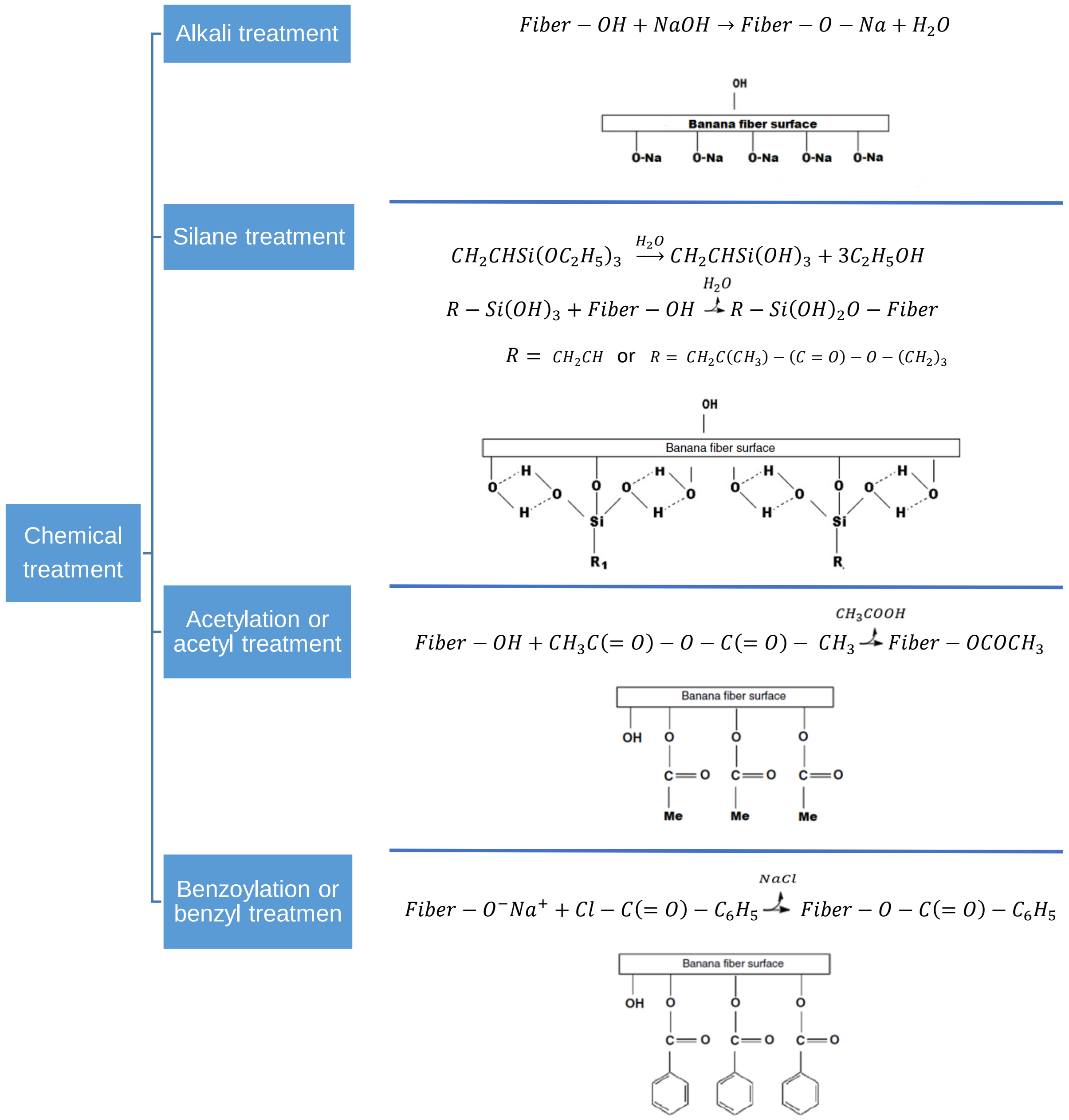

Regarding the literature review, it will mainly focus on alkali treatment since it was the chemical treatment used in this work.

Alkali treatment or mercerization using sodium hydroxide is one of the most effective and economical technique used for treating natural fibers. It directly influences the cellulosic fibril, the degree of polymerization and the extraction of lignin, pectins, waxes and oils, present in the external surface of the cell wall as well as hemicellulosic compounds, as shown in *Figure 13*. Overall, it will disrupt hydrogen bonds in the network structure and depolymerize cellulose further exposing the short length crystallites while also changing its orientation forming amorphous regions. Furthermore, with the removal of hemicellulose the interfibrillar region decreases its density and rigidity, thus the fibrils are more likely to rearrange themselves in the direction of mechanical loads. Thus, this treatment is responsible for an increase in surface roughness and increase in the number of possible reaction and bonding establishment between the fiber surface and the polymeric matrix. It also allows for a decrease in micro voids, reduction of the hydrophilicity and water absorption of natural fibers which leads to better mechanical interlocking between fibers and matrix, providing better mechanical and thermal properties and improves the stress transfer capacity. However, if the alkali concentration is higher than the optimum condition, the excess delignification of the fiber can take place, which results in weakening or damaging the fibre.[101–103,106,110] *Motaleb, Mizan, and Milašius*, studied three types of non-woven materials fabricated through wet laid web formation from different parts of the bark of the banana tree (outer, middle and inner bark). All fibers were extracted chemically with 15% sodium hydroxide and the outer bark non-woven material showed the highest mechanical properties with high values of tensile strength, elongation at break and Young´s modulus. Inner bark nonwoven showed the lowest results.[108]

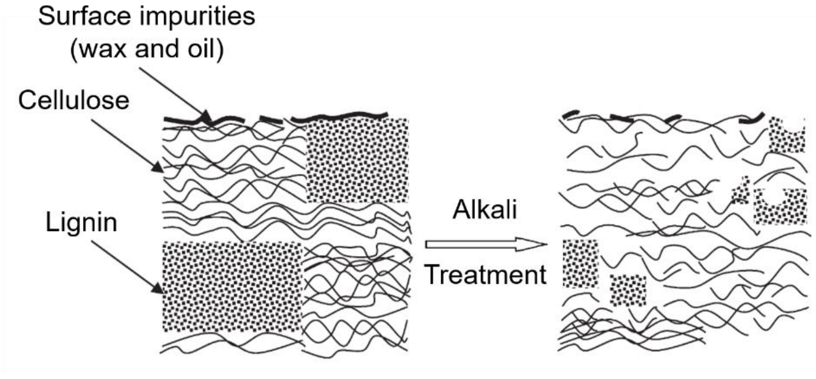

Figure 13 – Schematic representation of the structure of raw and alkali treated natural fiber. Adapted from *Kabir et al.* [102], *A. K. Mohanty, Misra, and Drzal* [103]

Meanwhile, another technique to improve mechanical properties, storage modulus, glass transition temperature and reduce water absorption of the composites is acrylic acid treatment. In this case this method reduces the hygroscopicity of the natural fiber.[110] When comparing both chemical treatments in blends of LDPE/fiber/LDPE-g-MAH, *Prasad et al.* found that biocomposites with acrylic acid fiber treatment showed the most effective improvement in the flexural and impact strength and also exhibited a reduction in the water absorption capacity. Moreover, 25 wt% of fiber was deemed the optimum content on the basis of biodegradability and mechanical properties.[110]

In what regards silane based treatments, silane undergoes hydrolysis reactions generating silanol species ($Si - OH$) in the presence of humidity/moisture, which react with hydroxyl groups belonging to cellulose forming stable covalent bonds that are chemisorbed onto the fiber surface. This reduces the hydroxyl groups at the fiber-matrix interface. Meanwhile, the hydrocarbon chains restrain the swelling of the fiber by creating a crosslinked network due to covalent bonding between the matrix and the fiber. Overall, it enhances the adhesion and thus improves the strength of the fiber.[101,106] *Pothan et al.* studied the fiber/matrix interactions of blends containing 40 wt% chemically modified with either NaOH, acetylation or silane treated fibers with 30 mm length prepared by compression molding. Even though silane A174 (γ-methacryloxypropyl trimethoxy silane) presented a more pronounced improvement in mechanical properties of the composites, reflected in the increase of the storage modulus value at high temperatures, NaOH also had positive effects. Furthermore, fibers treated with silane A174 also presented higher shifts in the loss modulus curve and maximum lowering of tan δ peak.[120,121]

Additionally, in acetyl treated fibers a esterification reaction takes place and plasticizes the cellulosic content. This promotes hydrophobicity, dimensional stability and compatibility of the biocomposite. It can also improve the resistance to biological attack and photo degradation. However, since acetic acid (CH_3COOH) is generated as a by-product, it must be removed from the lignocellulosic material before the fiber is used.[101,103,106]

Finally, in benzyl treated fibers benzoyl chloride, that contains benzoyl ($C_6H_5C = O$), is used to substitute hydroxyl groups to benzoyl groups. Once again this treatment will decrease the hydrophilic nature of the fibers and enhance the adhesion and compatibility of the biocomposite thereby considerably increasing the strength while decreasing the water absorption and improving the thermal stability.[101,106]

Table 18 list the few Banana fiber/LDPE composites found in the literature along with the corresponding mechanical properties, water absorption, rheological and thermal behaviour.

Chapter 2: Materials and methods

This chapter will present the detailed description of the materials, methods and processes used for the production of the PBAT/banana fiber powder composites. It is divided into three subsections: materials, methods and characterization techniques. A review of the literature was carried out in order to uncover the best methods for fiber extraction, fiber treatment and extrusion of PBAT/natural fiber composites, since no articles were uncovered for composites of PBAT/banana fiber. The research boundary starts with the harvesting of the banana trunks and handling of the material. In order to obtain the composites, the fibers were extracted from the pseudo-stem, dried, grinded and subject to carefully designed treatments, and blended, by extrusion, with PBAT pellets with different powder loadings. Fibers and fiber powders were characterized before and after treatment by scanning electron microscopy (SEM), optic microscopy, Fourier transform infrared (FTIR) spectroscopy and thermogravimetric and derivative thermogravimetric analysis (TGA/DTG) to analyze the chemical, morphological and thermal structure changes. For the composites, first an optimization was performed for the extrusion profile (parameters: heating temperatures, screw speed, spooling and wending velocities) and after obtaining the extrudates these were evaluated by scanning electron microscopy (SEM), Fourier transform infrared (FTIR) spectroscopy, thermogravimetric and derivative thermogravimetric analysis (TGA/DTG), water adsorption, dynamic mechanical analysis (DMA) and tensile tests. Samples were prepared to be tested by these two latter techniques.

2.1. Materials

Untreated and alkali treated banana fiber powder along with PBAT were used in this thesis to produce eleven different composites. The powders were prepared from the grinded fibers of matured banana plants supplied by local farmers in Barrocalvo, Leiria and Sobreiro, Mafra. *Figure 14* shows the pseudo-stem received with an average trunk length between 49 and 104 cm. A sample of PBAT was kindly supplied by Cabopol S.A. and sodium hydroxide (NaOH) was purchased from Panreac (reagent grade pellets). The supplier of PBAT did not have a technical data sheet for the material but was able to provide the marketing name: PBAT A400, from Kingfa (Ecopond). Moreover, cutting instruments (knives and spatulas), sieves, aluminum trays (to use in ovens), plastic containers and standard laboratory equipment were also frequently used.

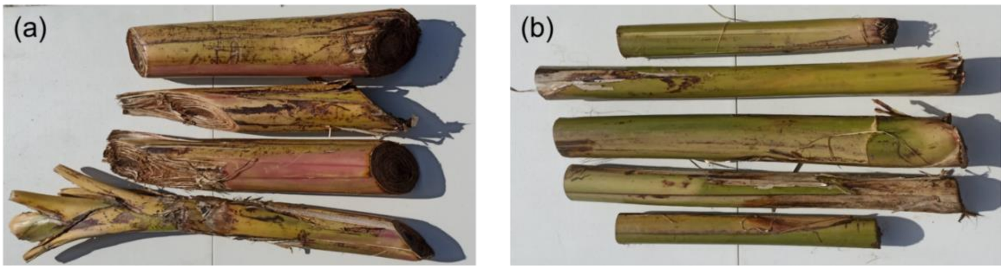

Figure 14 - Pseudo-stem from (a) Barrocalvo, Leiria and (b) from Sobreiro, Mafra

The tools used can be divided into three categories: processing, material characterization and software. The complete list of materials by category is presented in *Table 2*. Processing involves the most important equipment used for the preparation of the composites while characterization shows the equipment handled for determining the chemical composition, thermal behavior analysis, thermo-mechanical properties, imaging and mechanical analysis of the composites. Lastly, regarding the software category, three main programs were used for writing, data logging and analysis. *Figure 15* shows the processes followed to obtain the composites along with the characterization techniques used.

Table 2 - List of most important equipment used in the laboratory work

Equipment Category	Equipment
Processing	Pelletizer (Brabender)
	Oven (Nahita, model 631 Plus)
	Injection moulding (Ray-Ran)
	Mini extruder (3Devo® composer 450 desktop)
	Cryogenic impact mill (SPEX SamplePrep 6770 Freezer/Mills)
	Cutting mill (Reisch SM2000)
	3D Printer (Creality CR-5 Pro)
Characterisation	FTIR-ATR (Perkin Elmer, Spectrum Two)
	SEM (ThermoFischer Scientific, Phenom ProX G6 benchtop SEM)
	DMA (TA Instruments DMA Q800)
	TGA (Hitachi STA7200)
	Microscope with digital head
	Universal testing machine (Hounsfield)
	Water absorption
Software	Microsoft Office 2013
	OriginPro 2016
	TA Universal Analysis 2000

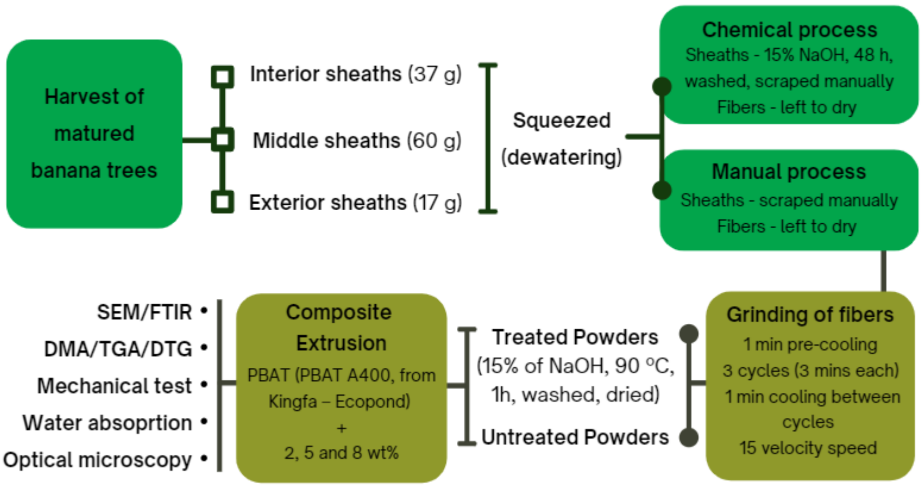

Figure 15 - Overview diagram of the processes and materials for the experimental phase

2.2. Methods

2.2.1. Tree segmentation and fiber extraction

Banana tree was separated in three groups (1) outer sheath (2) middle sheath and (3) inner sheath of the pseudo-stem in order to make three categories of composite materials. Layers were sorted one by one and cut into strips of about 90-100 cm length and 30 cm wide. After separation all sheaths were squeezed with a car wheel for dewatering. This step allows to reduce the moisture content up to 45-50%.[100] Two processes were employed for the extraction of banana fibers i) manual process and ii) chemical process.

2.2.1.1. Manual extraction of fibers

The sheaths were combed/scraped manually against a plastic board until a silky white color fiber was obtained with the minimum residual bark attached. Strip from the inner sheaths took less time to extract (around 15 mins per strip) while strips from the outer sheaths took the longest (around 20 mins per strip). After extraction, fibers were left to dry overnight.

2.2.1.2. Chemical extraction of fibers

Sheaths from the middle section were dipped in a solution of 15% NaOH for 48h. Afterwards they were washed with distilled water to make them free from alkali and other components and combed until a yellow color fiber was obtained with the minimum residual bark attached. They were left to dry overnight.

2.2.2. Fiber powder preparation

After obtaining the fibers, those were transformed into powders, by grinding within liquid nitrogen. Fibers were grinded in a cryogenic impact mill with the program set to 3 cycles (3 mins each), 1 min pre-cooling followed by 1 min interval between cycles at 15 velocity speed. *Figure 36* in appendix B shows the cryogenic impact mill apparatus.

2.2.3. Fiber powder alkali treatment

Chemical treatment of fiber powders were performed to improve the adhesion strength of the interface fiber/PBAT and to remove the wax and other organic compound from the fiber powders´ surface. The powders were immersed and treated with 15% of NaOH with a temperature of 90 °C for 1 h until they become yellowish. To control the temperature of the reaction, the solution was previously heated to 90 ºC in a parafine bath and only after were the powders added to the solution. To maintain the temperature the lid was partially closed. Afterwards, the boiled mixture was kept aside for 30 min to cool and was further rinsed with distilled water to carefully remove sodium hydroxide and other components. This allows to remove all the unwanted materials. Finally, the treated powders were left in an air oven at 60ºC until they were fully dried. Interior, exterior and middle treated powders took 2, 3 and 7 days, respectively.

2.2.4. Composite preparation and extrusion

Treated and untreated fiber powders were joined with PBAT pellets, at 2, 5 and 8 wt%, to produce eleven composites with the help of the single screw, mini extruder from 3Devo®. Both PBAT pellets and powders were dried in an air oven at 60ºC overnight, before extrusion. *Table 3* shows all the composites prepared in this study along with the pseudo-stem of origin of the extracted fiber. Throughout this thesis composites will be named according to the powder content (number) followed by sheath extraction origin (interior, exterior or middle) and if treated will present a big "T", as shown in the following table.

Table 3 – Composites of PBAT and its respective fiber percentage and origin

	Fiber percentage					
PBAT	**2 wt%**		**5 wt%**		**8 wt%**	
	Interior Untreated [a]	2I				
	Interior Alkali Treated [a]	2IT				
	Middle Untreated [a,b]	2M	Middle Untreated [a,b]	5M	Middle Untreated [a,b]	8M
	Middle Alkali Treated [a,b]	2MT	Middle Alkali Treated [a,b]	5MT	Middle Alkali Treated [a,b]	8MT
	Exterior Untreated [b]	2E				
	Exterior Treated [b]	2ET				

a – Sheaths from pseudo-stem (a) from *Figure 14* ; b - Sheaths from pseudo-stem (b) from *Figure 14*.

All extruders possess a barrel which runs from the hopper to the die. The screw located inside the barrel, is the most important element of this equipment and is designed to pick up, mix, compress, and move the polymer as it changes from solid granules to a viscous melt. In order to do so its geometry varies along the length.[23] The screw is generally made up of the following sections: the feed section (solid conveying zone), the compression section (plasticating or melting zone), and the metering section (melt flow).[23,122] The mini extruder used for this thesis was the single screw 3Devo® composer 450 desktop with a 4 heated zone screw. The parameters optimized for the extrusion profile include: screw speed (3.9 or 4.1 rpm), wending velocities (25, 35 or 42%) and heating temperatures (140-147-(152/155)-(156/159). Diameter control (puller) and spooling were automatic. The diameter chosen for the extrudates was 1.75 mm. *Figure 37* in the appendix shows the 3Devo® composer 450 desktop apparatus. In order to perform the mechanical tests and dynamic mechanical analysis tests on untreated and treated banana fiber powder/PBAT composites, tensile test specimens had to be prepared with the aid of an injection molding desktop machine. The filaments were pelletized in order to obtain small sized pellets and introduced in the machine. The barrel temperature was set to 150ºC while the bed was set to 80ºC. Five specimens were produced for each composite to be tested for tensile tests.

2.3. Characterization techniques

For material characterization several equipment and techniques were used. These include fourier transform infrared (FTIR) spectroscopy, scanning electron microscopy (SEM), thermogravimetric and derivative thermogravimetric analysis (TGA/DTGA), for fiber, fiber powders and composites, and dynamic mechanical analyses (DMA), mechanical testing and water absorption for composites. All relevant micrographs and spectra are presented in the Results and Discussion section.

2.3.1. Fourier transform infrared (FTIR) spectroscopy

Fourier transform infrared spectroscopy of treated, untreated fibers, fiber powder and composites was carried out with a Perkin Elmer, Spectrum Two, FTIR spectrometer equipped with an attenuated total reflection, UATR Two, accessory. The spectra were collected at 4 cm^{-1} resolution, in the range of 4000 to 400 cm^{-1}, using eight scans of data accumulation. The samples were heat treated overnight at 60ºC before the acquisition of the IR data.

2.3.2. Scanning electron microscopy (SEM)

Scanning electron microscopy (SEM) photos and EDS data were used to investigate the banana treated and untreated fiber surface, the morphology of the different types of composites (filler/matrix interface) and the banana treated and untreated fiber powders. These were obtained using a Phenom ProX G6 benchtop SEM (ThermoFischer Scientific, Waltham, MA, USA). The composites were frozen under liquid nitrogen, fractured immediately after freezing, mounted and coated with A 15 nm layer of gold-palladium before observation using a turbomolecular pumped coater Q150T ES (Quorum Technologies, Lewes, UK). Micrographs of each specimen were taken at various magnifications.

2.3.3. Mechanical test

The mechanical behavior was studied using a Hounsfield universal testing machine with a load cell of 2000 N. Tests were performed according to ISO 527-2:2012. Experiments were performed with a cross head speed of 10 mm min^{-1} at room temperature, 25 °C. First, each specimen was measured for its relevant dimensions (3 regions: width, depth and length) with a calliper (Mahr Type 16ER). After placement of the test specimen in the clamps, a tension was applied until the fracture of the material took place. The force is recorded as a function of the increase in gauge length. During the application of tension, the elongation of the gauge section is recorded against the applied force. Five stress-versus-strain graphs were generated and plotted to obtain the tensile test parameters (modulus of elasticity, tensile strength and elongation at break) and respective average and standard deviation values. The relevant equations for the determination of these parameters are provided below. The stress is given by:

$$\sigma = \frac{P}{A_0} \tag{1}$$

Where σ is the stress (MPa), P is the load (N) and A_0 is the initial cross section area (m^2). It provides measurements of strength, stiffness and resistance to stretching of the material. The strain is calculated with the equation:

$$\varepsilon = \frac{L - L_0}{L_0} = \frac{\delta}{L_0} \tag{2}$$

Where ε is the strain (no dimension), L_0 is the original distance between gage marks (mm), L is the distance between gage marks at any time (mm) and δ is the displacement (mm), or increment of distance between gage marks. Elongation within the elastic regime is defined as the ability of a material to resist to a distorting stress and to return to its original size and shape when said stress is removed. To determine Young's modulus (or modulus of elasticity), *E* (GPa), Hooke's Law was used:

$$\sigma = E\varepsilon \tag{3}$$

The modulus of elasticity is determined by finding the linear region of the stress-strain curve and doing a linear regression on that set of points. This value designates the specimen stiffness and resistance to elongation in use. The yield strength σ_y is the stress at which a material exhibits a specified limiting deviation from the proportionality of stress to strain (Hooke´s Law). It is determined by visual inspection and by the 0.2% offset method.

2.3.4. Dynamic mechanical analysis (DMA)

The TA Instruments Q800 Dynamic Mechanical Analyser (DMA) was employed for dynamic mechanical property evaluation of the composites. Samples of similar dimension were cut from unused tensile test specimens and used for testing. All sizes were measured with a calliper (Mahr Type 16ER). Before insertion in the machine the adequate sample holder was mounted. *Table 19* in appendix C shows all the dimensions of the specimens used. Testing temperatures ranged from -50 to 100 ºC and the experiments were carried out at frequencies of 1 Hz, 15 µm, at 2ºC/min.

2.3.5. Thermogravimetric and derivative thermogravimetric analysis (TGA/DTG)

Thermogravimetric and derivative thermogravimetric analysis (TGA/DTG) of middle untreated and treated powders and composites were carried out using Hitachi STA7200 thermal analysis system to analyze the thermal stability of the samples. The weight of the samples varied significantly from approximately 1 to 13 mg. Heating scan of 10°C/min from 30 to 600°C was applied and the % residual mass and decomposition temperature were measured under nitrogen atmosphere. The samples were placed in an open aluminum 5 mm diameter (600 ºC máx.) crucible for testing. Values for the onset degradation temperature and peak temperature were determined from the derivative TGA curves.

2.3.6. Water absorption

Moisture absorption test is used to study the water absorption behavior of the composite. This was determined by immersing pre-dried samples with various sizes, cut directly from the composite extrudates, in distilled water at room temperature. The thickness and length of each sample was measured and is shown in *Table 20* in appendix C. Five samples were tested for each composite. At specific time intervals (2, 5 and 8 days) the samples were removed from water, carefully blotted to remove the excess water on the surface, and immediately weighed using digital balance. The water absorption (WA) percentage is calculated with the following equation:

$$WA = \left[\frac{m - m_0}{m_0}\right] \times 100\% \tag{4}$$

Where m_0 (mg) and m (mg) are the sample weights before and after the immersion in distilled water at a specific time interval, respectively.

2.3.7. 3D printing

The 3D print of a bunny was conducted with a Creality CR-5 Pro, with a printing temperature of 190 ºC and a build plate temperature set to 80 ºC. The infill density was programed to 20% and the fine as 0.1 mm.

Chapter 3: Results and Discussion

This section will be divided into two subsections: fiber and fiber powder; PBAT/banana powder composite. Results will be presented along with the discussion for better understanding. Each subsection will present the main method used for the samples preparation and the analysis on the chemical and morphological structure (scanning electron microscopy (SEM); optical microscopy; Fourier transform infrared (FTIR) spectroscopy), the thermal behavior analysis (thermogravimetric and derivative thermogravimetric analysis (TGA/DTGA)), thermo-mechanical properties analysis (dynamic mechanical analysis (DMA)), mechanical testing and water absorption analysis.

3.1. Fiber and fiber powder

The goal of the project consisted in developing and characterizing a high end value product made of PBAT, a biodegradable polymer and agro-food waste left over from the banana production.

The first stage aimed at obtaining the adequate materials for the composite. In order to acquire the polymer, several international companies were contacted, i.e. BASF and three Chinese companies, and due to either a lack of response or overpriced budgets, mainly due to transportation costs, these were discarded as possibilities. Recently we found that B-Plast 2000® is a company that supplies PBAT from BASF, at 880 euros per 50 Kg of PBAT. In this work, PBAT was kindly supplied by Cabopol S.A., which is one of the biggest European companies that produces thermoplastics located in Leiria, Portugal, and works with our group in a partnership. Regarding the natural fibers, five Indian companies, one Brazilian and two in Madeira were reached out to and all but two Indian and the Brazilian company did not respond. Madeira was the ideal option since it is an archipelago belonging to Portugal and presents a prosperous climate for banana cultivation. This fruit has been a staple of this region for many years, being produced with high quantity and quality due to high temperatures (monthly average between 24ºC to 29ºC) and a moderate humidity all year round.[123] Initially the goal was to create a partnership with local companies or businesses that could make an indirect link to production. This could help the local economy by increasing the income on an otherwise waste and help with the reduction of the greenhouse gas emissions from the disposal of the pseudo-stems. However, in spite of big efforts developed with some companies based in the island, the materials never came through.

Considering that the banana plant can have a satisfactory growth in climates where temperatures can range from 15ºC to 35 ºC,[123] the pseudo-stem samples used where donated by local farmers from Barrocalvo, Leiria and Sobreiro, Mafra regions, as these natural resources are surprisingly abundant and available in continental Portugal.

According to the literature fibers can be extracted in several different ways. One of the easiest and less labor intensive method is through mechanical extraction with a mechanical decorticator. This machine is comprised of a rolling drum with blades positioned on its circumference (scrapper roller) that when in motion create a beating action. When the sheaths are inserted through the squeezing feed rollers the pulp gets separated and fibers are extracted. This process has a capacity to extract around two tonnes of dry fiber per day.[42,116] *Figure 16* illustrates this machine and its apparatus. Nevertheless, no such equipment (or similar equipment) was found in the facilities used for this project nor in other potential companies in the regions where the banana pseudo-steam were obtained. Therefore, the options were to either grind the full bark in a cutting mill (Reisch SM2000) or do the manual extraction of the fibers.

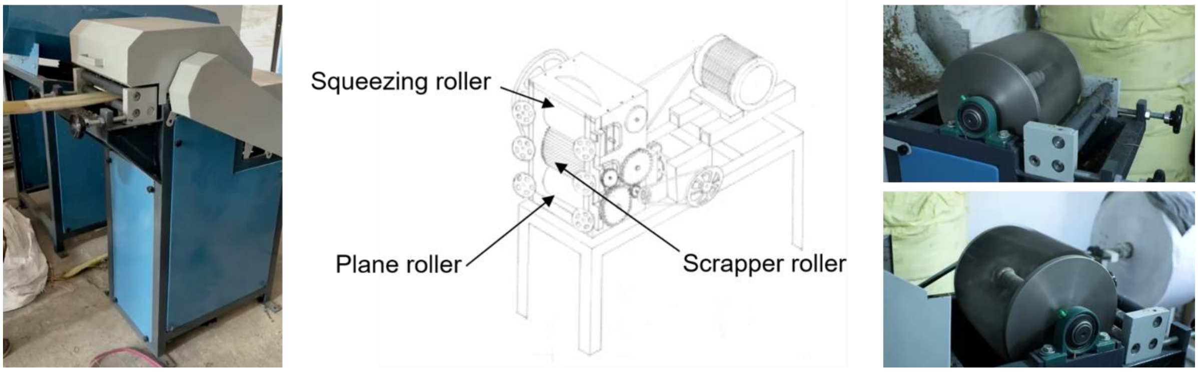

Figure 16 – Mechanical decorticator that extracts banana fiber and its apparatus. Adapted from *Mukhopadhyay et al.* [116]

The first trial included the grinding of the full bark where exterior and interior were separated. Exterior grinded bark was alkali treated with different concentrations to examine the results as a potential reinforcement/filler for the PBAT composite. Even though the chemical composition of the full grinded bark is similar to the raw extracted fibers (*Figure 38* in appendix D), no visible or clear tendencies were revealed in the FTIR spectra to proceed with these materials. Therefore, the second option was considered and fibers were manually extracted and treated for further studies.

Manual extraction, or stripping, is an extremely inefficient and impractical practice that requires continuous attention, a lot of physical work and is slower than the mechanical extraction.[42,107] This process required the use of knives and spatulas for extraction of fibers.

First, the trunk is cut along the intersection (core) into four pieces. Afterwards, the sheaths are manually sorted into their specific groups (inner, middle and outer sheaths). Even though this cataloging is essentially subjective as no guidelines where uncovered from the literature, the sheaths did present different intensities in coloring of the outer surface, dark green and dark brown, to a yellowish green shade, assisting the process. Regarding the structure of the bark it is mainly composed of two sections that need to be extracted to reach the fiber. These include an interior section that confer a robust structure to the sheath while the outer surface is extremely hard and tough. However, as you move towards the inner most layers the hardness of the outer surface decreases and becomes easier to remove. Furthermore, the fibers extracted from sample shown in *Figure 14* (b) of the banana trunk were easier and, therefore, faster to obtain as the trunk had less layers, presumably due to a lower maturity of the plant, than the sample shown in *Figure 14* (a).

The extraction of the fibers begins by squeezing the sheaths to remove excess water. This will also promote the cracking/breaking of the interior section that becomes fragile and is easily removed. Then comes the scraping of the outer surface where the fibers lie.[100,104] In case of chemical extraction after squeezing, the sheaths are dipped in a 15% sodium hydroxide solution for 48 hours and further scraped as previously described. *Figure 17* shows all the steps mentioned and a schematic representation of the cross section of a sheath with the respective sections. Another important issue to consider is the waste generated with this extraction as the interior section and the outer surface have no useful purpose. A very low percentage of the bark actually contains fibers, therefore biomass generated could be used for compost.

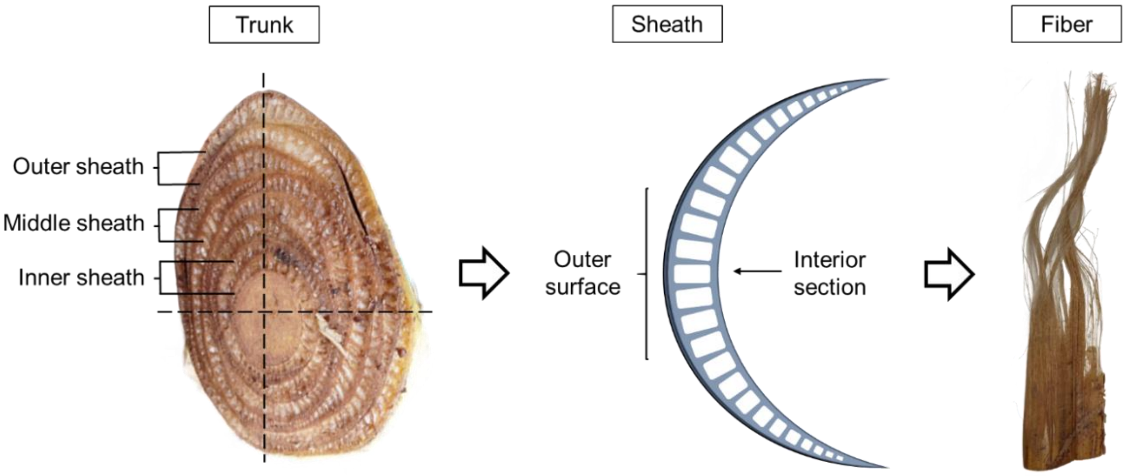

Figure 17 – Steps for the manual extraction of fibers and a schematic representation of the cross section sheath and morphology

After approximately four to five weeks' worth of intense labor, 37 g of inner fiber, 60 g of middle fiber and of 17 g of outer fiber were obtained from the banana pseudo-stem trunks. Fibers have a hair like texture and a characteristic smell. Furthermore, when comparing the chemical composition (FTIR spectra) of fibers obtained from the two different banana pseudo-stem trunk (*Figure 38* in appendix D) it can be seen that they have similar characteristics.

Banana fiber and fiber powders were alkali treated to promote a better compatibility with the polymer matrix by reducing the hydrophilicity and water absorption of natural fibers while preserving the mechanical properties of cellulose. These fibers were evaluated structurally, chemically and thermally.

3.1.1. Fiber powder preparation

After extraction, the fibers were grinded into small particles to be used as reinforcement/fillers for the PBAT composite to be prepared in the mini extruder. Their size could not exceed 500 μm. Once again the cutting mill (Reisch SM2000) was tested to grind the fibers. However, this task was unsuccessfully as the fibers were too light and did not enter the feed section even with the aid of liquid nitrogen. Even though no literature was found for the use cryogenic laboratory mill, this equipment was tested for grinding, with successful results and, therefore, remained unchanged for the rest of the process. This machine cools samples to cryogenic temperatures, and pulverizes them by magnetically shuttling a steel impactor back and forth against two stationary end plugs.[124] The integrity of the content is maintained and key aspects are preserved as the vials stay closed and are immersed in liquid nitrogen for the whole process. Two types of vials were used, one with metal and another with polycarbonate blunt and flanged end-plugs and impactor. Even though the metal vials had longer waiting period for defrosting and therefore were used less (two runs per hour on average), they could carry a bigger load for grinding and presented almost no loss of material. Meanwhile the plastic vials could do more runs per hour (four runs on average) but grinded a smaller load and, with excessive use, created a small gap between the cylinder and the blunt end-plug leading to loss of material (loss of 4%). *Figure 18* shows a schematic representation of the steps followed to transform fiber to fiber powder.

Fibers were separated into bundles/groups of either 1 g or 0.5 g (on average) to insert in the grinding metal or polycarbonate vials, respectively. To load it properly, first the blunt end-plug was pushed into a center cylinder, then came the bundles of fiber and the impactor, finally the flanged end-plug was fitted to close the vial. To make sure that the impactor has room to move back and forth the vial were shaken before inserting into the mill. The lid was unlatched and raised to first fill the chamber with liquid nitrogen until the fill mark (4.5 cm below the lip of the tub) and then the vials were inserted in the circular hole in the coil housing. If there is no vial in this region, the yoke will automatically drop. Otherwise, if it is closed, the toggle is pulled outward to open the yoke. Furthermore, it is also important to make sure that the yoke is moving freely for proper closing and opening of the upper section of the mill. The lid is closed slowly to avoid splashing of the liquid nitrogen, the latch is engaged and the grinding program is run. Then the process is repeated as many times necessary. If the vials are not opening properly an extractor from the vial opener set can aid in this regard.

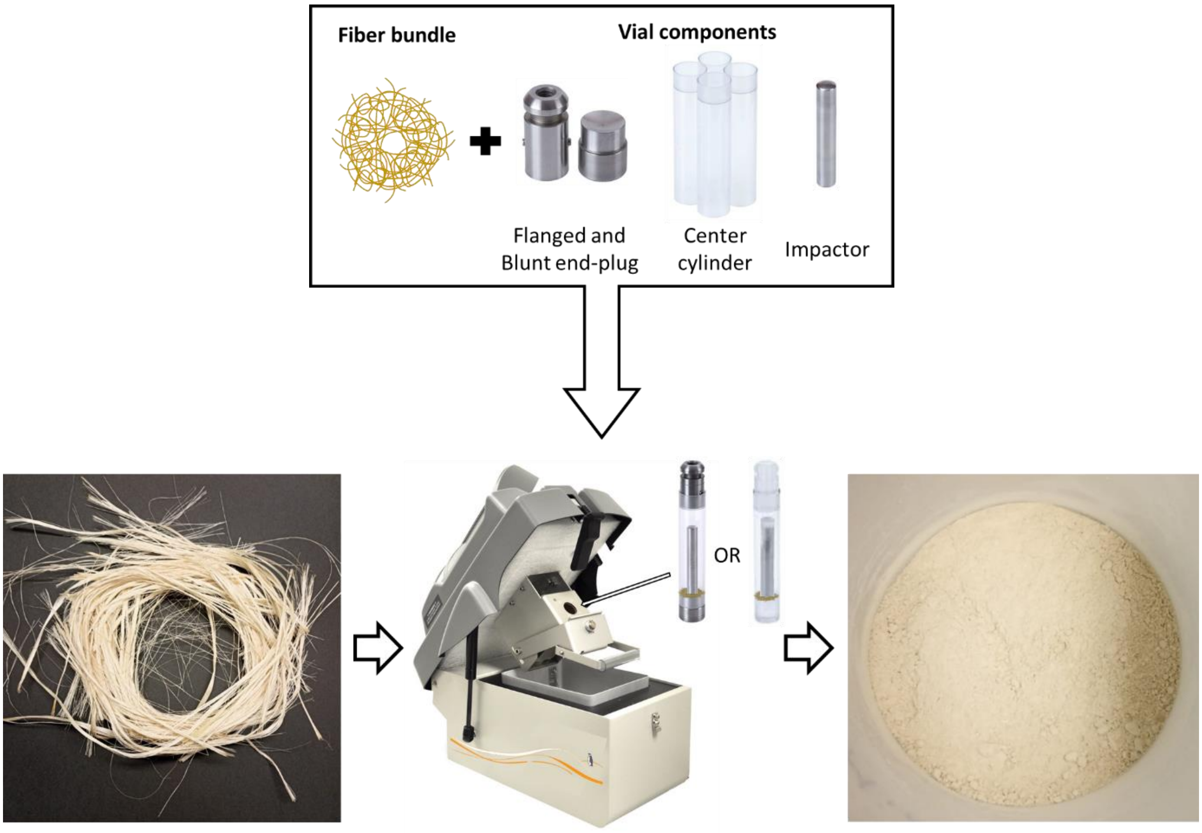

Figure 18- Schematic representation of the steps followed to transform fiber to fiber powder [125,126]

3.1.2. Chemical and morphological structure

FTIR spectroscopy was used to obtain information regarding the presence of the functional groups in the fiber and fiber powder samples and evaluate the efficiency of the alkali treatment. By irradiating samples with infrared light certain chemical bonds will vibrate to specific wavelengths. These changes in vibration are detected and translated from an interferogram to spectra by Fourier series. The

FTIR spectra obtained span across the range 4000 - 400 cm^{-1} (mid-IR). The most important regions are located in the 3550 – 1600 cm^{-1} and 1500 - 400 cm^{-1} range (fingerprint region). For the peak assignment and analysis several articles were selected from the literature and used for comparison. Not all articles specifically studied the banana fiber but did analyze other lignocellulosic fibers which have similar chemical composition. The ones that used fibers as reinforcement/fillers did not transform them into powders. *Table 4* summarizes the peak assignment in agreement with the literature.

The FTIR spectra of untreated and treated fibers are shown in *Figure 19* (a-b) and *Figure 20* (a-b). The main components of the lignocellulosic fiber are cellulose, hemicellulose, lignin and pectin which are predominantly composed of alkanes, esters, aromatics, ketones and alcohols, with different oxygen-containing functional groups.[98] All the data attained followed the same carefully drying process (overnight drying in over at 60 ºC) of the samples prior to the spectra acquisition, however the water adsorbed in the cellulose molecules is very difficult to extract due to the cellulose–water interaction.[98]

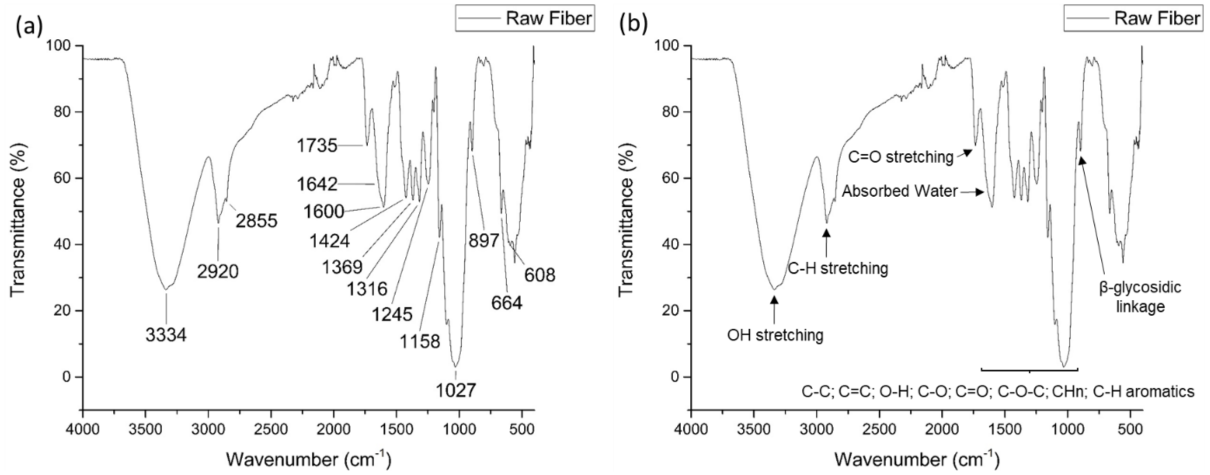

Figure 19- FTIR spectra of (a) raw manually extracted fiber and (b) the absorbance peaks of interest for banana fiber

Table 4 – FTIR spectra peak list of raw banana fiber with absorption, assignment and references from the literature for comparison

Absorption (cm^{-1})	Assignment	Refs
3334	O-H stretching vibrations	108,127–131
2920	C–H stretching vibration	108,127–130
2855	C–H stretching vibration	127,131
1735	C=O stretching	98,128,132128132130
1642	O–H bending vibrations	98,108,128,131
1600	C=O or C=C stretching vibration	133
1424	CH_2 symmetric stretch/bending, Methyl C–H asymmetric and wagging medium deformation, bending vibrations of the C–H and C–O groups of the polysaccharides rings	98,108,131,133
1369		
1316		
1245	OH in-plane bend	108

Absorption (cm^{-1})	Assignment	Refs
1158	C–O–C and C-O stretching vibration	108,128,131
1027	C–C stretching vibration	98,108,128
897	β-glycosidic linkage	127,132,134
664	out-of-plane bending vibration of intermolecular H-bonded O-H group	127,133,134
608		127,133,134

Figure 19 (a-b) shows the IR spectra of raw fiber and its peaks of interest. The broad absorption band in the 3550-3200 cm^{-1} (3334 cm^{-1}) region is ascribed to the stretching of OH groups, associated with the hydrophilic tendencies of the banana fibers due to their main lignocellulosic component, cellulose.[100,127,128] Other typical absorption peaks can be seen at around 2920 cm^{-1} and 2855 cm^{-1} for C-H stretching vibrations of cellulose and hemicellulose polysaccharides and aliphatic moieties in lignin.[108,127–131] Meanwhile the band at 1734 cm^{-1} indicates the presence of C=O stretching of carbonyl groups (>C=O) from acetyl and uronic ester groups of hemicelluloses or the ester linkage of carboxylic group of the ferulic and *p*-coumaric acids of the lignin and/or hemicellulose or even from the methyl ester and carboxylic acid in pectin.[128–131] The shoulder at 1642 cm^{-1} can indicate the O–H bending vibrations of absorbed water, as stated by *Abraham et al.*[98] and *Alonso et al.* [131]. Meanwhile the peak at 1600 cm^{-1} can be assigned to either conjugated carbonyl present in typical lignin groups (C=C in plane alkenes) or for C=O stretching vibration of the α-keto carbonyl from cellulose, according to *Guimarães et al.* [128], *El-Zawawy* [133] and *Motaleb, Mizan, and Milašius* [108]. Between 1424 cm^{-1} and 1316 cm^{-1} peaks are assigned to the symmetric bending of CH_2, bending vibrations of the C–H and C–O groups of the polysaccharides rings, associated to the existence of lignin and hemicellulose .[108,130,131] Furthermore, the peak at 1245 cm^{-1} was assigned to the aromatic skeletal vibration of lignin, by *Abraham et al.*[98], while *Mwaikambo and Ansell* [134], *Cherian et al.* [130] *Guimarães et al.* [128] mencione that it is indicative of the presence of hemicellulose. Additionanly, the region of 1158–1027 cm^{-1}, can be attributed mainly to the carbohydrates, including C–O–C and C–O stretch bonds (primary and secondary hydroxide and ester groups) and CH in the plane deformation of CH_2 groups belonging to lignin, cellulose, hemicelluloses, and extractives.[128,133] The band at 897 cm^{-1} (symmetric in-phase ring-stretching mode) is due β-glycosidic linkage between the monosaccharides.[127,132,134,133] Bands at 664 cm^{-1} and 606 cm^{-1} are due to the out of plane bending vibration of intermolecular H-bonded O-H group and out of plane O-H bending.[127,133,134]

The raw fiber was manually extracted. In order to compare the chemical and manual extracted fibers were either treated or bathed in a sodium hydroxide solution with the same concentration (15% NaOH). The main differences of both methods lies in the time of the reaction and temperature used. The choice for the concentration of 15% sodium hydroxide solution came from the required high concentration for the chemical extraction according to some Indian companies that were previously contacted. Furthermore, *Motaleb, Mizan, and Milašius* studied the properties of inner, middle and outer banana fibers extracted with that same concentration allowing for a more detailed comparison.[108] *Figure 20* shows the alkali treatment attempts.

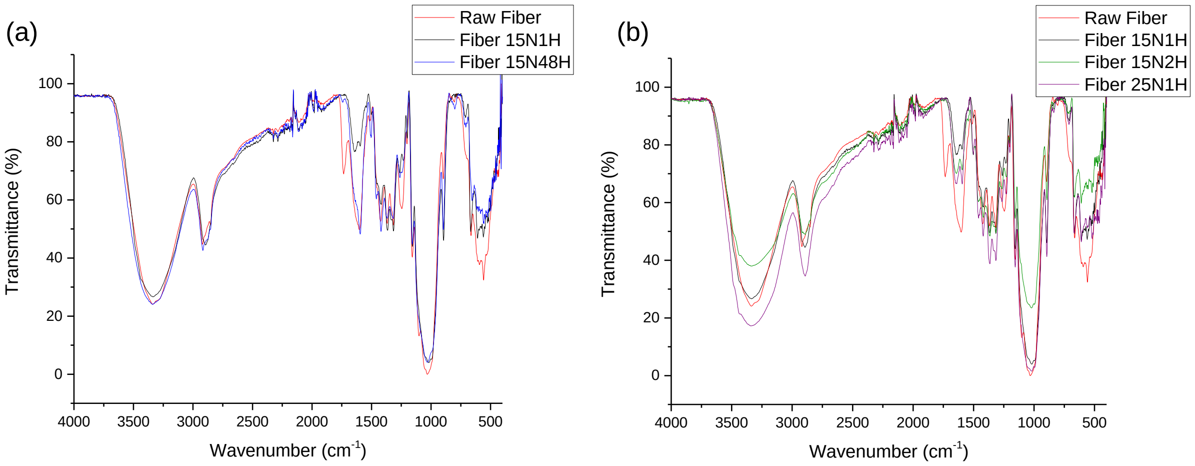

Figure 20 - FTIR spectra of (a) raw, manually extracted treated (15% NaOH for 1 h) and chemically extracted fibers (15% NaOH for 48 h); (b) alkali treated fibers (15% NaOH for 1 h; 15% NaOH for 2 h; 25% NaOH for 1h)

From the figure, it can be observed that the raw, the alkali treated and chemically extracted fiber present similar spectra.[108] *Figure 20* (a) shows the IR spectra of manually extracted fiber (or raw fiber), manually extracted treated fiber and chemically extracted fiber. For the scope of the analysis the proposed reaction for the alkali treatment is once again presented below:

$$Fibre\text{–}OH\ +\ NaOH\ \rightarrow\ Fibre\text{–}O^{-}Na^{+}\ +\ H_2O + surface\ impurities$$

When treated, the dissolution of hemicellulose, pectin and lignin takes place as they are sensitive to this reagent, increasing the numbers of reactive hydroxyl groups on the fiber surface available for H-bonding.[108,130,132] This will also decrease the quantum of binding components present in the fibers and reduces its hygroscopicity.[34,98] Therefore, according to the literature, the OH bands tend to decrease in intensity while bands at 1735 cm^{-1} and 1245 cm^{-1} (primary or secondary OH in-plane bend)[108] either disappear completely or reduce their intensity due to the removal of hydroxyl groups by reacting with sodium hydroxide and aldehyde/carboxylic group by deesterification reaction.[108,134] When trying to identify which lignocellulosic components belongs to each specific band, the information available from the literature was not entirely clear, in part, because many chemical bonds are common to varied components. However, since cellulose and hemicellulose are laid down first in the fiber structure while pectin and lignin serve as cementing materials, the latter might be more easily removed with the alkali treatment and therefore the peak might be fully absent.

The chemical and the alkali treated fibers both presented absence of 1735 cm^{-1} peak and reduction of 1245 cm^{-1} peak. This might indicate that the cementing materials, oils and waxes were preferentially removed while hemicellulose was only partially eliminated. Meanwhile, the chemically extracted fibers had no visible reduction in the 1642 cm^{-1} shoulder nor in the 1600 cm^{-1} peak.

Figure 20 (b) presents the raw fiber along with three different alkali treatments. All treatments were successful due to absence of 1735 cm^{-1} peak, reduction of 1245 cm^{-1} peak and reduction of the 1642 cm^{-1} shoulder and the 1600 cm^{-1} peak. In addition, when 25% of sodium hydroxide was used the characteristic peaks had higher intensities possibly due to improper drying.

Finally, *Ramesh, Palanikumar and Reddy* reported an intense peak at 1500 cm^{-1} for alkali treated abaca fibers which present a different lignin content when compared to banana fibers.[104] This band was attributed to carboxylate salts, which might indicate the formation of R–C=O–ONa groups on the surface of the fibers, through the substitution of COOH groups to COONa. The same effect was observed for the decrease in intensity for the 1600 cm^{-1} peak. *Figure 21* shows the SEM images of untreated and alkali treated fibers.

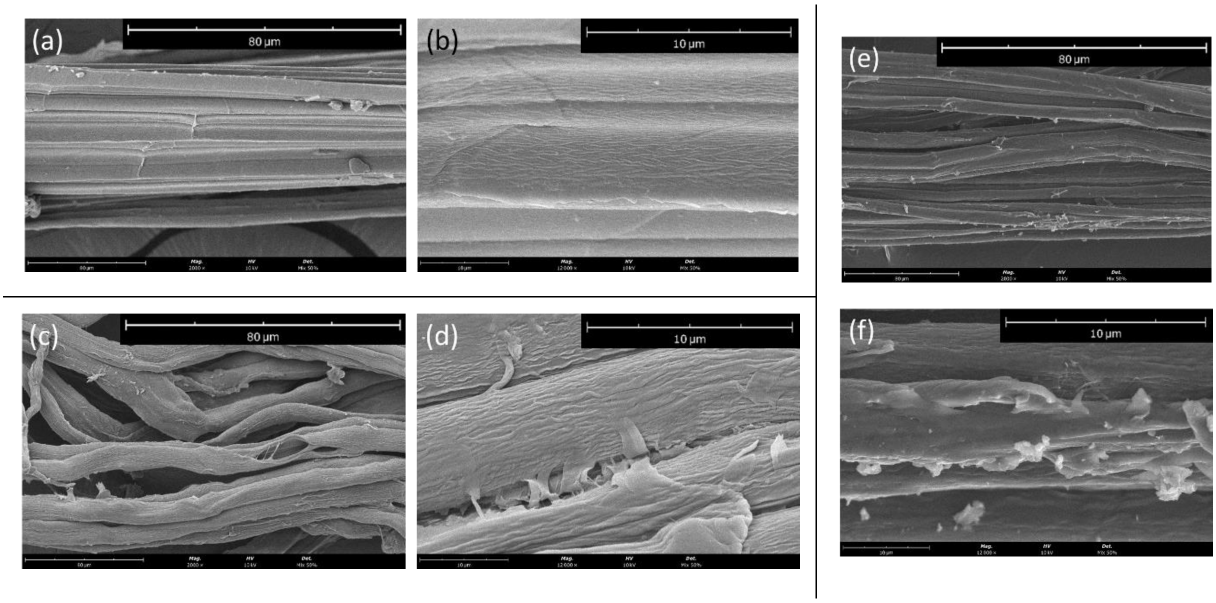

Figure 21 – SEM images of (a: 2000x, scale bar 80 µm; b: 12000x, scale bar 10 µm) raw fiber; (c: 2000x, scale bar 80 µm – d: 12000x, scale bar 10 µm) alkali treated fiber (15% NaOH for 1 h); (e: 2000x, scale bar 80 µm – f: 12000x, scale bar 10 µm) chemically extracted fiber (15% NaOH for 48 h)

When observing *Figure 21* (a – b) that shows the surface morphology of raw lignocellulosic fibers, it is evident that these present a smooth surface on account of oils and waxes, with the presence of oval shape particles and lumps that partake in the division of the fiber surface into sections. The particles can be impurities that stayed in the surface due to an ineffective manual removal of the bark and the lumps come from the natural layers of substances. *Annie et al.* also attributed the smoothness of the surface of raw banana fiber to the existence of oils and waxes,[119] while *Pereira et al.* recorded lumps and the presence of particles before washing the fibers with distilled water.[105] In addition, fibers also tend to form bundles rather than a single fibrillary condition. *Motaleb, Mizan, and Milašius* described the outer bark banana fibers in the same entangled state.[108]

Meanwhile, *Figure 21* (c – d) and (e – f) shows the surface morphology of the alkali treated lignocellulosic fiber and chemically extracted fiber. The surface is altered with the treatment, becoming rougher and exposing the fiber backbone structure that corresponds to the cellulosic phase. This difference stems from the removal of impurities like oil, wax, hemicellulose and cementing materials like lignin and pectin. The removal of impurities effectively cleans the fiber surface while the elimination of cementing materials successfully separates the bundles into individual strands and increases interfibrillar pores exposing more anchoring points for mechanical interlocking. The decrease in cementing materials also promotes a greater amount of disorientation in the cellulose morphology and leads to better packing and increase of the crystallinity index. *Motaleb, Mizan, and Milašius* noted the same effectiveness of the 15% NaOH, 90 ºC, 1 h treatment and washing with distilled water, with increase in surface roughness of the outer bark banana fiber,[108] while *Pothan, Thomas, and Groeninckx* saw the same results with a 0.5 and 1 % solution of sodium hydroxide for half an hour at room temperature and washed with a very diluted acid and distilled water.[120] Meanwhile, *Mohan and Kanny* treated with 1 mol/L NaOH for 4 h, rinsed with dilute acid and washed the fibers which lead to the exposure of the backbone structure.[135] When observing the EDS data of the alkali treated fiber surface *Figure 21* (c – d)) only trace amounts of sodium hydroxide were detected (*Figure 42* in appendix E). *Figure 22* shows the optical microscopy photographs taken for the same types of fibers observed in SEM.

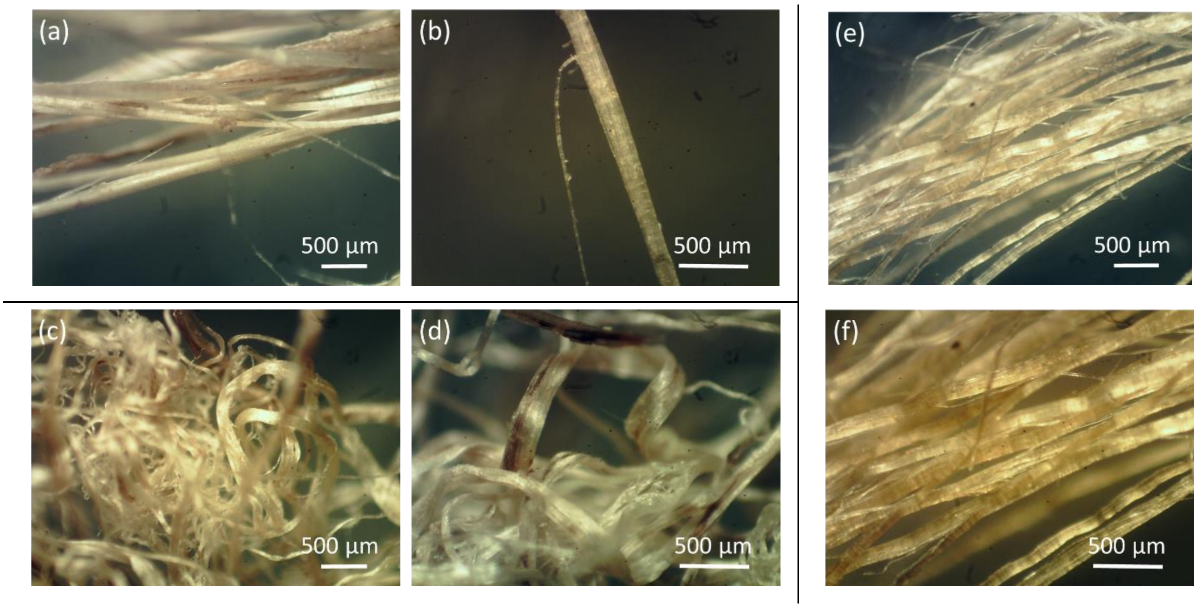

Figure 22 – Optical microscopy photographs of (a: 2.5x – b: 4.5x) raw fiber; (c: 2.5x – d: 4.5x) alkali treated fiber (15% NaOH for 1 hour); (e: 2.5x – f: 4.5x) chemically extracted fiber (15% NaOH for 48h)

Figure 22 (a – b) shows the surface morphology of the raw lignocellulosic fiber while *Figure 22* (c – d) and (e –f) shows the surface morphology of the alkali treated lignocellulosic fiber and chemically extracted fiber, respectively. Once again the photographs demonstrate that the fibers exist in a bundled structure and are separated after the treatment. The images also corroborate the findings in SEM, where the dark and light brown sections are impurities attached to the surface leftover from the bark. Since the extraction is done manually, there is always some margin of error in this method that others could potentially avoid. The untreated fibers present a white color like silk and a hair like texture. When treated with sodium hydroxide their color changes instantaneously to yellowish shade, and only after washing with distilled water is the color less prominent. To the naked eye, fibers that stayed longer in solution presented a cleaner exterior (15% NaOH for 48H) and were less likely to form a complex intertwined structure and curl up in a sphere.

Even though chemically extracted fibers presented a rougher surface and the absence of peaks at 1735 cm^{-1} (mainly assigned to cementing materials) and 1245 cm^{-1} (mainly assigned to hemicellulose) indicating a successful treatment, had lower amounts of attached residual bark and lower tendency to bundle up but presented no visible reduction the 1642 cm^{-1} shoulder or 1600 cm^{-1} peak. Additionally, this method is more complex by not eliminate the labor intensive part of the process while also increasing the amount of solution needed for treatment and thus making it less economically viable when compared to the manual extracted treated fibers. Therefore, no further studies were conducted with this process. *Figure 23* shows the comaprison between all types of extracted fibers and the chemical treatment.

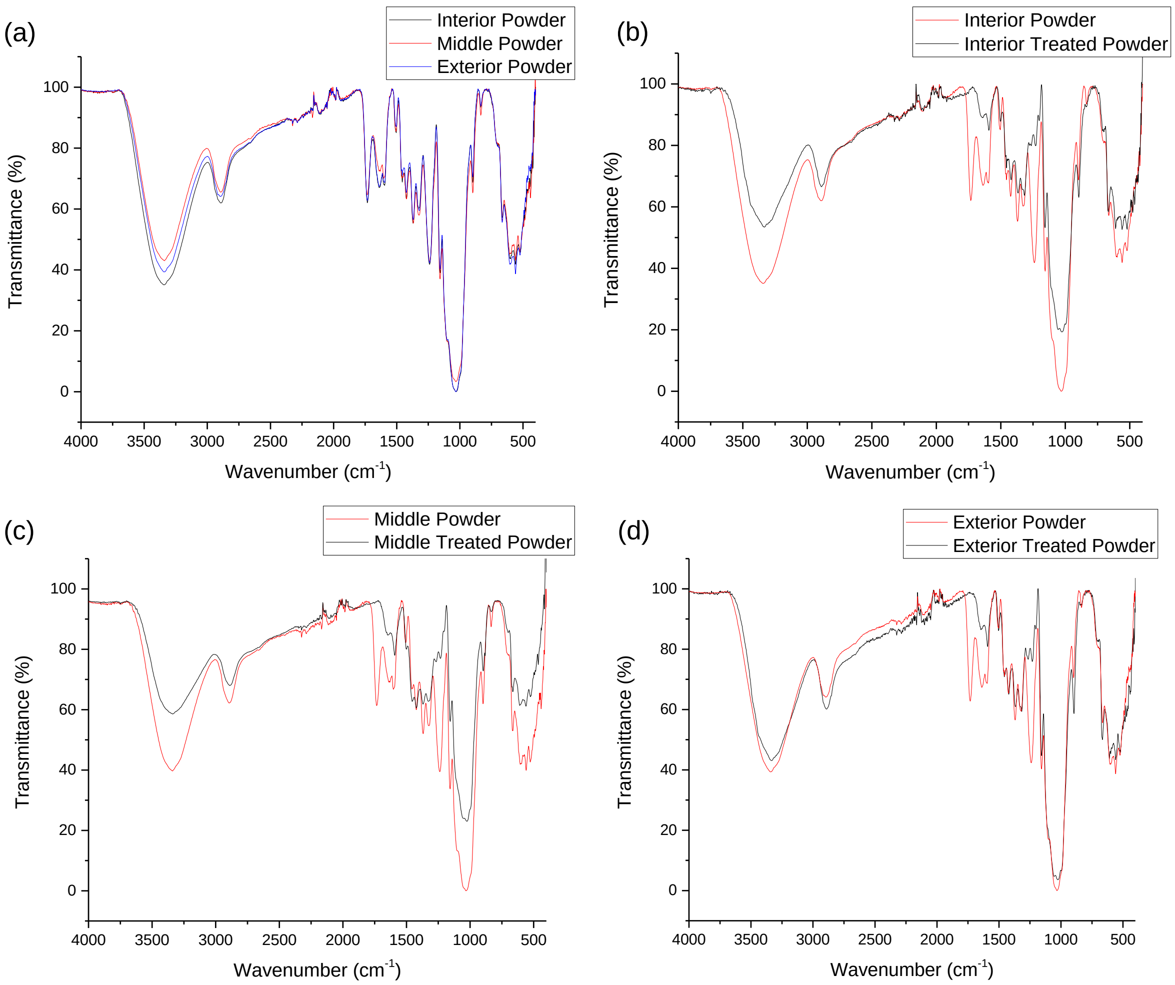

Figure 23- FTIR spectra of (a) interior, middle and exterior fiber powder; (b) interior treated and untreated fiber powder; (c) middle treated and untreated fiber powder; (b) exterior treated and untreated fiber powdes

Figure 23 (a-d) shows that the powders from the different section presented very similar chemical structures where the main difference lies on the intensity of the OH band and therefore quantity of lignocellulosic components or just improper drying before the acquisition of the spectra. Even though the 2 hours process with 15 % NaOH at 90 ºC presented good results for fiber treatment, the first tests conducted on the powders were with 15% sodium hydroxide for 1 hour at 90 ºC. As fibers were grinded into powders the bundled structure would cease to form itself in the solution and the degree of contact of the powder surface with the treatment would increase. Looking at the results all treatments were successful, judging by the absence of peaks at 1735 cm^{-1} (mainly assigned to cementing materials) and 1245 cm^{-1} (mainly assigned to hemicellulose). After treatment all products were washed with distilled water. This was a progressive process as they were washed, dried in an air oven at 60 ºC and analyzed by FTIR spectroscopy, to see if all alkali and other contaminants were removed. In total, interior treated powders were washed twice while middle treated powders and exterior treated powders needed three washes. The yields obtained were, 76.35 %, 55.94 % and 79.32% for interior, middle and exterior treated powders, respectively.

3.1.3. Thermal behavior analysis

Thermogravimetric and derivative thermogravimetric analysis was performed in order to study the thermal stability and thermal decomposition of the powders while observing the influence of alkali treatment. The composition was determined through the number of stages in the degradation curves and the quantification of inorganic filler content was obtained as the residual weight at the end of the analysis (600 ºC). This technique measures the amount and rate of change in the weight of a material as a function of temperature or time in a controlled atmosphere.[104] *Figure 24* shows the weight loss percentage over temperature and DTG curve for middle treated and untreated powder while *Table 5* summarizes the results. For the purpose of this thesis only the middle powders were tested for their thermal behavior as the composites produced with these powders had a more diverse degree of powder loading.

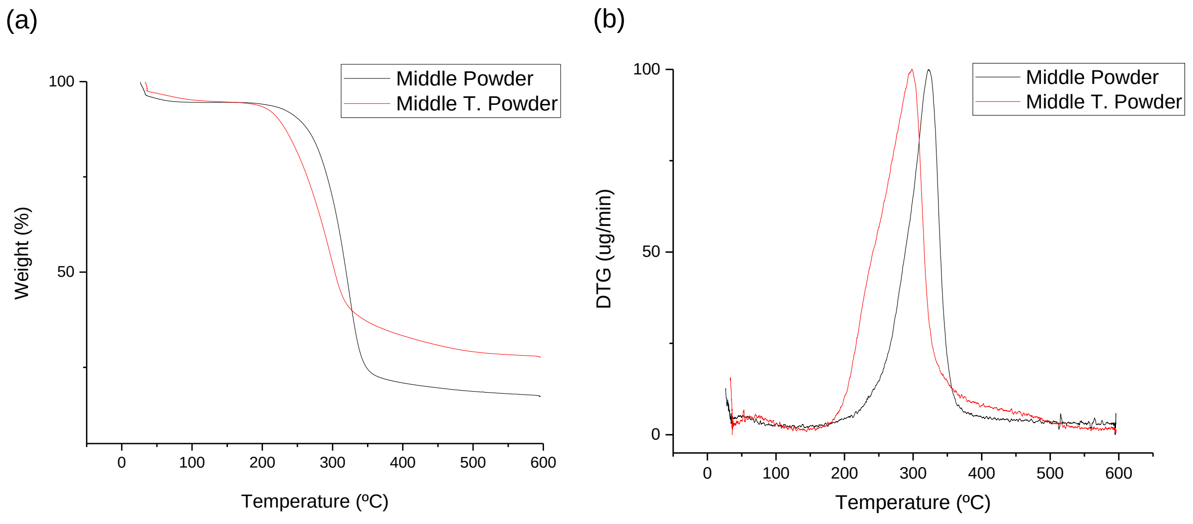

Figure 24– (a) Thermogravimetric analysis (TGA) of untreated and treated middle fiber powder (b) Differential thermogravimetric analysis (DTG) of untreated and treated middle fiber powder

Table 5 - Thermal stability of untreated and treated powders compared with the literature

Sample		ΔT (ºC)	T_d (ºC)	T_{onset} (ºC)	Residual Weight (%)	Ref
Middle Powder	1st stage	35.11 – 276.06	323.13		94.65	
	2nd stage	276.06 - 345			21.61	
	3rd stage	345 - 600			17.36	
Middle T. Powder	1st stage	37.21 – 232.83	296.54		94.00	
	2nd stage	232.83 – 334.75			34.41	
	3rd stage	334.75 - 600			27.66	
Banana fiber			284.4	249.2	12.2 (800 ºC)	21
Banana fiber			231			98
			317			
Banana fiber	2nd stage	200 - 300	321.08		4.14 (500 ºC)	128
	3rd stage	300 - 400				
	4th stage	400 - 500	445.19			
Banana peel powder		299.45 – 312.99		287.22	34.75 (600 ºC)	136

Lignocellulosic components present differences in chemical structure, therefore hemicellulose, cellulose and lignin have specific temperature intervals for their decomposition. Cellulose is known to start its decomposition at 310 ºC, and persists until 400 ºC, hemicellulose decomposes between 220 ºC and 300 ºC while lignin has a more extensive range of decomposition that spans the whole temperature spectra, initiating below 200 ºC and persisting above 700 ºC.[98]

From *Figure 24* (a), it can be seen that the thermal degradation of the fiber powders took place in three stages or one step for both treated and untreated samples. The initial decrease in slope from 28 ºC to 35 ºC can be disregarded as a step of decomposition. Just like in the case of *Abraham et al.* and *Liu, Wu and Zhang* an initial small weight loss was observed due to the evaporation of the humidity of the material or low molecular weight compounds remaining from the isolation procedure.[21,98] Therefore, the first weight loss, or first stage, occurred over the temperature range of 35 ºC to 276 ºC and 37 ºC to 232 ºC for untreated and treated powder, respectively. This step was attributed to the removal of moisture or solvents (dehydration) from the powders which resulted in about 5.35 - 6% weight loss. Furthermore, *Guimarães et al.* attributed this loss of moisture in the first stage to the hydrophilic nature of the fibers which present structurally bound water molecules.[128] Therefore, even when samples are previously dried before data acquisition, the complete elimination of water is a difficult task. In addition, within the first degradation stage of the untreated powder, there is a range of temperatures where a plateau is formed and no significant loss in mass is observed (maintained at around 94.54 %). This range corresponds to temperatures from 106 ºC to 169 ºC and indicates the region where the powder is thermally stable. This value can be seen as the maximum temperature up to which these powders can be used since above it, mass loss is high. *Guimarães et al.* also attribute this maximum observed temperature to 200 ºC for banana fibers.[128]

After 232 ºC and 276 °C, the decomposition rate had a drastic increase with temperature. The second stage, where the major weight loss takes place, occurred from 276ºC to 345 ºC and from 232 to 334ºC, for untreated and treated powder, respectively. This degradation is attributed to the pyrolysis of fragments of the fiber lignocellulosic compounds in the presence of nitrogen (hemicelluloses, cellulose and lignin), which resulted in about 60% loss of specimens' weight for treated powder and a loss of 73% for untreated powder. As the untreated powder possess higher lignocellulosic contents, its weight loss is greater (no removal was previously performed with treatment). These results are in agreement with the FTIR spectra as the expected peaks disappeared and the OH band decreased in intensity. *Liu, Wu and Zhang* attributed the onset degradation temperature at 249.2 ºC to the degradation of lignin and hemicellulose for untreated banana fibers.[21] Furthermore, it could be seen that treated powder showed a higher weight loss at lower temperature when compared to the untreated powder which showed a lower weight loss at lower temperature. Therefore, the untreated powder is more thermally stable than the treated one, during this temperature range, but results in a lower char residue at the end temperature of the analysis, 600ºC. The same results were observed by *Abraham et al.* where the thermal stability of the natural fibers was decreased when they were subjected to chemical modifications.[98] *Mitra, Basak, and Sarkar* justified this occurance with the imparted flame retardency to the treated sample.[137]

The final stage takes place after 345 and 334 ºC and goes to 600 ºC attributed to the char content which are 17% and 28% for untreated and treated powders, respectively. Meanwhile, *Guimarães et al.* reported a lower char content of 4.14 % (at 500 ºC) and three steps of decomposition, [128] while *Liu, Wu and Zhang* observed a 12.2 % at 800 ºC.[21]

From *Figure 24* (b) that shows the DTG results of untreated and treated powders, the maximum weight loss is seen at 323 ºC and 296 ºC. *Abraham et al.* identified two main peaks from the DTG analysis of the banana fiber at 231 ºC and 317 ºC assigned to hemicellulose and α-cellulose degradation, respectively.[98] Both values are within the range of temperatures observed for the powder samples. Regardless, both maximum peaks can be assigned to the loss of cellulose which was pyrolyzed leaving a small char content behind (0.33 to 1 wt %). Once again the treated powder recorded lower decomposition temperatures than untreated ones.

3.2. PBAT/Banana powder composites

This section will discuss the extrusion of the composites reinforced with the fiber powders, along with their characterization and 3D printing of the filaments as a proof of concept. Results will be presented along with the discussion for better understanding. Several techniques were used to analyze the composites and these are divided into four subsections: chemical structure and morphological studies (scanning electron microscopy (SEM); optical microscopy; Fourier transform infrared (FTIR) spectroscopy), thermal behavior analysis and thermo-mechanical properties (thermogravimetric and derivative thermogravimetric analysis (TGA/DTGA); dynamic mechanical analysis (DMA)), mechanical testing and water absorption.

3.2.1. Composite extrusion

Extrusion is the term used to describe the continuous manufacture of a semifinished plastic product (film, sheet, pipe, profile).[23] In this process, cold thermoplastics materials (in powdered or granular form – pellets) are propelled continuously along a screw through regions of high temperature and pressure where they are converted into a homogenous polymer melt, compacted, and finally forced through a shaping die forming items of uniform cross-sectional area (profile).[138,139] High temperatures are attained through the use of external heaters and the friction of viscous flow, while pressure increases along the barrel and is highest right before the plastic enters the die. This allows the shaping to occur in the extruded product, also known as extrudate.[122] The screw of the extruder is its most important element and influences the extrusion process according to the screw or barrel diameter and the length-to-diameter ratio (L/D) - effective screw length.[23,122,140] Longer L/D extruders can have a higher throughput, mixing capacity, die pressure and greater melt capacity with less shear heating. Meanwhile, short L/D extruders require less floor space, are more affordable ((initial investment and replacement of parts), are better for processing temperature sensitive materials (lower residence time), require less torque and less horsepower or have lower motor size.[140]

The extruder used for this project was a single screw 3Devo® composer 450 desktop. The single-screw extruder is a very important equipment employed in the polymer industry as it presents low cost, straightforward design, ruggedness, reliability, and a favorable performance/cost ratio.[141] The parameters that influence the extrusion process are the feed rate, the rotor speed and the barrel temperatures.[138] Furthermore, since the extruder consisted of a single screw with feed, compression, and metering sections, it can often fail to homogenize the liquid/melt satisfactorily when compared to twin screw extruders (co-rotating and counter-rotating) which are extremely important for difficult mixing operations.[138] Proper mixing involves two actions: distributive and dispersive mixing. As their names describe, distributive mixing evenly distributes particles throughout the melt, while dispersive mixing breaks up agglomerates or large particles and disperses them evenly throughout the melt.[140]

Therefore, in order to promote a more efficient mixing, each composite was extruded twice showing a more homogeneous appearance in the second run based on a visual inspection (color wise). *Figure 25* shows the untreated and treated middle powders along with the extrudates. Even though it is not clearly visible in the pictures, the powders gained a more yellowish color after their treatment, just like in the case of the treated fibers. Composites with treated powders also tended to have more intense coloring. Moreover, after washing yields obtained for the powders were: 76.35 %, 55.94 % and 79.32% for interior, middle and exterior treated powders, respectively. Looking at *Figure 25* (c –d) the powders showed good adhesion to the PBAT pellet's surface due to adequate drying of the materials. As the powder loadings increased, a deposit was observed at the bottom of the container.

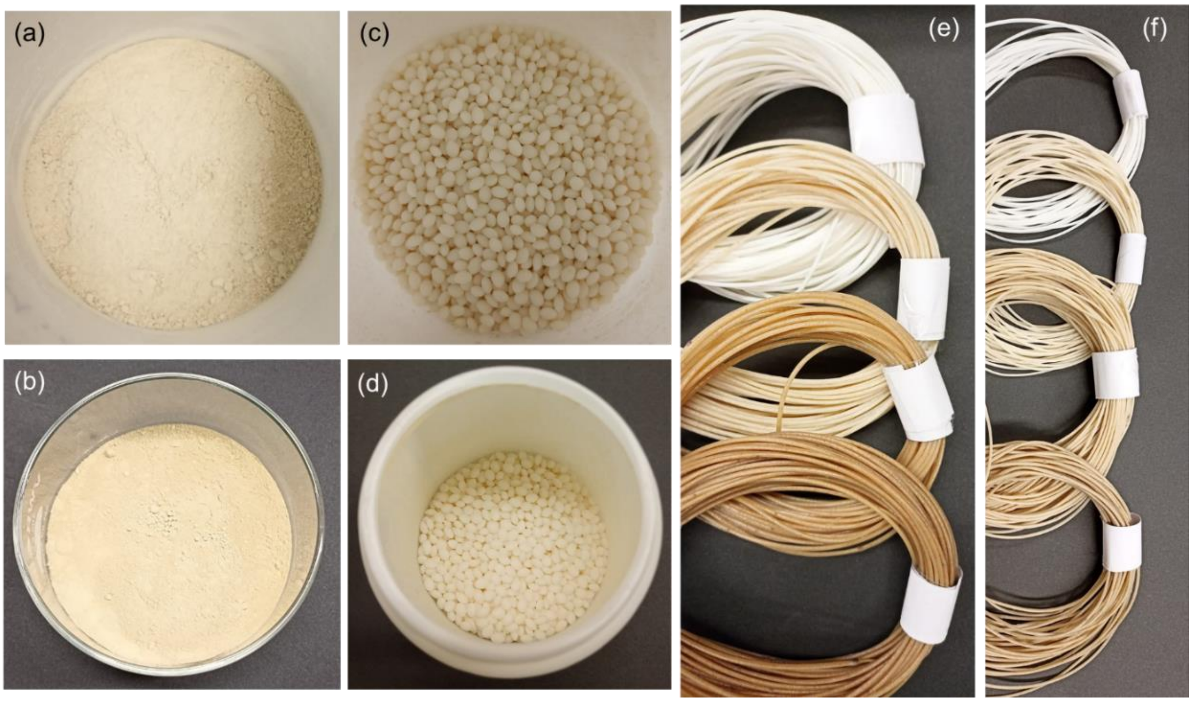

Figure 25 – (a) Untreated middle powder; (b) Treated middle powder; (c) PBAT/untreated middle powder at 2 wt%; (d) PBAT/ treated middle powder at 2 wt%; (e) neat PBAT and composites of PBAT with 2, 5 and 8 wt% treated middle powder (f) neat PBAT and composites of PBAT with 2, 5 and 8 wt% untreated middle powder

Initial trials were performed to gain sensitivity and a better understanding on how to handle the material and the equipment. As suggested by the 3Devo® support manual for the starting temperatures, these were set 10% above the materials´ melting temperature for all heaters. This could guarantee a proper output flow of material and allow to gradually decrease the temperatures until the range was set to the optimal conditions.[142] Furthermore, *Ratanakamnuan and Aht-Ong* reported using temperatures of 100, 135, 140, 145 and 150 ºC in a twin-screw extruder for banana starch/LDPE.[109] *Liu, Wu, and Zhang* blended HDPE/Nylon-6 with banana fiber in a two-step extrusion, with the temperatures set between 160 to 175 ºC for the fiber mixing step.[21] *Botta et al*. prepared blown films of extruded PBAT/biochar pellets in a single screw extruder at 150, 160, 160 and 180 ºC.[32] Finally, *Tavares et al*. obtained PBAT/kraft lignin films through extrusion with 132, 135, 135, 138, 138 and 140 °C from the feeder to the die as the temperature profile.[30] These parameters can be used as reference points but do not guarantee a successful extrusion. Prior to the extrusion process, all authors mention the drying of materials for either 24h or 8h, at temperatures ranging from 60 to 90 ºC, to avoid hydrolytic scission of PBAT during processing [32] or to avoid void formation, due to moisture evaporation during the extrusion process [110]. The same was done with the materials used to extrude the PBAT/banana fiber powder composites, where banana fiber powders and PBAT were dried in an air oven overnight at 60 ºC.

After carefully tuning and customizing the extrusion parameters (temperature profile, screw speed, fan speed and orientation) the initial temperature profile used was set between 130-145 ºC with 3.5 rpm and 40% of fan speed for PBAT alone. With the introduction of fiber powders the parameters were slightly altered to assure a good quality filament as shown in *Table 6*. Overall, heaters 2 and 1 (closest to the die) presented the highest fluctuation of temperatures, while screw speed varied between 3.9 and 4.1 rpm and fan speed went as low as 35 % to 44 %. Furthermore, the second extrusion either presented lower or the same temperatures as the first extrusion, to prevent any type of degradation of materials.

The diameter of the filaments were assessed with the average and standard deviation values specified in *Table 6*. All measurements were taken for samples of 1 m with 50 data points.

Table 6 - First and second extrusion processing parameters and diameter control measurements for PBAT/banana fiber powder treated and untreated composites

Comp.	Screw Speed (RPM)	Fan speed (%)	H4 (˚C)	H3 (˚C)	H2 (˚C)	H1 (die) (˚C)	Avg Diameter (mm)	Diameter Stdev (mm)
PBAT	3.5	40	130	135	140	145	1.70	0.05
2I	4.1	42	141	147	156	161	1.57	0.05
2IT	4.1	42	141	147	155	159	1.60	0.04
			141	147	155	157		
2M	4.1	35	141	147	160	165	1.65	0.05
	3.9	44	141	147	153	156		
2MT	4.1	42	141	147	153	159	1.68	0.03
5M	4.1	35	141	147	160	165	1.56	0.03
	3.9	44	141	147	153	156		
5MT	4.1	25	141	147	154	159	1.66	0.05
			141	147	154	156		
8M	4.1	35	141	147	160	165	1.66	0.05
	3.9	44	141	147	153	156		
8MT	4.1	25	141	147	154	157	1.64	0.06
2E	4.1	42	141	147	155	157	1.71	0.05
2ET	4.1	42	141	147	155	156	1.67	0.04
			141	147	152	153		

2I: PBAT/2 wt% interior powder; 2IT: PBAT/2 wt% interior treated powder; 2M: PBAT/2 wt% middle powder; 2MT: PBAT/2 wt% middle treated powder; 5M: PBAT/5 wt% middle powder; 5MT: PBAT/5 wt% middle treated powder; 8M: PBAT/8 wt% middle powder; 8MT: PBAT/8 wt% middle treated powder; 2E: PBAT/2 wt% exterior powder; 2ET: PBAT/2 wt% exterior treated powder; H (heater) – H1 is closest to the nozzle/die

The diameter control data is imperative and a useful tool to compare and assess the quality of the filaments extruded, however the samples taken do not represent the entirety of the extrudates. No considerable diameter variations were observed as the standard deviation is quite low, however, some filaments presented values below the required standards for 3D printing (1.75±0.05 mm depending on printer tubes, bearings, motor and extruder).

When performing the extrusion process complications can occur with the handling of the equipment and also the extrudates obtained. Typical problems encountered include: die swell, melt fracture, die exit instability (shark skin; orange peel; bambooing; oval or flat filament), impurities (gels; specks), output fluctuations (output too low or too thin; output it too liquid), thermal degradation of polymers, poor mixing, air bubbles or holes in filament, nozzle build-up, bumps/particle in filament, abnormal smoke production, filament thickness deviation, error messages during extrusion, etc.

Regarding the die swell, it can be calculated according to the following equation:

$$\%\ die\ swell = \frac{D_{Extrudate} - D_{die}}{D_{die}} \times 100 \tag{5}$$

Where $D_{Extrudate}$ is the diameter of the extrudate when leaving the die and D_{die} is the diameter of the die. For the composites extruded in this project, the die swell was so insignificant that calculations were incoherent as no significant differences could be detected between both diameters. Furthermore, filaments presented a good surface quality with no entanglements or twists. Meanwhile, composites with treated powders displayed more visible aggregates that could easily be distinguished with the naked eye. The higher the content of powder, the greater the quantity of agglomerates.

In addition, during the extrusion, the main problems faced were nozzle build-up, bumps and particles in the filaments, curling and waving of the filaments, polymer adhesion to the pulley, uneven quantity of material exiting the die and error messages from the equipment. The chart below summarizes the steps followed to assess and prevent bumps and particles in the filaments, which also includes nozzle build-up, and uneven quantity of material exiting the die.

(a)

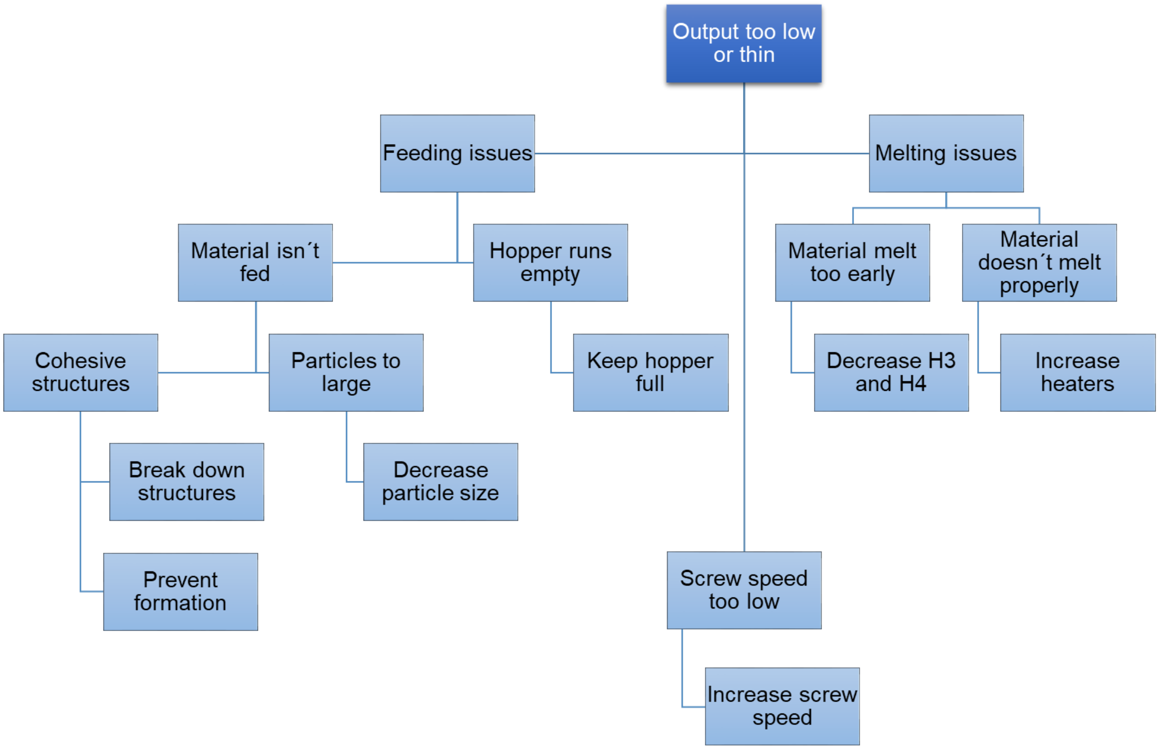

(b)

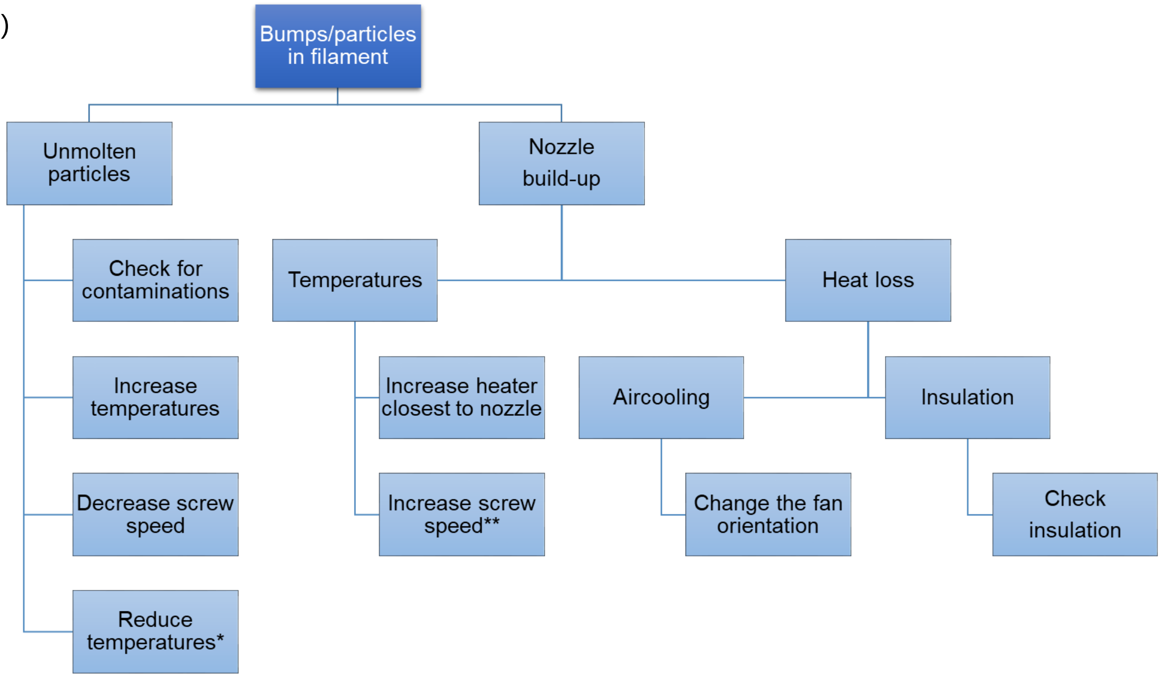

*Some rare cases (when working with amorphous polymers)

**Not systematically a good option (increase in small steps)

Figure 26 - Summary chart of potential causes and corrective actions when the (a) output is too low or tin and (b) the filament extruded presents bumps and particles [143]

Following the scheme, nozzle build up was decreased by increasing the temperature of the heater closer to the noozzle/die, allowing the material to flow at higher temperatures and being less likely to stick. Furthermore, the direct contact of the fans with the nozzle and extruded filament was minimized by position them with a downwards angle allowing for a slower cooling of the extrudate and maintaining a rubbery state. This rubbery state significantly improves the diameter variance since the puller can easily correct it as the material is still deformable. The prevention of particles and bumps was done by increasing the temperature of the first and second heater closest to the die to allow the polymer to melt correctly. However, when increasing these temperatures the extrudate tended to be in a molted state for longer and when in contact with the puller wheel could adhere to it inhibiting the coiling action. Therefore, the temperatures chosen for heater 2 and 1 needed to be optimal in order to prevent nozzle build-up, particles and bumps and adherence of the extrudate on the puller wheel for a proper extrudate acquisition.

Curling and waving of the extrudate occurred when the its output from the die was faster then the puller wheel/coiling action, leading to an accumulation of material before reaching the IR sensor. Therefore, when passing through the sensor results would be tampered and the equipment wouldn't ajust the puller speed automatically. To avoid this problem the speed would first be ajdusted manually until the filament would flow in a straight line from the nozzle to the IR sensor, and after the adjustment could be changed to automatic settings.

One noteworthy issue that occurred throughout every extrusion trial run was an initial error message from the equipment stating that the screw was unable to move. Thus, in the beginning of every run, the heaters needed to be around 20 ºC higher than the optimal conditions stated in *Table 6*, to allow the first batch of composite to fully melt and be “expelled” from the barrel. This process usually took about 10 to 15 mins. Afterwards, extrusion could take place normally.

3.2.2. Chemical and morphological structure

This section will cover PBAT/banana fiber powder composites regarding their chemical structure and morphology, also looking at the differences between treated and untreated composites. The FTIR spectra obtained span across the range 4000 - 400 cm^{-1} (mid-IR). *Figure 27* presents the FTIR spectra of pure PBAT with its characteristic peaks while *Table 7* summarizes the absorption bands and compares with the literature. *Figure 28* presents the comparison of FTIR spectra of neat PBAT and PBAT/powder blends. The regions that possess characteristic peaks for PBAT are: 3300 – 3700 cm^{-1} (C-H stretching in aliphatic and aromatic portions), 1700 – 1760 cm^{-1} (carbonyl groups (C=O) in the ester linkage), and 500 - 1500 cm^{-1} (C-O in the ester linkage, C=C vibrations, methylene (-CH2-) groups, bending peaks of the benzene substitutes), as stated by *Wu* and *Al-Itry, Lamnawar and Maazouz*. [33,93]

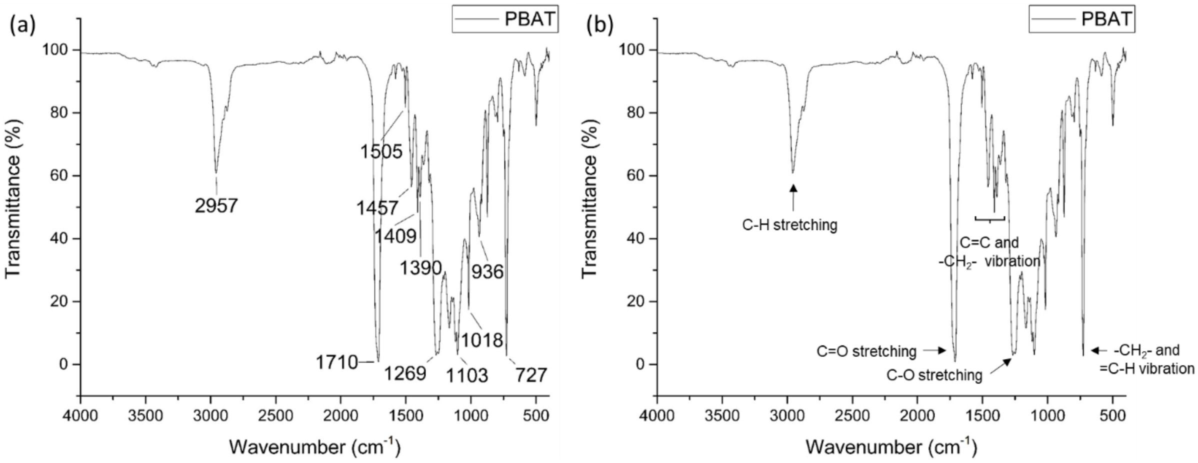

Figure 27 – FTIR spectra of (a) neat PBAT and (b) the absorbance peaks of interest of PBAT

Table 7– FTIR spectra peak list of neat PBAT with absorption, assignment and references from the literature for comparison

Absorption (cm^{-1})	Assignment	Ref
2957	CH_2 asymmetric stretching vibration	15,25,32,38,93
1710	C=O stretching vibration	15,25,32,38,84,93,95,144
1505	Skeleton vibration of the benzene ring and phenylene group	15,38,144
1457	phenylene group stretching vibration	38
1409, 1390	Bending vibration *trans*-CH_2-plane	15
	phenylene group stretching vibration	38
1269	C-O symmetric stretching vibration	15,25,32,38,93,144
1103	C-O left-right symmetric stretching vibration absorption	15,25,144
1018	Bending vibration absorption at the surface of adjacent hydrogen atoms on the phenyl ring	15,38

Absorption (cm^{-1})	Assignment	Ref
936	Symmetric stretching vibration *trans*-C-O	15,25,93
727	Bending vibration absorption of CH-plane of the benzene ring	15,25,38,76,93
	Methylene group	32,93,144

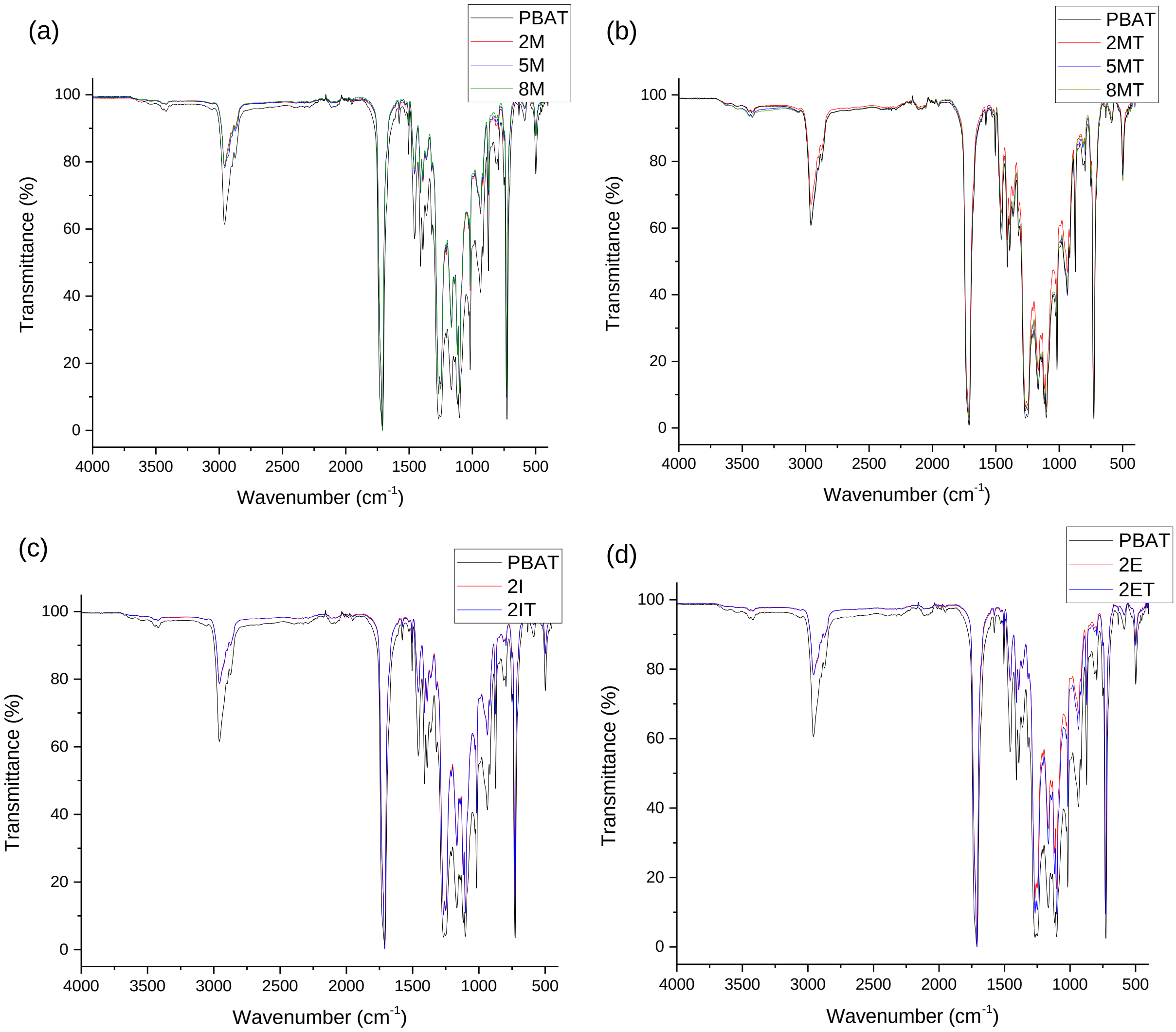

Figure 28 – FTIR spectra of (a) neat PBAT and PBAT/middle fiber powder composites (b) neat PBAT and PBAT/middle treated fiber powder composites (c) neat PBAT and PBAT/interior treated and untreated fiber powder (d) neat PBAT and PBAT/exterior treated and untreated fiber powder composites

Overall, the addition of banana fiber powder as reinforcement/filler in the composite did not induce significant qualitative changes in the evolution of the infrared spectra with respect to the PBAT matrix. Typically, differences would be expected in the 3300 – 3700 cm^{-1} region and at 1710 cm^{-1} peak, with either more intense bands, widened peaks or appearance of new ones as stated in the literature by different authors. *Wu* reported an intensified peak in the 3200-3700 cm^{-1} region due to the O-H stretching contribution of the OH groups of peanut husks in composites with 20 wt% PH and PBAT.[24] Meanwhile, in composites of PBAT and 10 wt% cellulose acetate the same phenomena was observed, once again due to the contributions of the OH groups of CLA.[33] In addition, *Kashani Rahimi et al.* used PBAT-g-MAH copolymer as the matrix material, reinforced with 9 wt% cellulose nanocrystals and observed the broadening of the 3100−3600 cm^{-1} peak, assigned to the H-bonded stretching vibration of OH groups of cellulose and the appearance of a peak at 1740 cm^{-1} attributed to the formation of interfacial ester bonds resulting from transesterification reaction between the anhydride groups and the surface hydroxyl groups of the cellulose.[38] *González Seligra et al.* prepared films of PBAT/TPS (starch plasticized with glycerol containing citric and stearic acids) and 0.6 wt% starch nanoparticles. When amplifying the zone of asymmetric and symmetric C−H stretching of CH_2, the composite showed a shift of the peaks to higher wavenumbers (around 2948 cm^{-1} and 2884 cm^{-1}) and widened bands. Therefore, it was concluded that the nanoparticles had a proper interaction with the PBAT/starch matrix.[145] Finally, *Olivato et al.* stated that the peak at 1715 cm^{-1} attributed to the presence of ester carbonyl stretch (C = O) from the PBAT structure presented an enhanced intensity in a starch/PBAT composite with maleic anhydride and citric acid as compatibilizers. This was due to a esterification or interesterification reactions promoted by both compatibilizers.[146]

Figure 28 (a - b) show the spectra of the composites with middle treated and untreated fiber powders, respectively. Regarding the untreated composites, all fiber loads presented lower intensity peaks when compared to pure PBAT and had overlapped spectra for the whole span of the absorption region studied. Meanwhile, composites with treated middle powders also had lower intensity peaks when compared to pure PBAT with the exception in the 3300 – 3700 cm^{-1} region. As the fiber powder loadings increased (5 and 8 wt%), so did the tendency to form a band due to the OH stretching contributions of OH groups of mainly cellulose (the major component). Moreover, when comparing peaks at 1710 cm^{-1}, treated middle powder composites presented a shoulder, closer to the one observed for pure PBAT. *Figure 39* in appendix D shows these zoomed regions of the spectra for all composites. Therefore, the lower intensities peaks only demonstrate that the composites had smaller amounts of the original chemical composition/groups from the PBAT matrix. In addition, the formation of an OH band and a shoulder at 1728 cm^{-1} might indicate a proper interaction or a good adhesion due to a reaction between the fiber powder with the PBAT matrix as the carboxylic acid peak is normally seen at 1725-1700 cm^{-1} and the ester is seen at 1750 – 1725 cm^{-1}.[147]

Figure 28 (c - d) shows the spectra of PBAT treated and untreated interior and exterior fiber powder composites. Just like in the case of untreated middle powder composites, these spectra were overlapped and had lower intensity peaks throughout the absorption region when compared to pure PBAT. In addition, no differences where spotted in 3300 – 3700 cm^{-1} region and 1710 cm^{-1} peak. This could be explained by the very low weight percentages used in these composites. In fact, also no significant difference in the OH stretching band was noted for the middle treated fiber powders for low loadings of 2 wt%. Only those with loadings at treated 5 and 8wt% exhibited a more intense OH stretching band.

SEM images and optical microscopy photographs of nitrogen-fractured cross-section surfaces of banana fiber powder composites are shown in Table 8.

Table 8 - SEM images and optical microscopy photographs (at 4.5x for a;c;f;h;k;m;p) of PBAT/treated and untreated middle fiber powder composites with 2, 5 and 8 wt% and neat PBAT (1500x, scale bar 20 µm – b;d;g;i;l;n;q; 8400x, scale bar 3 µm – e;j;o)

	PBAT/Untreated Fiber Powder composite		PBAT/Treated Fiber Powder composite		
2 wt%	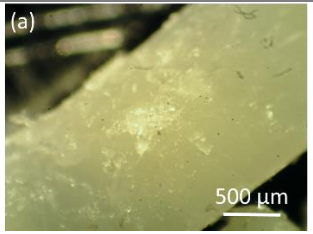	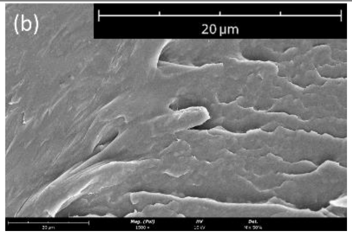	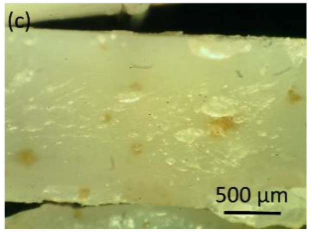	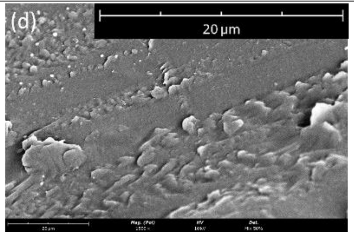	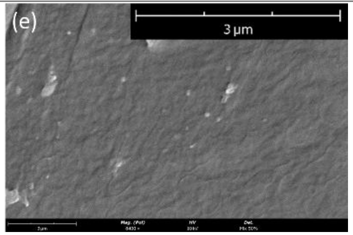
5 wt%		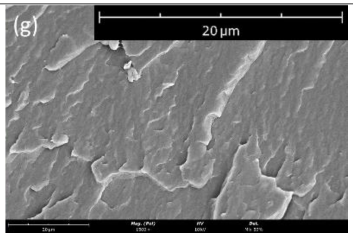	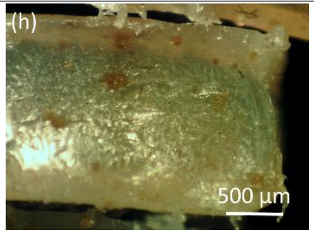	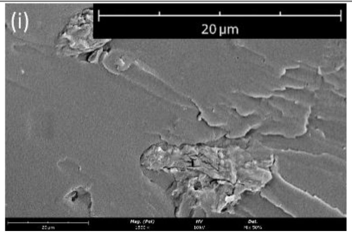	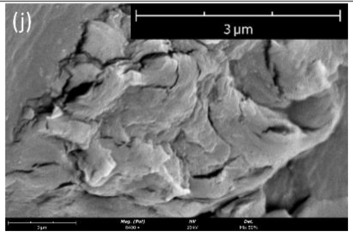
8 wt%		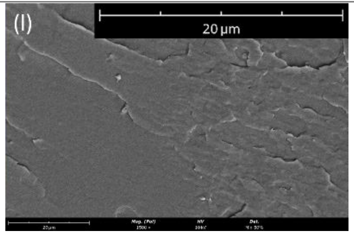		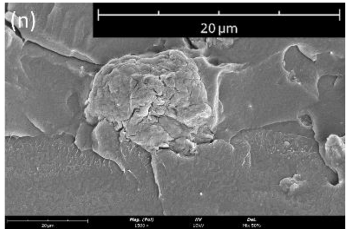	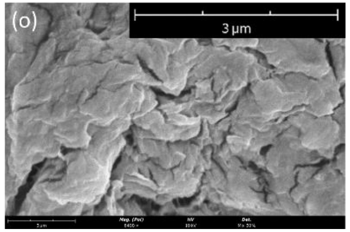
Neat PBAT		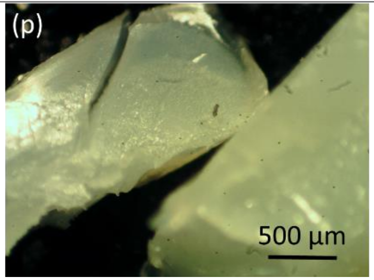	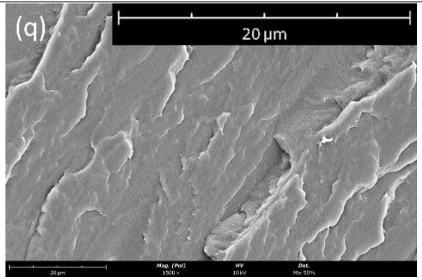		

Examining the SEM images and the optical microscopy photographs gives information on how the powders affect the interphase of the composites. Effective wetting and uniform dispersion of the reinforcements in the matrix and strong interfacial adhesion between the phases are required to obtain composites with satisfactory mechanical properties.[136] SEM images of the middle powder particles show nearly parallelepiped particles in a variable granulometry in the range of 16 µm to 157 µm. Neat PBAT presents a smooth and homogenous surface with a uniform white color observed in the optical microscopy photograph. Since banana fiber powders are totally hydrophilic in nature and PBAT is hydrophobic in nature, in theory it is expected that fiber–matrix adhesion will be poor. Composites with untreated fiber powder have a similar surface morphology as pure PBAT without any morphological difference in the nitrogen fractured surfaces with increasing powder content, with no visual agglomerates in the SEM images for the magnification chosen (1500 x, scale bar 20 µm). The only exception observed is in the optical microscope photograph of 5 wt% composite were two small dot can be distinguished with the naked eye. Meanwhile, the remaining optical microscopy photos from the untreated composites show very clean surfaces without a clear separation between filler and matrix and no holes or voids are detected. The lack of visible effect of the dispersed fiber powder might be indicative of insufficient adhesion. In the FTIR spectra no visible differences were also observed. Furthermore, with the increase in powder loadings the color of the composites only presented a mild change possibly due to a lack of interaction with the filler and the matrix.

Because treated powders were washed they had a more homogenous size particle display (from 10 µm to 85 µm) and therefore the agglomerates shown are not big particles but rather a cohesion of several particles due to a non-uniform dispersion of the powders. This is also verified in the EDS data shown in the *Figure 43* in appendix E, where the areas of agglomeration showed the presence of sodium while the clean surface did not. However, these agglomerates seem to be embedded in the polymer matrix, suggesting a good interfacial adhesion. Furthermore, they were also observed right after the extrusion of the filaments. Meanwhile, higher powder loading present some gaps in the fractured area around the agglomerates. Therefore, the used processing method (single screw extruder) was possibly not as efficient for promoting a good dispersion of the powders in the matrix as expected, which is in line with the fact that twin screw extruders in counter rotating mode are more efficient for dispersive mixing, which involves the breaking of particle agglomerates.

3.2.3. Thermal behavior analysis and thermo-mechanical behavior

Thermogravimetric and derivative thermogravimetric analysis was performed in order to study the effect of fiber powder addition on the thermal stability, thermal decomposition and structure/properties relationships of the untreated and treated composites. The composition was determined through the number of stages in the degradation curves correlated to significant mass loss and volatilization of specific components in the samples. The quantification of inorganic filler content was obtained as the residual weight at the end of the trial. This technique measures the amount and rate of change in the weight of a material as a function of temperature or time in a controlled atmosphere.[104] *Figure 29* shows the weight loss percentage over temperature and DTG curve for inner, middle and outer treated and untreated composites along with the corresponding powders.

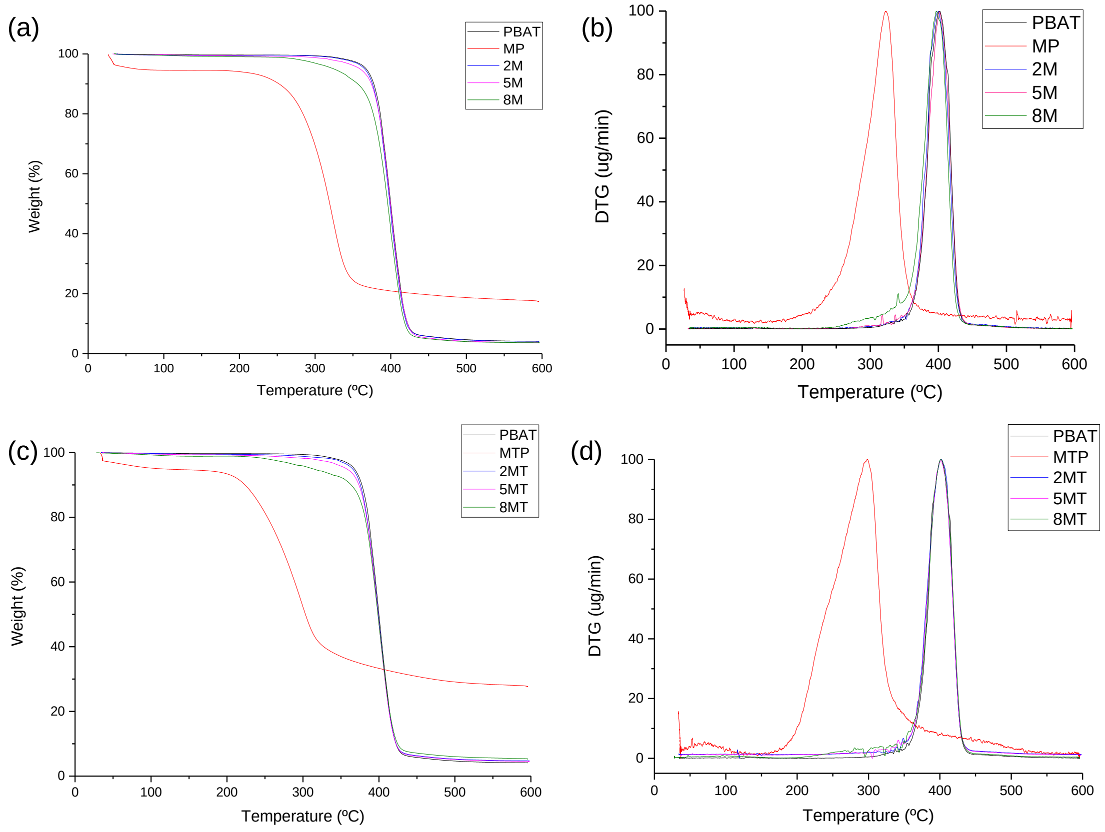

Figure 29 - (a -b) Thermogravimetric analysis (TGA) of untreated and treated middle fiber powder composites (b) Differential thermogravimetric analysis (DTG) of untreated and treated middle fiber powder composites

When looking at the curve for PBAT alone, the polymer presents one step degradation just like the powders. Furthermore, the plateau where no significant mass loss is observed (maintained between 99.89 and 99.62 %) extends to higher temperatures around 262.64 ºC when compared to the banana powders, therefore presenting a higher thermal stability and a higher maximum temperature up to which the polymers can be used without severe decomposition. The major weight loss takes place between 378 ºC and 420 ºC, with a maximum decomposition temperature at 402 ºC. Several authors reported similar temperatures and ranges for the main degradation step of the thermograms of pure PBAT. *Chang, Trinh and Mekonnen* reported the degradation of PBAT ranging from 350 to 440 ºC,[54] similar to *W. Liu et al.* and *W. Liu et al.* who observed it between 340 °C to 450 °C.[61,67] Meanwhile *Dang et al.* observed the major weight loss between 385 ºC and 395 ºC,[62] *Mohanty and Nayak* reported the initial degradation at 310.58 ºC and final degradation peak at 412°C (residue 6.5 wt%),[46] and *Kumar et al*. reported between 314.53 and 556.13 ºC (char 4.32%).[86] In regards to the main decomposition peak *Olivato et al.* observed it at 439 ºC,[60] *W. Liu et al.* at 428 °C,[67] *W. Liu et al.* at 413 ºC (with residue of 4.77% at 500ºC),[61] and *Dang et al.* at 391 and 481 °C,[62] attributed to the degradation of PBAT chains and of some additives in PBAT, respectively. The onset degradation temperatures, the maximum decomposition temperature and the residue obtained at the end of the degradation process are summarized in *Table 9* and presented in *Graphic 1* for an easier assessment.

Table 9 – Thermal decomposition parameters of PBAT and PBAT/powder blends

Composites	**T_{onset}**		**T_d (ºC)**	**Weight loss (%) at T_2**	**Residues at 600 ºC (%)**
	T_1 (ºC)	**T_2 (ºC)**			
PBAT	377.88	419.70	401.49	94.14	4.12
2 wt% Interior	376.13	420.18	401.82	94.89	3.98
2 wt% T. Interior	376.29	420.50	401.82	93.70	4.50
2 wt% Middle	376.13	417.94	400.00	95.43	4.12
5 wt% Middle	376.60	419.06	402.03	94.49	3.72
8 wt% Middle	370.99	417.78	399.53	95.64	3.63
2 wt% T. Middle	376.33	419.29	401.49	94.01	4.69
5 wt% T. Middle	376.61	419.22	401.49	94.52	4.50
8 wt% T. Middle	373.89	420.82	401.49	93.50	5.29
2 wt% Exterior	378.36	417.31	401.49	94.35	4.35
2 wt% T. Exterior	376.29	420.18	401.49	94.58	4.00

Graphic 1 - Thermogravimetric and derivative thermogravimetric analysis of PBAT and PBAT powder composites

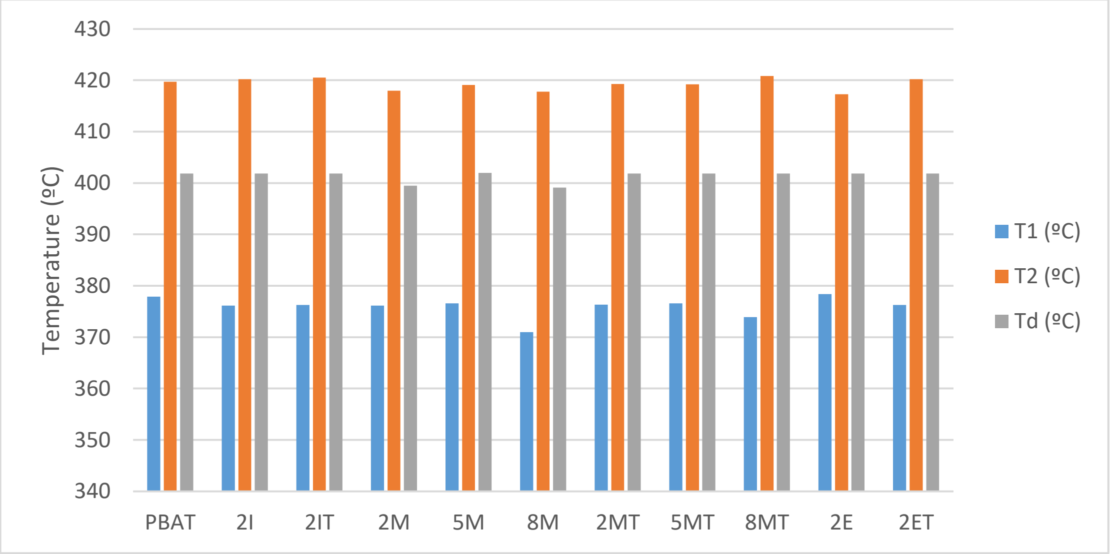

Figure 29 (a), shows the composites with middle treated and untreated fiber powders. The thermograms for interior and exterior untreated and treated composites are located in appendix D, *Figure 41*. The thermal degradation of all composites took place in one step. Just as in the case of the powders, the degradation of the composites presented an initial removal of solvents or moisture from the matrix with a weight loss between 0.80 and 1.60 % as the banana powders are hydrophilic/hygroscopic. The weight loss was slightly higher for treated composites

than untreated ones. Once again, composites with only 2 wt% had no significant or visible changes in the thermograms just like in the FTIR spectra, only at higher powder contents was there visible changes. *Ramesh, Palanikumar and Reddy* reported the same type of weight loss for epoxy reinforced with banana fiber where the initial temperature weight loss was 190ºC.[104] Meanwhile *Ratanakamnuan and Aht-Ong* observed the loss of moisture from banana starch because of its hydrophilicity at around 100 ºC,[109] and *Okafor et al*. for untreated and alkali treated banana fiber polyester resin composite between 50 to 250 ºC (15% weight loss).[99] With the addition of powders it was verified that there was a slight reduction in thermal stability as the first decomposition temperature was attained sooner than pure PBAT and the slope of weight percentage over temperature tended to be more prominent with increase in powder loading for both treated and untreated powders. This can be better observed from *Figure 40* in appendix D. This effect is more visible in the case of middle powder reinforced composites as higher weight percentages were tested. Composites prepared by *Wu* [33] with PBAT and cellulose acetate (natural fibers) also presented lower initial degradation temperatures as the content of fiber increases (up to 20 wt%). The interactions between both elements of the composite was reported to be hydrogen bonds, possibly similar bonds occur in the banana fiber powder composites.

The thermal stability of the composites was affected by the proportions of powder and PBAT. The higher weight fractions of PBAT provided the blends with higher thermal stability because of less moisture absorption and with greater weight losses taking place at higher temperatures. Similarly observed by *Dang et al.* for composites of TPS/PBAT (80/20; 50/50; 20/80 wt%),[62] by *Chang, Trinh and Mekonnen* for TPS/PBAT films (50/50; 60/40; 70/30 wt%) [54] and *Sadhasivam, Ramamoorthy and Dhamodharan* for PBAT-nano chitin nanocomposite (90/10; 70/30; 50/50 wt%).[10] Furthermore, treated composites presented a lower initial degradation temperatures than untreated composites either simply due to the fact that the powders themselves have lower initial degradation or they present lower thermal stability. *Xiong et al.* studied composites of PBAT/lignin (60/40; 50/50; 40/60 wt%) and noted that the filler could significantly decrease the thermal stability of PBAT by 10−19 °C.[11] *Kargarzadeh, Galeski and Pawlak* also reported that the introduction of kraft lignin particles in the PBAT composites lowered the initial decomposition temperature.[31] Meanwhile, *Okafor et al.* reported opposite results where the alkali treated with 5% NaOH at 30ºC for 1 h banana fiber composite joined with polyester resin tended to be more thermally stable due to the removal of organic impurities on the surface of the fiber than the untreated composites.[99]

The stage where the decomposition takes place at a much faster rates started over the temperature range of 370 to 377 ºC for all composites. This step was assigned to degradation or volatilization of the matrix along with the powder contents (hemicellulose, lignin, cellulose, pectin, waxes and oils or just cellulose and residues) present in the composite resulting in an average weight loss of 94.89, 93.70, 95.19, 94.01, 94.35 and 94.58 % for interior untreated and treated, middle untreated and treated and exterior untreated and treated composites, respectively. As the untreated powder possess higher lignocellulosic contents, its weight loss is greater (no removal was previously performed with treatment). *Ramesh, Palanikumar and Reddy* also observed the initial major weight loss around 380 ºC for a banana fiber resin composite.[104] *Ratanakamnuan and Aht-Ong* studied a LDPE film with different amounts of banana starch which showed a the major weight loss at around 450 ºC due to the complete thermodegradation of the LDPE backbone.[109]

The final stage is the carbonization phase and it takes place after around 417 ºC and goes up to 600 ºC where what is left is the ash content (around 4 %). The addition of interior treated, middle treated and exterior powder in the pure polymer increased the amount of residue after the major thermal degradation stage due to the decomposition of some powder components that have degradation temperatures over 600 °C as seen by the thermograms of the pure middle powders. Meanwhile, for untreated interior and middle composites and treated exterior composites the opposite occurred. When comparing the residue results from the middle composites and the powders, the values were higher for treated than for untreated composites just as in the case of the powders. *Ratanakamnuan and Aht-Ong* also attributed the higher residues percentage left at 550°C to residue left by the banana starch.[109] *Dang et al.* studied blends of PBAT/HNTs that similarly had higher residual weight in the nano-biocomposites because of the presence of thermally stable HNTs inorganic material,[62] and *Xiong et al.* studied composites of PBAT/lignin which yielded significantly higher residual masses at 600 °C due to the filler.[11] *Kargarzadeh, Galeski and Pawlak* attributed the 3% increase in ash residue at 600 ºC for PBAT due to lignin content.[31]

Finally, the maximum decomposition temperature of the composites either maintained the value presented by pure PBAT or was slightly lowered possibly due to the hydrophilic nature of the powders or low interactions between the filler and the matrix as reported by *Mohanty and Nayak* for PBAT/TPS blends (4ºC lower) since TPS is also hydrophilic in nature,[46] and *Dang et al.* for PBAT/HNTs composites (unchanged) due to low interaction and a rather poor affinity.[62] *Kargarzadeh, Galeski and Pawlak*reported a slight reduction of T$_{max}$ due to the presence of KLPs presence in the composites.[31] Nevertheless, the decrease was very insignificant as the weight percentages tested were very small. Meanwhile, *Ratanakamnuan and Aht-Ong* observed no interference of banana starch in the T$_d$(onset) temperature for their composites.[109] *Table 10* presents the summary of the thermal behavior of the articles mentioned in the analysis above.

Table 10– Thermal behavior of either banana fiber, LDPE or PBAT blends from the literature

Sample		**ΔT (ºC)**	**T$_d$ (ºC)**	**Weight loss (%)**	**Residue (%)**	**Ref**
30 wt% BaF/polyester resin (5% NaOH)	1st stage	50 - 250		15		99
	2nd stage[a]	250 - 500		85		
	2nd stage[b]	250 - 450				
LDPE/ 5% banana starch	1st stage	100	-	0.02 (120 ºC)	3.31 (550 ºC)	109
	2nd stage	290 - 300	295	1.65 (350 ºC)		
	3rd stage	450	451.1	15.87 (450 ºC)		

Sample		ΔT (ºC)	T_d (ºC)	Weight loss (%)	Residue (%)	Ref
LDPE/ 10% banana starch	1st stage	100	-	0.22 (120 ºC)	3.96 (550 ºC)	[109]
	2nd stage	290 - 300	295.2	5.30 (350 ºC)		
	3rd stage	450	451.6	18.35 (450 ºC)		
PBAT/Lignin 60/40 wt%	1st stage	363.36			20.6	[11]
PBAT/CLA	95/5 wt%	405				[33]
	90/10 wt%	388				

a – treated; b – untreated

Dynamic mechanical analysis (DMA) presents enormous potential and reliability as one of the most important thermal analysis techniques. Its uniqueness is based on the capacity to monitor separately the elastic and viscous response of a sample under an oscillating load against time, temperature, or frequency of oscillation. [121] Therefore, the storage modulus (G′) that represents the elastic response of the sample, can be expressed as an in-phase component, while the loss modulus (G″) that characterizes the viscous response of the sample, can be expressed as an out-phase component, being Tan δ a measure of the capacity of the sample to dissipate energy (ratio G″/G′), namely damping capacity.[121] The latter informs us on how good a material will be at absorbing energy. Hence, DMA easily and accurately characterizes important relationships between the macroscopic properties, including the mechanical and thermal properties associated to the viscoelastic behavior, conformational changes, and microscopic rearrangements at the molecular level of the composites allowing to infer the structure/properties correlations.[121]

This technique was used to study the effect of fiber powder loading on the mechanical and thermal properties of the reinforced composites while also evaluating the morphology, visco-elastic properties and the interfacial interactions of the materials by measuring the stiffness and damping of the sample in terms of modulus and Tan δ.[104121] These properties can alter according to the nature of the matrix material, the chemical and physical nature of the fiber powder, the distribution of the reinforcing powder, the nature of the powder–matrix interfaces and the interphase region. The G′ and G″ values, with T_g for neat PBAT and the composites are listed in *Table 12* for comparison purposes along with the graphical representation for an easy analysis in *Graphic 2*. Furthermore, *Figure 30* shows the storage modulus, *Figure 31* the loss modulus and *Figure 32* the damping peaks of neat PBAT and PBAT/powder blends.

Table 11– Storage modulus G' (at -45 ºC and 35 ºC), glass transition temperature Tg and loss modulus G″ of neat PBAT and PBAT/powder blends.

Composites	G′ (MPa) at -45 ºC	G′ (MPa) at 35 ºC	T_g (ºC)	G″ (MPa)
PBAT	2447.2	68.6	-21.72	305.0
2 wt% Interior	2272.6	68.6	-20.47	295.0
2 wt% T. Interior	2063.0	49.5	-19.66	282.4
2 wt% Middle	2151.9	55.9	-20.25	263.4
5 wt% Middle	2393.3	74.9	-18.74	310.0
8 wt% Middle	2229.2	74.9	-19.44	311.3
2 wt% T. Middle	2291.7	74.9	-19.57	310.3
5 wt% T. Middle	2529.0	82.3	-18.69	340.6
8 wt% T. Middle	2658.5	105.2	-18.87	351.5
2 wt% Exterior	2498.5	82.3	-20.21	330.3
2 wt% T. Exterior	3293.8	150.4	-19.85	458.8

Graphic 2 - Storage modulus G' (at -45 ºC and 35 ºC), glass transition temperature Tg and loss modulus G″ of neat PBAT and PBAT/powder blends

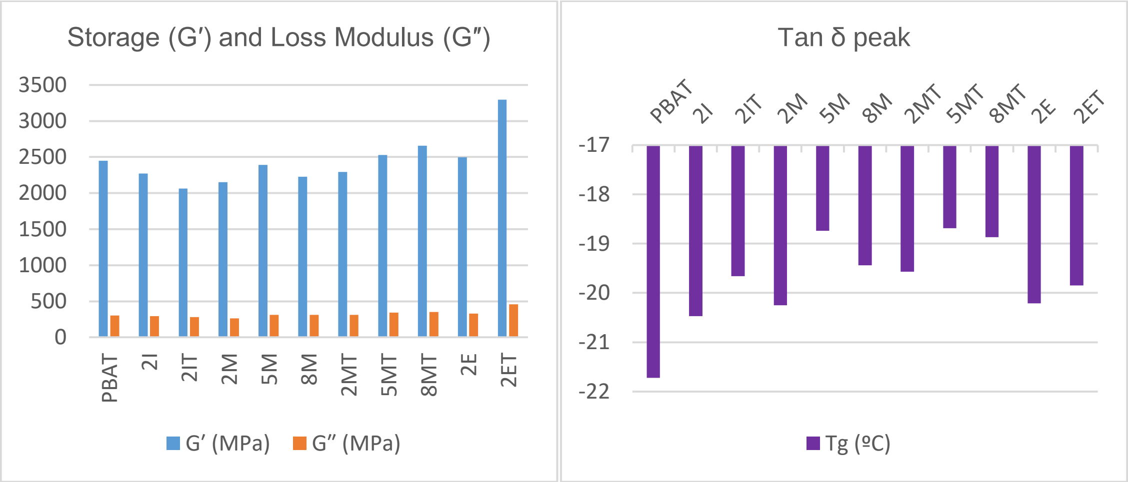

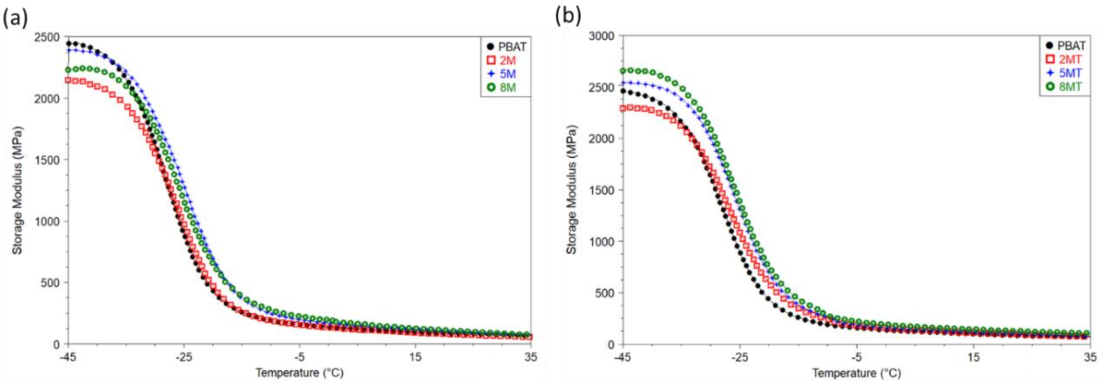

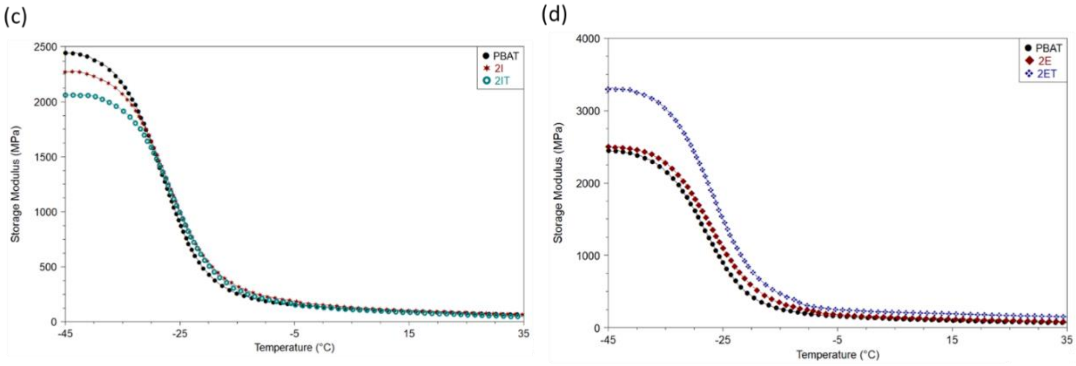

Figure 30 - Effect of powder loading and alkali treatment with temperature on the storage modulus of neat PBAT and PBAT composites for (c) interior, (a-b) middle and (d) exterior fiber powders in the temperature range of -45 ºC to 35 ºC

Figure 30 shows the evolution of storage modulus (G′) as a function of temperature from -45 ºC to 35 ºC for all untreated and treated composites. All curves present typical behavior of a semi-crystalline polymers with three distinct regions, before the melting stage: an elastic plateau or glassy region, a glass transition region, and a rubbery plateau. In the first region, almost all untreated composites had lower storage modulus values when compared to PBAT. The exception to this case was 2 wt% untreated exterior powder composite, where the value of G' increases from 2447.2 MPa for neat PBAT to 2498.5 MPa, respectively. Meanwhile in the case of treated composites, middle 5 and 8 wt% and exterior 2 wt% presented superior values of storage modulus compared to pure PBAT. Furthermore, all curves maintained this tendency over the entire experimental temperature range. Only 2 wt% middle treated presented values below PBAT for the glassy region. These values increased from 2447.2 MPa for neat PBAT, to 2529.0 MPa, 2658.5 MPa and the highest registered value 3293.8 MPa for treated middle 5 and 8 wt% and exterior 2 wt%, respectively. The increase in G' denotes the enhanced stiffness of the material with incorporation of the fiber powders which reduces the viscous constituent imposing a restriction on the molecular motion. Furthermore, this increase can also be attributed to a proper/uniform powder dispersion in the PBAT matrix and consequently a good PBAT-powder interaction. However, when observing the SEM and optical microscopy images, composites with 5 and 8 wt% treated middle powder have visible agglomeration of powders, therefore these agglomerates did not negatively affect the dynamic properties of the composites. Meanwhile, composite with 2 wt% exterior treated powders were not observed in SEM and optical microscopy images did not reveal any major differences between the treated and untreated composites (*Figure 44* in appendix E). However, these treated composites might present a better dispersion, lower agglomerates and enhanced intermolecular interactions as they present an extremely high storage modulus (enhancement of 134.6 %). *Kargarzadeh, Galeski and Pawlak* observed that composites of PBAT reinforced with kraft lignin particles (wide distribution of particle sizes ranging from 6 to 150 μm) had higher storage modulus values in the glassy state when compared to neat PBAT, and these values increased with higher amounts of filler content (up to 6 wt%).[31] This enhancement was also due to a stiffening effect or the reinforcement with an increase in uniform dispersion of the particles in the matrix and desirable intramolecular interaction such as hydrogen bond, and π-π interaction between aromatic structures in lignin and PBAT.

In all thermograms storage modulus decreases with increasing temperature. Even with the imparted stiffness from the incorporation of powders, the increasing temperatures will reduce said stiffness. The sharp decline is due to the increase in molecular mobility after passing the glass transition temperature (T_g). However, this drop is less prominent for 5 and 8 wt% of untreated middle powder, 2, 5 and 8 wt% of treated middle powder and 2 wt% untreated and treated exterior powder composites. Meanwhile, the curves with less pronounced slopes for each category are the 5 wt% for untreated middle powder, 8 wt% for treated middle powder and 2 wt% for treated exterior powder composite. Hence, the treated composites presented better results for the reinforcing effect of powders on the modulus above the glass transition temperature (T_g).

Finally, in the rubbery plateau composites with untreated interior powders presented the same values for the modulus as neat PBAT while treated had slightly lower values. All composites with middle powder, with the exception of 2 wt% untreated, presented higher G′ values when compared to pure PBAT. Meanwhile, for exterior powders both untreated and treated had higher values than neat PBAT. At 35 ºC, i.e., above T_g region, the G′ for neat PBAT goes from 68.6 MPa to 105.2 MPa and 150.4 MPa for 8 wt% middle treated powder and 2 wt% exterior treated powder, respectively. The improved modulus above the glass transition temperature (T_g) shows the high temperature utility of the material. Thus, composites with 5 and 8 wt% treated middle powder and 2 wt% exterior treated and untreated were the only samples with a higher storage modulus over the entire temperature range tested. *Ramesh, Palanikumar and Reddy* and *Tavares et al.* also reported a positive impact on the storage modulus value over the entire temperature range tested for epoxy reinforced with banana fiber (up to 31 wt%) [104] and PBAT/kraft lignin blends (up to 10 wt%) [30], respectively. For the fiber reinforcement this enhancement was attributed to an increase in stress transfer at the fiber interface or due to the interference of neighboring chains that promoted greater molecular cooperation to allow the relaxation process to occur. For the kraft lignin a proper dispersion and intermolecular interaction of the filler with the matrix such as π hydrogen bonding between the hydroxyl group of lignin and the aromatic ring of PBAT, as well as π-π complex between aromatic structures in lignin and PBAT.

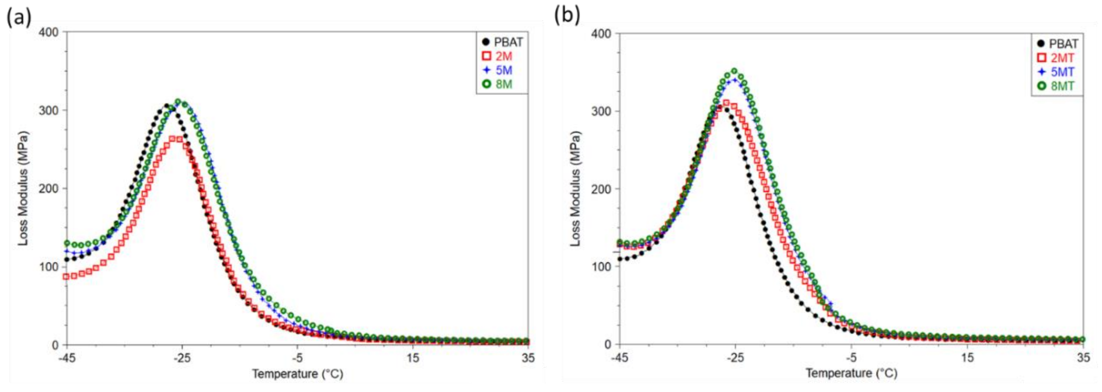

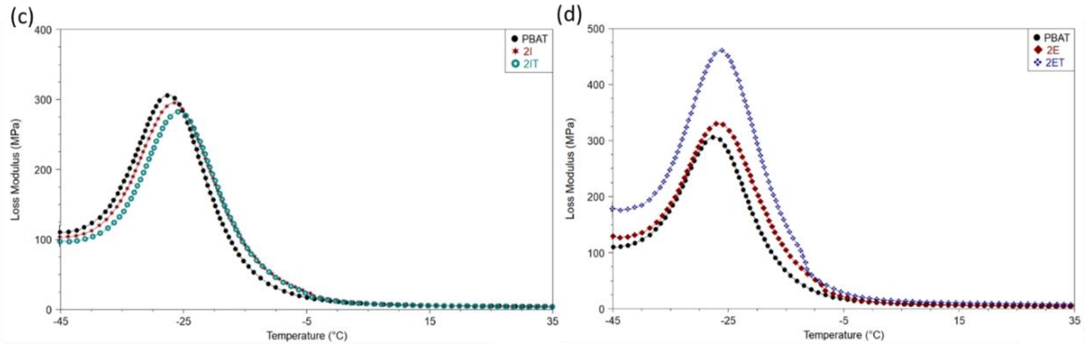

Figure 31 - Effect of fiber loading and alkali treatment with temperature on the loss modulus of neat PBAT and PBAT composites for (c) interior, (a-b) middle and (d) exterior fiber powders in the temperature range of -45 ºC to 35 ºC

When observing the loss modulus for the untreated middle composites, 5 and 8 wt% were overlapped, had the same band width, presented slightly higher values of G″ and were shifted to higher temperatures when compared to pure PBAT. The composite with 2 wt% was the only one that had a lower G″ and a thinner band. Regarding the treated middle composites, the height of the peaks and therefore the loss modulus increased with powder loading. All composites presented wider bands when compared to neat PBAT and the peaks were once again shifted to higher temperatures. Composites with 8 wt% treated middle powders had the highest loss modulus value at 351.5 MPa. Furthermore, considering the composites with interior and exterior powders it is clear that the exterior samples had more promising results. For interior powders the treated composite presented lower values of G″, lower band width and higher temperature shift. Meanwhile, exterior powders had better results for the treated composites as they present values up to 458.8 MPa, very wide band and a slight temperature shift. The broadening of the peaks emphasizes the enhanced adhesion between the powders and the matrix. Just like in the storage modulus, composites with 5 and 8 wt% for treated middle composites and 2 wt% treated exterior composite presented the best results. *Kargarzadeh, Galeski and Pawlak* observed that composites had higher loss modulus peaks with increasing lignin content indicating higher dissipative energy through internal molecular motion and higher viscose response.[31] Moreover, they also attributed this phenomena as possible increase in friction between KLPs and PBAT matrix during cycling loading. *Tavares et al.* indicated that the shift of the loss modulus peak for higher temperatures and the presence of a single peak for the blends indicate miscibility between the biopolymers of lignin and PBAT.[30]

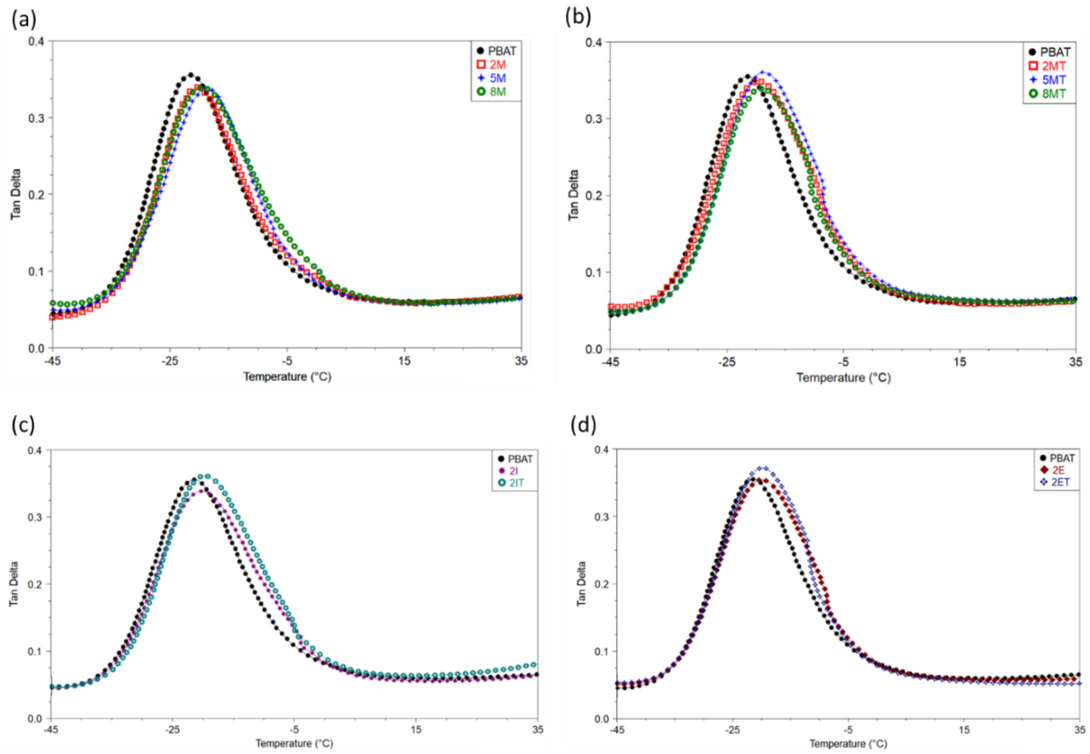

Figure 32- Effect of fiber loading and alkali treatment with temperature on the tan δ peaks of neat PBAT and PBAT composites for (c) interior, (a-b) middle and (d) exterior fiber powders in the temperature range of -45 ºC to 35 ºC

PBAT has been reported to present two distinct T_g values in the tan δ curve. The primary transition is detected at about – 20 ºC, due to the motion of the poly(butylene adipate) unit, associated to the glass transition temperature, whereas the secondary transition was noticed at 62 °C or 35 ºC corresponding to the relaxation of the relatively stiffer terephthalate unit. [38,148,149] From *Figure 32* it is evident that the glass transition temperature of PBAT is located at around -22 ºC, similar to the values reported in the literature. Furthermore, when observing the tan δ of PBAT a small indentation is perceived at about 44.2 ºC, between the values stated from the previous authors. However, for the sake of an easier comparison of the behavior of the composites the temperature range chosen went from -45 ºC to 35 ºC just as in the storage and loss modulus.

When observing the tan delta peak for the untreated banana fiber powder composites, it is evident that they presented a slight shift to higher temperatures and had lower and broader peaks when compared to pure PBAT (2 wt% untreated middle composite was the exception). This decrease in the damping peak is expected as the volume fraction of the matrix is lowered with the incorporation of the powders. Furthermore, the broadening of the band indicates a decrease in stress transfer from the powder to the matrix and possibly a higher agglomeration and interaction between the powders, revealing a higher heterogeneity of the composite material. Meanwhile, the positive shift in temperature is indicative of the effectiveness of the powder as a reinforcement/filler. Regarding the treated banana fiber powder composites, almost all presented an increase in the damping peak (except 2 and 5 wt% treated middle composite), with a positive shift in temperature and broader peaks when compared to neat PBAT. Once again, the positive shift indicates the decreased mobility of the polymer chains with the addition of powders, and that shift is more prominent when compared to the untreated composites. *Tavares et al.* detected an increase in Tg with the addition of lignin (up to 10 wt%).[30] This increase was due to the high glass transition temperature of lignin resulting from its aromatic structure. Meanwhile, *Kargarzadeh, Galeski and Pawlak* perceived slightly shifted to lower temperatures for the Tg due to the liberation effect of the KLPs enhancing the chain mobility of the amorphous regions of PBAT composites in the vicinity of KLPs particles.[31] Finally, *Ramesh, Palanikumar and Reddy* reported that the incorporation of banana fiber in epoxy as reinforcements had a lowered but broader loss modulus and a positively shifted lower damping peak, emphasizing the improved fiber/matrix adhesion.[104]

3.2.4. Mechanical tests

The tensile tests were performed to attain the mechanical properties of PBAT and PBAT/powder blends allowing to compare the results for: the ultimate tensile strength (UTS, maximum stress the test specimen can take until failure) and the nominal strain at failure or elongation at break (ε_B),

The Young's Modulus, the yield strain, the yield strength and modulus of resilience were not considered for the analysis and comparison of the PBAT/powder blends as the stress-strain curves did not present a linear behaviour in this region, resembling an elastomer. Therefore the data obtained was incoherent. *Table 12* and the graphic representation of the data summarizes the tensile strength and elongation at break values for PBAT and PBAT/powder blends. Furthermore, *Figure 33* shows the representative stress-strain curves obtained for the treated and untreated composites.

Table 12– Tensile strength and elongation at break of PBAT and PBAT/powder blends

	Tensile strength (MPa)		**Elongation at break (%)**	
Composites	**Average**	**SD**	**Average**	**SD**
PBAT	19.11	0.24	646.60	3.59
2 wt% Interior	18.44	1.31	550.37	5.94
2 wt% T. Interior	17.55	0.70	538.44	16.49
2 wt% Middle	16.03	0.73	573.76	40.30
5 wt% Middle	13.94	0.31	442.37	2.02
8 wt% Middle	13.20	0.62	244.82	10.49
2 wt% T. Middle	15.86	0.46	487.16	7.22
5 wt% T. Middle	14.12	0.41	354.84	11.07
8 wt% T. Middle	11.51	1.00	334.11	8.68
2 wt% Exterior	18.10	0.23	573.44	3.14
2 wt% T. Exterior	18.17	0.36	594.48	4.66

Graphic 3 - Tensile strength (MPa) and Elongation at break (%) for PBAT and PBAT/powder blends

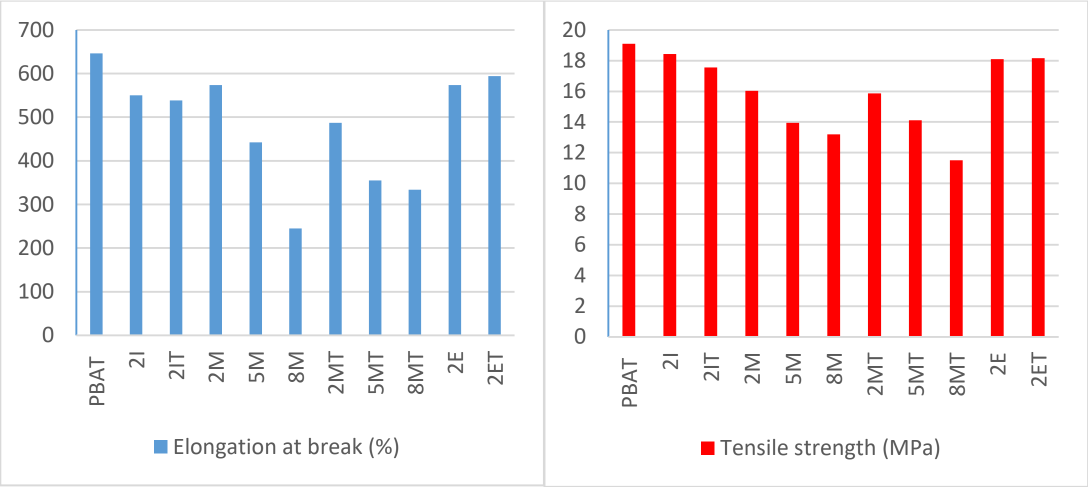

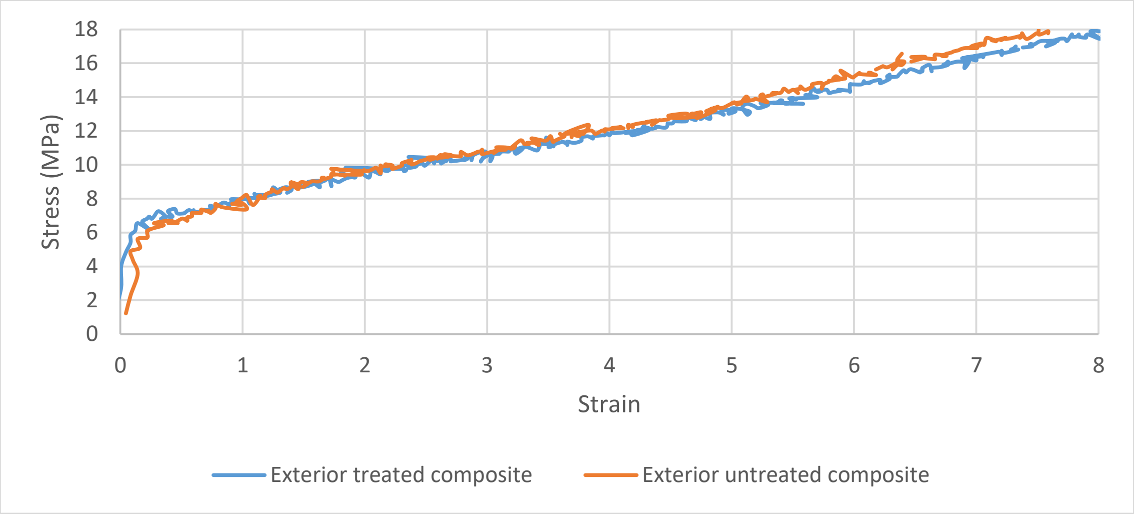

Figure 33 - Representative stress-strain curves for exterior untreated and treated composites

Neat PBAT is highly ductile due to its high value of elongation at break. With the introduction of the powders both tensile strength and elongation at break tended to be lower. For interior powders composites, the treated composites presented a decrease in tensile strength and elongation at break when compared to the untreated composites. This is indicative that the powders might have acted as points of failure. *Pinheiro, Morales, and Mei* observed similar results in biocomposites prepared with treated and untreated Munguba fibers in a PBAT matrix.[34] No significant improvement in mechanical properties were obtained when compared to natural fiber. They attributed these result to the partial modification of the fibers, which was insufficient to increase the fiber/ matrix interactions.

Meanwhile, when observing middle treated and untreated composites it is evident that with increase in powder loading both tensile strength and elongation at break decreased, being the reduction in tensile strength more significant in the treated composites while the decrease in elongation is more prominent in untreated composites. These values went from 16 MPa to 13 MPa, and from 574 % to 245 % for untreated composites, while for treated composites they varied from 16 MPa to 11 MPa, and from 487 % to 384 %. The decrease in tensile strength could be explained by the formation of agglomerates when higher quantities of powder content were employed in the blends that can cause a premature rupture of the materials. This poor dispersion incapacitated the stress transfer to occur properly in the particle-polymer interface, concentrating its effect in the continuous phase around the powder particles. This was also evident in the SEM images, where the treated composites presented visible aggregates of powders on the nitrogen-fractured surface while the untreated composites had a cleaner surface morphology. Meanwhile, since the elongation also depends on state of the interface, its decrease suggests that there was a poor adhesion of the untreated powders with the PBAT matrix as these powders are hydrophilic and the matrix is hydrophobic rendering them immiscible and compromising the ductile matrix, also in agreement with SEM and FTIR spectra. *Ratanakamnuan and Aht-Ong* studied the starch content effect on the tensile properties of LDPE blends and reported that both tensile and elongation at break decreased with increasing amounts of starch.[109] *Wu* studied blends of PBAT with cellulose acetate up to 20 wt% content. Both tensile strength and elongation at break decreased markedly and continuously with increasing CA content, due to the poor dispersion and compatibility (forming bundles) of the cellulose acetate in the PBAT matrix.[33] *Xiong et al.* also reported that the presence and increased content of lignin particles decreased the mechanical properties of the PBAT blends, as these particles had limited compatibility and poor adhesion promoting an interruption in the continuous PBAT matrix, which promoted to stress concentration effects.[11] One interesting study presented by *Kargarzadeh, Galeski, and Pawlak* described that the simple addition of 0.5 wt% of KLPs, increased tensile strength, strain at break, and modulus of the PBAT by 30%, 38.7%, and 29% respectively.[31] Meanwhile, at 6 wt% both tensile strength and elongation at break reduced dramatically. They attributed these results to closer packing of KLPs at higher concentrations.

Lastly, exterior treated composites present slightly higher values for elongation at break, from 573 % to 594%, and almost unchanged values for tensile strength, from 18.10 MPa to 18.17 MPa, when compared to untreated composites. However, no significant changes can be seen in the optical microscopy photographs to infer if the powders are well dispersed (*Figure 44* in appendix E), one can only assume. *Motaleb, Mizan, and Milašius* also reported that the tensile strength, elongation at break and Young's Modulus had higher values for outer bark nonwoven and lowest for inner bark nonwoven.[108] This was to be expected as outer bark layer of the pseudo-stem are harder and the fibers extracted present higher strength. Meanwhile, *Pinheiro, Morales, and Mei* proposed that the increase in elastic modulus and tensile strength while the decrease in elongation at break of Munguba fibers was due to the increase in stiffness of the mercerized fiber as the amorphous fraction of cellulose was removed.[34] *Table 13* summarizes the mechanical properties of the studies reported above in the analysis.

Table 13 – Mechanical properties of LDPE or PBAT blends with banana fibers or other natural fibers and fillers from the literature

Sample		**Elastic Modulus (MPa)**	**Tensile Strength (MPa)**	**Elongation at break (%)**	**Ref**
PBAT/ Resyflex®/ Munguba fiber 80/10/10 wt%	Treated*	94	9	316	34
	Untreated	87	10	349	
PBAT/Cellulsoe Acetate 95/5 and 90/10 wt%	95/5		11	670	33
	90/10		9	600	
PBAT/ Kraft Lignin 94/6 wt%		225	17	545	31
Non-woven banana fibers**	IB	67	1.23	3.82	108
	MB	165	6.33	9.65	
	OB	215	8.56	12.56	
LDPE/Banana Fiber 50/50 wt%		155.39	9.056		100
LDPE/Banana Starch 80/20 wt%			12	100	109

1. *mercerization (2% NaOH, 30 mins) and acetylation (glacial acetic acid and acetic anhydride 1:1.5, 95ºC, 2h)
2. **IB: inner bark;MB: middle bark;OB: outer bark - Treated with 15% NaOH at 90ºC

3.2.5. Water absorption

The water absorption behavior of the untreated and treated composites along with the fiber content was studied and the results are shown in *Figure 34* and sumarized in *Table 14*. The tests were done over a peroid of 8 days and samples were weight in a specific order to minimize errors. In theory, the treated powders joined with the PBAT matrix should minimize the absortion of water as the alkali treatment replaces hydroxyl groups with sodium. However, when observing the values and the graphs, it is evident that only the exterior treated composite had better results than the untreated exterior composite. On the other hand, the composites probably had better chemical linkage or improved adhesion between the treated powders and the PBAT matrix with a proper dispersion of powders which reduced the microvoids formation. This could only be confirmed if observed in SEM. Furthermore, in all cases, after just 2 days of imersion the results show how hydrophilic the composites are and how they tend to absorb water, attaining a maximum and then maintained its value after 5 days to 8 days on average. In addition, when observing the results for middle treated and untreated composites, it is apparent the water absorption capacity of the composite increased by increasing powder loading from 2 to 8 wt %. One theory proposed by Cassie–Boxter theory on Lotus effect mentions that that the rougher the surface the more air-trap on the contact area between surface and water promoting a more hydrophobic effect.[108] However, when observing the SEM images it is apparent that the untreated middle composites presented the same type of surface roughness while the treated middle composites had an increase due to the appearance of agglomerates. Therefore, the water absorption capacity of the composites is mainly due to the increase in powder loading as they possess cellulose as the main constituent which is comprised of free hydroxyl groups that create hydrogen bonds with the water molecules. Meanwhile, treated composites presented higher water absprtion due to the formation of agglomerates that lead to the apperance of microvoids. *Wu* also reported that with the increase in cellulose acetate in a PBAT/CLA blend, from 10 to 20 wt%, the percent water gain increase.[33] This was attributed to the decrease in chain mobility of the presumably random polymer chain arrangement in these systems with greater amounts of CLA, while also presenting contribution from the hydrophilic character of CLA, which adheres weakly to the more hydrophobic PBAT.

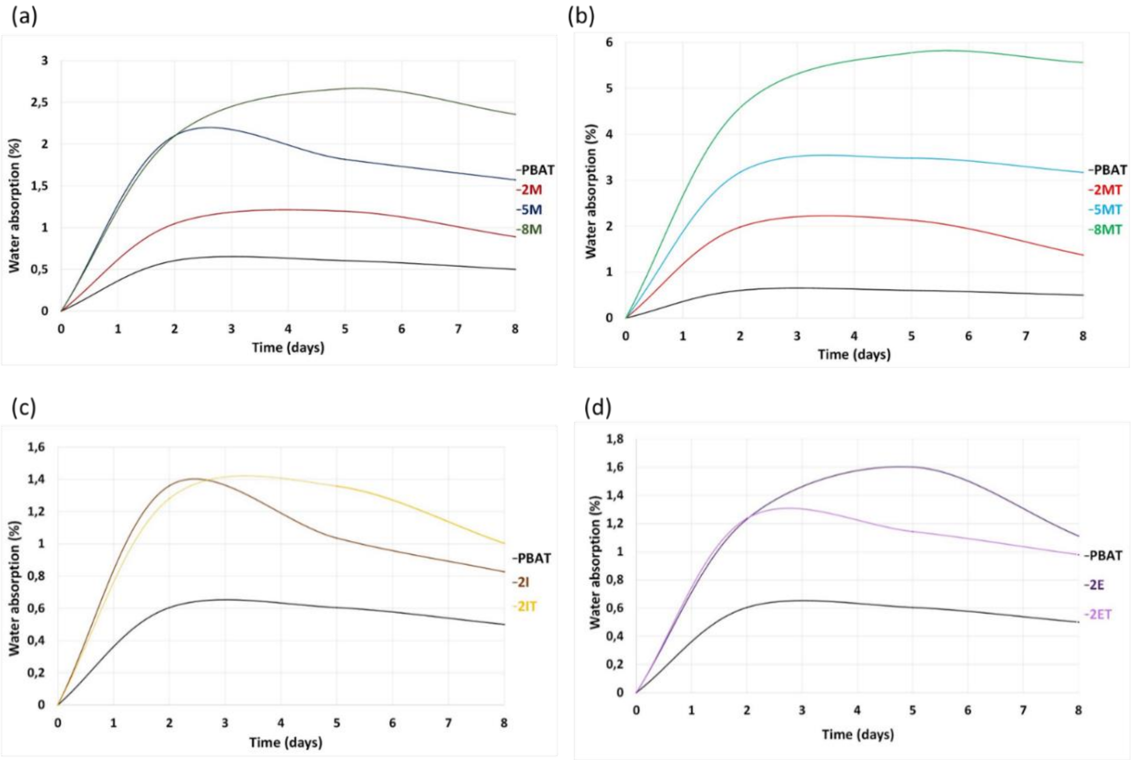

Figure 34 – Water absorption behavior of neat PBAT and (a) untreated middle composites, (b) treated middle composites, (c) untreated and treated interior composites, (d) untreated and treated exterior composites

Table 14– Water absorption values along with standard deviation for 2, 5 and 8 days for PBAT and PBAT/powder blends

Days	**2**		**5**		**8**	
Composites	**Average**	**SD**	**Average**	**SD**	**Average**	**SD**
PBAT	0.60	0.0	0.60	0.0	0.50	0.1
2 wt% Interior	1.36	0.2	1.04	0.1	0.83	0.1
2 wt% T. Interior	1.28	0.1	1.36	0.2	1.00	0.0
2 wt% Middle	1.05	0.0	1.20	0.2	0.89	0.2
5 wt% Middle	2.10	0.2	1.82	0.1	1.57	0.2
8 wt% Middle	2.10	0.1	2.66	0.2	2.36	0.2
2 wt% T. Middle	1.98	0.2	2.13	0.4	1.37	0.2
5 wt% T. Middle	3.18	0.6	3.48	0.3	3.17	0.2
8 wt% T. Middle	4.58	0.1	5.78	0.4	5.57	0.1
2 wt% Exterior	1.23	0.2	1.60	0.1	1.11	0.1
2 wt% T. Exterior	1.24	0.2	1.14	0.1	0.98	0.1

3.2.6. 3D printing of extrudates

Fused Deposition Modelling (FDM) has attracted a lot of attention in the last year as a 3D printing technique that enables the manufacture of macroscopic well-defined, spatially resolved objects from a 3D digital model data.[122,150] The main advantages of the use of this technique include shortening the design-manufacturing cycle through high speed production, minimizing the cost for low production runs, being able to build intricate geometries and complex shapes, reducing the production waste, tailoring the microstructure and properties in each layer, not employing health concerning solvents or glues and providing high value to research applications. [150151152] The basic functioning of FDM lies on the deposition of viscous thermoplastic materials layer-by-layer through a heated nozzle onto a platform or over previously printed layers.[151] The printing process depends on a series of factors, namely extruder-related (filament width and nozzle diameter), process-related (processing temperatures and printing speed) and structural parameters (patterning of the deposited material onto the workspace).[152]

Moreover, this process allows to use a wide range of materials making it one of the most commonly employed additive manufacturing technique today.[150] These materials can vary from neat thermoplastics to composites and even biocomposites, mainly in the form of discontinuous fibers or powder-like reinforced polymer. [150151] However, the latter present some restricting factors due to the incorporation of plant fibers or powders that influence the mechanical properties according to the fiber type, orientation/size of particles, geometry, content, dispersion, crystallinity, aspect ratio (length/diameter) and quality of interface between the reinforcement and the polymer matrix.[150151] Therefore, the choice of the polymer matrix is a key point for obtaining high quality manufactured final product, preferentially polymers that don’t need high processing temperatures to preserve the properties of the plant walls.[150] *C. Badouard, et al.*[150] reported that

PBAT appeared to be a suitable candidate for 3D printing of biocomposites with flax fibers due to its flexibility, the possibility of enabling higher loadings (up to 30 wt%) and having a relatively low melting temperature (around 115 ºC).

As proof of concept, some attempts were made to print a bunny with the extrudates obtained in this thesis, as shown in *Figure 35*. In both attempts the printing was interrupted as the filament presented some small variations in diameter and clogged the equipment. However, when handling the most printed sample, a good movement and malleability was apparent in the reticulated joined regions between each small section of the bunny, suggesting the high potential of this material for 3D printing.

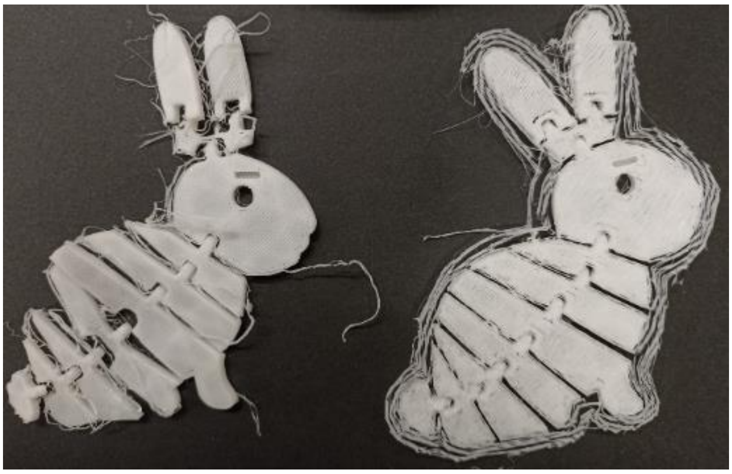

Figure 35 – 3D printed bunnies with PBAT extruded filament

Concluding remarks

The goal of this thesis consisted in developing and characterizing a high end value product made of PBAT, a biodegradable polymer and agro-food waste left over from the banana production. This polymer was chosen due to its similarity to an extremely used commodity plastics, LDPE. Even though PBAT is biodegradable, tough and thermally stable polymer, it still possesses some shortcomings such as its high production cost and low physical and mechanical resistance in comparison to non-biodegradable polymers. Therefore, when blended with other materials to form a composite, it offers the possibility to adjust the cost-performance balance and fulfill the specific properties needed for a given application. Several approaches have been stated in the literature for blends with various types of additives and other biopolymers.

The choice of reinforcement/filler was directed towards agro-food waste. The banana fibers from the pseudo-stem were ellected as excellent candidates due to their high cellulose content, high tensile and flexural strength, high stiffness and low microfibrillar angle (11°). These fibers were extracted from three different parts of the pseudo-stem, dried, grinded and subject to carefully designed treatments, before blended, by extrusion, with PBAT pellets with different powder loadings (2,5 and 8 wt%). A known economical and effective chemical treatment, *i.e.* alkali treatment, was performed to enhance the interfacial bonding with the PBAT matrix. Fibers, fiber powders and PBAT blends were characterized by scanning electron microscopy (SEM), optical microscopy, Fourier transform infrared (FTIR) spectroscopy, thermogravimetric and derivative thermogravimetric analysis (TGA/DTG), water absorption, dynamic mechanical analysis (DMA), and tensile tests to analyze the chemical and morphological structure changes, the thermal, mechanical and dynamic mechanical behavior.

To better outline all the observations stated along the analysis of the thesis, a small list with the essential results is presented below:

- All three categories of banana fiber powder extracted from the three types of sheaths of the pseudo-stem (interior, middle, exterior) presented evidence of a successful alkali treatment, where the OH band had a reduction in intensity (enhanced hydrophobicity) and peaks at 1735 cm^{-1} and 1245 cm^{-1} either disappeared completely or reduced their intensity due to the effective removal of lignocellulosic components.
- Untreated middle powders presented a higher thermal stability and maximum decomposition temperature but had a higher char content at 600 ºC in comparison to middle treated powders (flame retardant behavior).
- All extruded composites had good surface quality with no entanglements or twists but middle treated composites displayed visible aggregates that increased in quantity with the content of powder.
- The only changes in the infrared spectra with respect to the composites was seen in treated middle composites with 5 and 8 wt% where the increase in powder load promoted an OH band formation and a shoulder that appeared at 1730 cm^{-1}.
- SEM images and optical microscopy photographs revealed that untreated middle composites had similar surface morphology as pure PBAT, regardless of the powder

content. Meanwhile, treated middle composites exhibited agglomerates that were embedded in the polymer matrix. Higher powder loads displayed more aggregates.

- Untreated middle composites presented a higher thermal stability and maximum decomposition temperature but had a higher char content at 600 ºC in comparison to treated middle composites, in line with what was observed for the corresponding fibres.
- All composites present typical behavior of a semi-crystalline polymer. Treated middle composites with 5 and 8 wt%, and treated exterior composites with 2 wt% presented superior values of storage modulus compared to pure PBAT over the entire experimental temperature range. Composites with 8 wt% treated middle powders and 2 wt% treated exterior powders had the highest loss modulus values, wide bands and a slight temperature shift to higher values. Treated composites presented a more prominent positive shift in the damping (tan δ) peaks than untreated composites.
- Treated composites presented a higher reduction in tensile strength values, while untreated composites had a more significant decrease in elongation at break. Only exterior treated composites presented higher values of both tensile strength and elongation at break than exterior untreated composites.
- The water absorption behavior demonstrated that only exterior treated composites had a lower tendency to absorb water then the untreated counter parts.

Overall, middle treated composites presented an interaction between the fillers and the polymer matrix, as seen in the FTIR spectra and SEM images. However, the addition of powders, both treated and untreated rendered the composite less thermally stable as the powders themselves tend to degrade at lower temperatures than neat PBAT. Nonetheless, these differences were very insignificant. On the other hand, due to improper dispersive mixing of treated middle composites the powders, especially the treated ones, had a tendency to agglomerate and form embedded aggregates in the extrudate which compromised some mechanical properties of the composites and water absorption behavior due to the formation of microvoids. Thus, the composite with most promising properties was the PBAT/2 wt% treated exterior composite since it meets almost all the theorized properties with enhanced mechanical, thermo-mechanical and water absorption capacity when compared to its untreated counterpart.

To conclude, when bioplastics with high performance (more specific and enhanced properties) are needed, exterior treated powders are a good solution as reinforcements of PBAT to reduce the cost of the material while not compromising its mechanical, thermo-mechanical properties and water absorption capacity. If the requirements for the bioplastic are more tolerant then undiscriminated fiber powders can be mixed, between interior, middle and exterior to once again reduce the cost of the material and allow to repurpose such agricultural waste.

Considerations for future work

After the results obtained in this thesis and experience acquired with the work, several other studies could be performed to further understand how to improve the preparation of the composites and how the powders interact with PBAT. First off, further studies need to be conducted to better understand the mechanical behavior of the composites extruded and more images need to be obtained by SEM for untreated middle composites and untreated and treated exterior composites to assess their surface morphology. Moreover, the extraction of the fibers could be done mechanically to compare the results with the manual extracted ones. Furthermore, more concentrations, times and temperatures could be assessed to establish the optimal conditions of alkali treatment for these specific fibers, and other chemical treatments could be analyzed and compared. Finally, regarding the extrusion process, filaments could be produced in a twin screw counter-rotating extruder to improve the dispersive mixing of the powders in the matrix. Additionally, this could also allow to introduce higher fiber powder or simply fiber content in the extrudate and possibly lead to the production of filaments with parameters that are more in line with the condition needed for 3D printing for further tests.

References

1 S. RameshKumar, P. Shaiju, K. E. O’Connor and R. B. P, Bio-based and biodegradable polymers - State-of-the-art, challenges and emerging trends, *Curr. Opin. Green Sustain. Chem.*, 2020, **21**, 75–81.

2 F. V. Ferreira, L. S. Cividanes, R. F. Gouveia and L. M. F. Lona, An Overview on Properties and Applications of Poly(butylene adipate-co-terephthalate)–PBAT Based Composites, Polym. Eng. Sci., 2019, **59**, E7–E15.

3 Plastics – the Facts 2020, https://plasticseurope.org/wp-content/uploads/2021/09/Plastics_the_facts-WEB-2020_versionJun21_final.pdf, (accessed December 2021).

4 M. Hong and E. Y.-X. Chen, Future Directions for Sustainable Polymers, Trends Chem., 2019, **1**, 148–151.

5 Biodegradable Plastics: breaking down the facts . https://www.greenpeace.org/static/planet4-eastasia-stateless/84075f56-biodegradable-plastics-report.pdf, (accessed October 2021).

6 J. Jian, Z. Xiangbin and H. Xianbo, An overview on synthesis, properties and applications of poly(butylene-adipate-co-terephthalate)-PBAT, Adv. Ind. Eng. Polym. Res., 2020, **3**, 19–26.

7 A. A. Shah, S. Kato, N. Shintani, N. R. Kamini and T. Nakajima-Kambe, Microbial degradation of aliphatic and aliphatic-aromatic co-polyesters, *Appl. Microbiol. Biotechnol.*, 2014, **98**, 3437–3447.

8 J. Fojt, J. David, R. Přikryl, V. Řezáčová and J. Kučerík, A critical review of the overlooked challenge of determining micro-bioplastics in soil, Sci. Total Environ., 2020, **745**, 140975.

9 D. Elvers, C. H. Song, A. Steinbüchel and J. Leker, Technology Trends in Biodegradable Polymers: Evidence from Patent Analysis, Polym. Rev., 2016, **56**, 584–606.

10 B. Sadhasivam, D. Ramamoorthy and R. Dhamodharan, Scale-up of non-toxic poly(butylene adipate-co-terephthalate)-Chitin based nanocomposite articles by injection moulding and 3D printing, *Int. J. Biol. Macromol.*, 2020, **165**, 3145–3155.

11 S. J. Xiong, B. Pang, S. J. Zhou, M. K. Li, S. Yang, Y. Y. Wang, Q. Shi, S. F. Wang, T. Q. Yuan and R. C. Sun, Economically Competitive Biodegradable PBAT/Lignin Composites: Effect of Lignin Methylation and Compatibilizer, *ACS Sustain. Chem. Eng.*, 2020, **8**, 5338–5346.

12 S. Kashi, R. K. Gupta, N. Kao and S. N. Bhattacharya, Viscoelastic properties and physical gelation of poly (butylene adipate-co-terephthalate)/graphene nanoplatelet nanocomposites at elevated temperatures, *Polymer* , 2016, **101**, 347–357.

13 R. Scaffaro, A. Maio, F. Sutera, E. ortunato Gulino and M. Morreale, Degradation and Recycling of Films Based on Biodegradable Polymers: A Short Review, *Polymers*, 2019, **11**, 651.

14 T. Mukherjee, M. Czaka, N. Kao, R. K. Gupta, H. J. Choi and S. Bhattacharya, Dispersion study of nanofibrillated cellulose based poly(butylene adipate-co-terephthalate)

composites, *Carbohydr. Polym.*, 2014, **102**, 537–542.

15 V. Titone, F. P. La Mantia and M. C. Mistretta, The Effect of Calcium Carbonate on the Photo-Oxidative Behavior of Poly(butylene adipate-co-terephthalate), *Macromol. Mater. Eng.*, 2020, **305**, 1–7.

16 D. Wei, H. Wang, H. Xiao, A. Zheng and Y. Yang, Morphology and mechanical properties of poly(butylene adipate-co-terephthalate)/potato starch blends in the presence of synthesized reactive compatibilizer or modified poly(butylene adipate-co-terephthalate), *Carbohydr. Polym.*, 2015, **123**, 275–282.

17 Y. Yang, C. Zhang and Y. Weng, Effects of CaCO3 surface modification and water spraying on the weathering properties of PBAT/CaCO3 films, *Polym. Test.*, 2021, **102**, 107334.

18 J. Jian, Z. Xiangbin and H. Xianbo, An overview on synthesis, properties and applications of poly(butylene-adipate-co-terephthalate)–PBAT, *Adv. Ind. Eng. Polym. Res.*, 2020, **3**, 19–26.

19 S. Ravati and B. D. Favis, Tunable morphologies for ternary blends with poly(butylene succinate): Partial and complete wetting phenomena, *Polymer*, 2013, **54**, 3271–3281.

20 N. Karthi, K. Kumaresan, S. Sathish, S. Gokulkumar, L. Prabhu and N. Vigneshkumar, An overview: Natural fiber reinforced hybrid composites, chemical treatments and application areas, *Mater. Today Proc.*, 2019, **27**, 2828–2834.

21 H. Liu, Q. Wu and Q. Zhang, Preparation and properties of banana fiber-reinforced composites based on high density polyethylene (HDPE)/Nylon-6 blends, *Bioresour. Technol.*, 2009, **100**, 6088–6097.

22 T. A. Osswald and G. Menges, in Material Science of Polymers for Engineers, Hanser, Munich, 3rd edn, 2012, ch. 3, pp.78.

23 B. Elves in Ullmann´s Polymers and Plastics, Wiley-VCH Verlag GmbH & Co. KGaA, Weinheim, Germany, 7th edn, 2016, ch. 1, p 179-183.

24 C. S. Wu, Utilization of peanut husks as a filler in aliphatic-aromatic polyesters: Preparation, characterization, and biodegradability, *Polym. Degrad. Stab.*, 2012, **97**, 2388–2395.

25 S. Y. Yap, S. Sreekantan, M. Hassan, K. Sudesh and M. T. Ong, Characterization and Biodegradability of Rice Husk-Filled Polymer Composites, *Polymers.*, 2020, **13**, 104.

26 T. G. Almeida, J. E. João, A. R. M. Costa, A. S. da Silva, L. H. Carvalho and E. L. Canedo, Degradation during processing in poly(butylene adipate-co-terephthalate)/vegetable fiber compounds estimated by torque rheometry, *Polym. Test.*, 2016, **55**, 204–211.

27 J. Phosee, J. Wittayakun and N. Suppakarn, Mechanical properties and morphologies of rice husk silica (RHS)/poly (butylene adipate-co-terephthalate) (PBAT) composites: Effect of silane coupling agent, *Adv. Mater. Res.*, 2010, **123**–**125**, 141–144.

28 F. Sarasini, F. Luzi, F. Dominici, G. Maffei, A. Iannone, A. Zuorro, R. Lavecchia, L. Torre, A. Carbonell-Verdu, R. Balart and D. Puglia, Effect of different compatibilizers on sustainable composites based on a PHBV/PBAT matrix filled with coffee silverskin,

Polymers, 2018, **10**, 1–16.

29 F. Sarasini, J. Tirillò, A. Zuorro, G. Maffei, R. Lavecchia, D. Puglia, F. Dominici, F. Luzi, T. Valente and L. Torre, Recycling coffee silverskin in sustainable composites based on a poly(butylene adipate-co-terephthalate)/poly(3-hydroxybutyrate-co-3-hydroxyvalerate) matrix, *Ind. Crops Prod.*, 2018, **118**, 311–320.

30 L. B. Tavares, N. M. Ito, M. C. Salvadori, D. J. dos Santos and D. S. Rosa, PBAT/kraft lignin blend in flexible laminated food packaging: Peeling resistance and thermal degradability, *Polym. Test.*, 2018, **67**, 169–176.

31 H. Kargarzadeh, A. Galeski and A. Pawlak, PBAT green composites: Effects of kraft lignin particles on the morphological, thermal, crystalline, macro and micromechanical properties, *Polymer*, 2020, **203**, 122748.

32 L. Botta, R. Teresi, V. Titone, G. Salvaggio, F. P. La Mantia and F. Lopresti, Use of biochar as filler for biocomposite blown films: Structure-processing-properties relationships, Polymers, 2021, **13**, 3953.

33 C. S. Wu, Characterization of cellulose acetate-reinforced aliphatic-aromatic copolyester composites, *Carbohydr. Polym.*, 2012, **87**, 1249–1256.

34 I. F. Pinheiro, A. R. Morales and L. H. Mei, Polymeric biocomposites of poly (butylene adipate-co-terephthalate) reinforced with natural Munguba fibers, *Cellulose*, 2014, **21**, 4381–4391.

35 M. Shahlari and S. Lee, Mechanical and Morphological Properties of Poly(butylene adipate-co-terephthalate) and Poly(lactic acid) Blended With Organically Modified Silicate Layers, *Polym. Eng. Sci.*, 2012,**52**, 1420-1428..

36 L. Botta, V. Titone, M. C. Mistretta, F. P. La Mantia, A. Modica, M. Bruno, F. Sottile and F. Lopresti, PBAT based composites reinforced with microcrystalline cellulose obtained from softwood almond shells, *Polymers*, 2021, **13**, 2643.

37 L. Lai, S. Wang, J. Li, P. Liu, L. Wu, H. Wu, J. Xu, S. J. Severtson and W. J. Wang, Stiffening, strengthening, and toughening of biodegradable poly(butylene adipate-co-terephthalate) with a low nanoinclusion usage, *Carbohydr. Polym.*, 2020, **247**, 116687.

38 S. Kashani Rahimi, R. Aeinehvand, K. Kim and J. U. Otaigbe, Structure and Biocompatibility of Bioabsorbable Nanocomposites of Aliphatic-Aromatic Copolyester and Cellulose Nanocrystals, *Biomacromolecules*, 2017, **18**, 2179–2194.

39 S. Adrar, A. Habi, A. Ajji and Y. Grohens, Combined effect of epoxy functionalized graphene and organomontmorillonites on the morphology, rheological and thermal properties of poly (butylenes adipate-co-terephtalate) with or without a compatibilizer, *Appl. Clay Sci.*, 2017, **146**, 306–315.

40 K. Behera, S. Veluri, Y. H. Chang, M. Yadav and F. C. Chiu, Nanofillers-induced modifications in microstructure and properties of PBAT/PP blend: Enhanced rigidity, heat resistance, and electrical conductivity, *Polymer*, 2020, **203**, 122758.

41 K. Post, W.; Kuijpers, L.J.; Zijlstra, M.; van der Zee, M.; Molenveld, Effect of Mineral Fillers on the Mechanical Properties of Commercially Available Biodegradable Polymers,

Polymers, 2021, **13**, 394.

42 S. Balda, A. Sharma, N. Capalash and P. Sharma, Banana fibre: a natural and sustainable bioresource for eco-friendly applications, Clean Technol. Environ. Policy, 2021, **23**, 1-13.

43 M. Nofar, M. C. Heuzey, P. J. Carreau and M. R. Kamal, Effects of nanoclay and its localization on the morphology stabilization of PLA/PBAT blends under shear flow, *Polymer*, 2016, **98**, 353–364.

44 L. Lendvai, A. Apostolov and J. Karger-Kocsis, Characterization of layered silicate-reinforced blends of thermoplastic starch (TPS) and poly(butylene adipate-co-terephthalate), *Carbohydr. Polym.*, 2017, **173**, 566–572.

45 J. B. Olivato, C. M. O. Müller, G. M. Carvalho, F. Yamashita and M. V. E. Grossmann, Physical and structural characterisation of starch/polyester blends with tartaric acid, *Mater. Sci. Eng. C*, 2014, **39**, 35–39.

46 S. Mohanty and S. K. Nayak, Starch based biodegradable PBAT nanocomposites: Effect of starch modification on mechanical, thermal, morphological and biodegradability behavior, *Int. J. Plast. Technol.*, 2009, **13**, 163–185.

47 Y. Fourati, Q. Tarrés, M. Delgado-Aguilar, P. Mutjé and S. Boufi, Cellulose nanofibrils reinforced PBAT/TPS blends: Mechanical and rheological properties, *Int. J. Biol. Macromol.*, 2021, **183**, 267–275.

48 Y. Parulekar and A. K. Mohanty, Extruded biodegradable cast films from polyhydroxyalkanoate and thermoplastic starch blends: Fabrication and characterization, *Macromol. Mater. Eng.*, 2007, **292**, 1218–1228.

49 Y. Nabar, J. M. Raquez, P. Dubois and R. Narayan, Production of starch foams by twin-screw extrusion: Effect of maleated poly(butylene adipate-co-terephthalate) as a compatibilizer, *Biomacromolecules*, 2005, **6**, 807–817.

50 J. M. Raquez, Y. Nabar, M. Srinivasan, B. Y. Shin, R. Narayan and P. Dubois, Maleated thermoplastic starch by reactive extrusion, *Carbohydr. Polym.*, 2008, **74**, 159–169.

51 D. Wu, Y. Tan, L. Han, H. Zhang and L. Dong, Preparation and characterization of acetylated maltodextrin and its blend with poly(butylene adipate-co-terephthalate), *Carbohydr. Polym.*, 2018, **181**, 701–709.

52 J. B. Olivato, J. Marini, F. Yamashita, E. Pollet, M. V. E. Grossmann and L. Avérous, Sepiolite as a promising nanoclay for nano-biocomposites based on starch and biodegradable polyester, *Mater. Sci. Eng. C*, 2017, **70**, 296–302.

53 Y. Fourati, Q. Tarrés, P. Mutjé and S. Boufi, PBAT/thermoplastic starch blends: Effect of compatibilizers on the rheological, mechanical and morphological properties, *Carbohydr. Polym.*, 2018, **199**, 51–57.

54 C. C. Chang, B. M. Trinh and T. H. Mekonnen, Robust multiphase and multilayer starch/polymer (TPS/PBAT) film with simultaneous oxygen/moisture barrier properties, *J. Colloid Interface Sci.*, 2021, **593**, 290–303.

55 R. P. H. Brandelero, F. Yamashita and M. V. E. Grossmann, The effect of surfactant Tween 80 on the hydrophilicity, water vapor permeation, and the mechanical properties of

cassava starch and poly(butylene adipate-co-terephthalate) (PBAT) blend films, *Carbohydr. Polym.*, 2010, **82**, 1102–1109.

56 Y. Fourati, Q. Tarrés, P. Mutjé and S. Boufi, PBAT/thermoplastic starch blends: Effect of compatibilizers on the rheological, mechanical and morphological properties, *Carbohydr. Polym.*, 2018, **199**, 51–57.

57 S. Zhang, Y. He, Z. Lin, J. Li and G. Jiang, Effects of tartaric acid contents on phase homogeneity, morphology and properties of poly (butyleneadipate-co-terephthalate)/thermoplastic starch bio-composities, *Polym. Test.*, 2019, **76**, 385–395.

58 J. B. Olivato, M. M. Nobrega, C. M. O. Müller, M. A. Shirai, F. Yamashita and M. V. E. Grossmann, Mixture design applied for the study of the tartaric acid effect on starch/polyester films, *Carbohydr. Polym.*, 2013, **92**, 1705–1710.

59 J. B. Olivato, M. V. E. Grossmann, A. P. Bilck and F. Yamashita, Effect of organic acids as additives on the performance of thermoplastic starch/polyester blown films, *Carbohydr. Polym.*, 2012, **90**, 159–164.

60 J. B. Olivato, J. Marini, E. Pollet, F. Yamashita, M. V. E. Grossmann and L. Avérous, Elaboration, morphology and properties of starch/polyester nano-biocomposites based on sepiolite clay, *Carbohydr. Polym.*, 2015, **118**, 250–256.

61 W. Liu, S. Liu, Z. Wang, J. Liu, B. Dai, Y. Chen and G. Zeng, Preparation and characterization of compatibilized composites of poly(butylene adipate-co-terephthalate) and thermoplastic starch by two-stage extrusion, *Eur. Polym. J.*, 2020, **122**, 109369.

62 K. M. Dang, R. Yoksan, E. Pollet and L. Avérous, Morphology and properties of thermoplastic starch blended with biodegradable polyester and filled with halloysite nanoclay, *Carbohydr. Polym.*, 2020, **242**, 116392.

63 M. A. B. S. Nunes, V. A. D. Marinho, G. A. M. Falcão, E. L. Canedo, M. A. G. Bardi and L. H. Carvalho, Rheological, mechanical and morphological properties of poly(butylene adipate-co-terephthalate)/thermoplastic starch blends and its biocomposite with babassu mesocarp, *Polym. Test.*, 2018, **70**, 281–288.

64 C. Yokesahachart, R. Yoksan, N. Khanoonkon, A. K. Mohanty and M. Misra, Effect of jute fibers on morphological characteristics and properties of thermoplastic starch/biodegradable polyester blend, *Cellulose*, 2021, **28**, 5513–5530.

65 E. Hablot, S. Dewasthale, Y. Zhao, Y. Zhiguan, X. Shi, D. Graiver and R. Narayan, Reactive extrusion of glycerylated starch and starch-polyester graft copolymers, *Eur. Polym. J.*, 2013, **49**, 873–881.

66 J. Bai, H. Pei, X. Zhou and X. Xie, Reactive compatibilization and properties of low-cost and high-performance PBAT/thermoplastic starch blends, *Eur. Polym. J.*, 2021, **143**, 110198.

67 W. Liu, S. Liu, Z. Wang, B. Dai, J. Liu, Y. Chen, G. Zeng, Y. He, Y. Liu and R. Liu, Preparation and characterization of reinforced starch-based composites with compatibilizer by simple extrusion, *Carbohydr. Polym.*, 2019, **223**, 115122.

68 R. P. H. Brandelero, M. V. Grossmann and F. Yamashita, Films of starch and

poly(butylene adipate co-terephthalate) added of soybean oil (SO) and Tween 80, *Carbohydr. Polym.*, 2012, **90**, 1452–1460.

69 L. Jiang, M. P. Wolcott and J. Zhang, Study of Biodegradable Polylactide / Poly (butylene adipate-co-terephthalate) Blends, *Biomacromolecules*, 2006, **7**, 199–207.

70 M. B. Coltelli, C. Toncelli, F. Ciardelli and S. Bronco, Compatible blends of biorelated polyesters through catalytic transesterification in the melt, *Polym. Degrad. Stab.*, 2011, **96**, 982–990.

71 M. Mohammadi, C. Bruel, M. C. Heuzey and P. J. Carreau, CNC dispersion in PLA and PBAT using two solvents: morphological and rheological properties, *Cellulose*, 2020, **27**, 9877–9892.

72 R. Y. Tabasi and A. Ajji, Selective degradation of biodegradable blends in simulated laboratory composting, *Polym. Degrad. Stab.*, 2015, **120**, 435–442.

73 P. Cinelli, N. Mallegni, S. Fiori, M. Seggiani, M. B. Coltelli, M. C. Righetti and A. Lazzeri, Polylactic Acid and Poly(Butylene Adipate-Co-Terephthalate) Blends Plasticised with Lactic Oligomers and Epoxy Reactive Plasticizers, *Chem. Eng. Trans.*, 2021, **88**, 1333–1338.

74 Y. Zhou, L. Lei, B. Yang, J. Li and J. Ren, Preparation of PLA-based nanocomposites modified by nano-attapulgite with good toughness-strength balance, *Polym. Test.*, 2017, **60**, 78–83.

75 W. Phetwarotai, M. Zawong, N. Phusunti and D. Aht-Ong, Toughening and thermal characteristics of plasticized polylactide and poly(butylene adipate-co-terephthalate) blend films: Influence of compatibilization, *Int. J. Biol. Macromol.*, 2021, **183**, 346–357.

76 W. Li, C. Sun, C. Li, Y. Xu, H. Tan and Y. Zhang, Preparation of effective ultraviolet shielding poly (lactic acid)/poly (butylene adipate-co-terephthalate) degradable composite film using co-precipitation and hot-pressing method, *Int. J. Biol. Macromol.*, 2021, **191**, 540–547.

77 M. Nofar, A. Tabatabaei, H. Sojoudiasli, C. B. Park, P. J. Carreau, M. C. Heuzey and M. R. Kamal, Mechanical and bead foaming behavior of PLA-PBAT and PLA-PBSA blends with different morphologies, *Eur. Polym. J.*, 2017, **90**, 231–244.

78 Y. Zhao, B. Zhao, B. Wei, Y. Wei, J. Yao, H. Zhang, X. Chen and Z. Shao, Enhanced compatibility between poly(lactic acid) and poly (butylene adipate-co-terephthalate) by incorporation of N-halamine epoxy precursor, *Int. J. Biol. Macromol.*, 2020, **165**, 460–471.

79 S. Y. Gu, K. Zhang, J. Ren and H. Zhan, Melt rheology of polylactide/poly(butylene adipate-co-terephthalate) blends, *Carbohydr. Polym.*, 2008, **74**, 79–85.

80 V. Gigante, I. Canesi, P. Cinelli, M. B. Coltelli and A. Lazzeri, Rubber Toughening of Polylactic Acid (PLA) with Poly(butylene adipate-co-terephthalate) (PBAT): Mechanical Properties, Fracture Mechanics and Analysis of Ductile-to-Brittle Behavior while Varying Temperature and Test Speed, *Eur. Polym. J.*, 2019, **115**, 125–137.

81 M. B. Coltelli, S. Bronco and C. Chinea, The effect of free radical reactions on structure and properties of poly(lactic acid) (PLA) based blends, *Polym. Degrad. Stab.*, 2010, **95**,

332–341.

82 P. Ma, X. Cai, Y. Zhang, S. Wang, W. Dong, M. Chen and P. J. Lemstra, In-situ compatibilization of poly(lactic acid) and poly(butylene adipate-co-terephthalate) blends by using dicumyl peroxide as a free-radical initiator, *Polym. Degrad. Stab.*, 2014, **102**, 145–151.

83 X. Ai, X. Li, Y. Yu, H. Pan, J. Yang, D. Wang, H. Yang, H. Zhang and L. Dong, The Mechanical, Thermal, Rheological and Morphological Properties of PLA/PBAT Blown Films by Using Bis(tert-butyl dioxy isopropyl) Benzene as Crosslinking Agent, *Polym. Eng. Sci.*, 2019, **59**, E227–E236.

84 H. Pan, Z. Li, J. Yang, X. Li, X. Ai, Y. Hao, H. Zhang and L. Dong, The effect of MDI on the structure and mechanical properties of poly(lactic acid) and poly(butylene adipate-co-butylene terephthalate) blends, *RSC Adv.*, 2018, **8**, 4610–4623.

85 S. Lee, Y. Lee and J. W. Lee, Effect of ultrasound on the properties of biodegradable polymer blends of poly(lactic acid) with poly(butylene adipate-co-terephthalate), *Macromol. Res.*, 2007, **15**, 44–50.

86 M. Kumar, S. Mohanty, S. K. Nayak and M. Rahail Parvaiz, Effect of glycidyl methacrylate (GMA) on the thermal, mechanical and morphological property of biodegradable PLA/PBAT blend and its nanocomposites, *Bioresour. Technol.*, 2010, **101**, 8406–8415.

87 N. Zhang, Q. Wang, J. Ren and L. Wang, Preparation and properties of biodegradable poly(lactic acid)/poly(butylene adipate-co-terephthalate) blend with glycidyl methacrylate as reactive processing agent, *J. Mater. Sci.*, 2009, **44**, 250–256.

88 S. Su, Prediction of the miscibility of pbat/pla blends, *Polymers*, 2021, **13**, 2339.

89 S. Su, R. Kopitzky and C. Berrenrath, Experimental determination of molecular weight-dependent miscibility of pbat/pla blends, *Polymers*, 2021, **13**, 3686.

90 N. Wu and H. Zhang, Mechanical properties and phase morphology of super-tough PLA/PBAT/EMA-GMA multicomponent blends, *Mater. Lett.*, 2017, **192**, 17–20.

91 Y. Ding, B. Lu, P. Wang, G. Wang and J. Ji, PLA-PBAT-PLA tri-block copolymers: Effective compatibilizers for promotion of the mechanical and rheological properties of PLA/PBAT blends, *Polym. Degrad. Stab.*, 2018, **147**, 41–48.

92 D. Y. Kim, J. Bin Lee, D. Y. Lee and K. H. Seo, Plasticization effect of poly(lactic acid) in the poly(butylene adipate-co-terephthalate) blown film for tear resistance improvement, *Polymers*, 2020, **12**, 1904.

93 R. Al-Itry, K. Lamnawar and A. Maazouz, Improvement of thermal stability, rheological and mechanical properties of PLA, PBAT and their blends by reactive extrusion with functionalized epoxy, *Polym. Degrad. Stab.*, 2012, **97**, 1898–1914.

94 T. Zhang, W. Han, C. Zhang and Y. Weng, Effect of chain extender and light stabilizer on the weathering resistance of PBAT/PLA blend films prepared by extrusion blowing, *Polym. Degrad. Stab.*, 2021, **183**, 109455.

95 X. Wang, S. Peng, H. Chen, X. Yu and X. Zhao, Mechanical properties, rheological behaviors, and phase morphologies of high-toughness PLA/PBAT blends by in-situ

reactive compatibilization, *Compos. Part B Eng.*, 2019, **173**, 107028.

96 S. Adrar, A. Habi, A. Ajji and Y. Grohens, Synergistic effects in epoxy functionalized graphene and modified organomontmorillonite PLA / PBAT blends, *Appl. Clay Sci.*, 2018, **157**, 65–75.

97 S. Girdthep, N. Komrapit, R. Molloy, S. Lumyong, W. Punyodom and P. Worajittiphon, Effect of plate-like particles on properties of poly(lactic acid)/poly(butylene adipate-co-terephthalate) blend: A comparative study between modified montmorillonite and graphene nanoplatelets, *Compos. Sci. Technol.*, 2015, **119**, 115–123.

98 E. Abraham, B. Deepa, L. A. Pothan, M. Jacob, S. Thomas, U. Cvelbar and R. Anandjiwala, Extraction of nanocellulose fibrils from lignocellulosic fibres: A novel approach, *Carbohydr. Polym.*, 2011, **86**, 1468–1475.

99 K. J. Okafor, S. O. Edelugo, I. C. Ezema Ike-Eze and S. A. Chukwunwike, Effect of soaking temperature on the tensile and morphological properties of banana stem fibre-reinforced polyester composite, *Polym. Bull.*, 2021, **78**, 5243–5254.

100 H. Das, P. Saikia and D. Kalita, Physico-mechanical properties of banana fiber reinforced polymer composite as an alternative building material, *Key Eng. Mater.*, 2015, **650**, 131–138.

101 X. Li, L. G. Tabil and S. Panigrahi, Chemical treatments of natural fiber for use in natural fiber-reinforced composites: A review, *J. Polym. Environ.*, 2007, **15**, 25–33.

102 M. M. Kabir, H. Wang, K. T. Lau and F. Cardona, Chemical treatments on plant-based natural fibre reinforced polymer composites: An overview, *Compos. Part B Eng.*, 2012, **43**, 2883–2892.

103 A. K. Mohanty, M. Misra and L. T. Drzal, Surface modifications of natural fibers and performance of the resulting biocomposites: An overview, *Compos. Interfaces*, 2001, **8**, 313–343.

104 M. Ramesh, K. Palanikumar and K. H. Reddy, Plant fibre based bio-composites: Sustainable and renewable green materials, *Renew. Sustain. Energy Rev.*, 2017, **79**, 558–584.

105 P. H. F. Pereira, K. C. C. Carvalho Benini, C. Y. Watashi, H. J. C. Voorwald and M. O. H. Cioffi, Characterization of high density polyethylene (HDPE) reinforced with banana peel fibers, *BioResources*, 2013, **8**, 2351–2365.

106 U. S. Gupta, M. Dhamarikar, A. Dharkar, S. Chaturvedi, S. Tiwari and R. Namdeo, Surface modification of banana fiber: A review, *Mater. Today Proc.*, 2021, **43**, 904-915.

107 A. Pappu, V. Patil, S. Jain, A. Mahindrakar, R. Haque and V. K. Thakur, Advances in industrial prospective of cellulosic macromolecules enriched banana biofibre resources: A review, *Int. J. Biol. Macromol.*, 2015, **79**, 449–458.

108 K. Z. M. A. Motaleb, R. Al Mizan and R. Milašius, Development and characterization of eco-sustainable banana fiber nonwoven material: surface treatment, water absorbency and mechanical properties, *Cellulose*, 2020, **27**, 7889–7900.

109 U. Ratanakamnuan and D. Aht-Ong, Preparation and characterization of low-density

polyethylene/banana starch films containing compatibilizer and photosensitizer, *J. Appl. Polym. Sci.*, 2006, **100**, 2717–2724.

110 N. Prasad, V. K. Agarwal and S. Sinha, Banana fiber reinforced low-density polyethylene composites: effect of chemical treatment and compatibilizer addition, *Iran. Polym. J.*, 2016, **25**, 229–241.

111 S. Bolduc, K. Jung, P. Venkata, M. Ashokcline, R. Jayasinghe, C. Baillie and L. Lessard, Banana fiber/low-density polyethylene recycled composites for third world eco-friendly construction applications – Waste for life project Sri Lanka, *J. Reinf. Plast. Compos.*, 2018, **37**, 1322–1331.

112 N. Prasad, V. K. Agarwal and S. Sinha, Banana fiber reinforced low-density polyethylene composites: effect of chemical treatment and compatibilizer addition, *Iran. Polym. J.*, 2016, **25**, 229–241.

113 M. Idicula, S. K. Malhotra, K. Joseph and S. Thomas, Dynamic mechanical analysis of randomly oriented intimately mixed short banana/sisal hybrid fibre reinforced polyester composites, *Compos. Sci. Technol.*, 2005, **65**, 1077–1087.

114 H. U. Zaman, M. A. Khan and R. A. Khan, Physico-mechanical and degradation properties of banana fiber/LDPE composites: Effect of acrylic monomer and starch, *Compos. Interfaces*, 2011, **18**, 685–700.

115 K. Bilba, M. A. Arsene and A. Ouensanga, Study of banana and coconut fibers. Botanical composition, thermal degradation and textural observations, *Bioresour. Technol.*, 2007, **98**, 58–68.

116 S. Mukhopadhyay, R. Fangueiro, Y. Arpaç and Ü. Şentürk, Banana Fibers – Variability and Fracture Behaviour, *J. Eng. Fiber. Fabr.*, 2008, **3**, 39-45.

117 J. S. Jayaprabha, M. Brahmakumar and V. B. Manilal, Banana pseudostem characterization and its fiber property evaluation on physical and bioextraction, *J. Nat. Fibers*, 2011, **8**, 149–160.

118 Y. Habibi, W. K. El-Zawawy, M. M. Ibrahim and A. Dufresne, Processing and characterization of reinforced polyethylene composites made with lignocellulosic fibers from Egyptian agro-industrial residues, *Compos. Sci. Technol.*, 2008, **68**, 1877–1885.

119 S. Annie, A. Boudenne, L. Ibos, Y. Candau, K. Joseph and S. Thomas, Effect of fiber loading and chemical treatments on thermophysical properties of banana fiber/polypropylene commingled composite materials, *Composites Part A: Applied Science and Manufacturing,* 2008, **39**, 1582–1588.

120 L. A. Pothan, S. Thomas and G. Groeninckx, The role of fibre/matrix interactions on the dynamic mechanical properties of chemically modified banana fibre/polyester composites, *Compos. Part A Appl. Sci. Manuf.*, 2006, **37**, 1260–1269.

121 C. S. M. F. Costa, A. C. Fonseca, A. C. Serra and J. F. J. Coelho, Dynamic Mechanical Thermal Analysis of Polymer Composites Reinforced with Natural Fibers, *Polym. Rev.*, 2016, **56**, 362–383.

122 F. Rodriguez, C. Cohen, C. K. Ober and L. Al Archer, *Principles of Polymer Systems*, CRC

Press, New York, 2014.

123 Produtos regionais da Madeira; Banana, https://www.visitmadeira.com/pt-pt/a-madeira/produtos-regionais/banana, (accessed October 2022).

124 O. Manual, 6770 freezer/mill ®, 1–26.

125 SPEX™ SamplePrep 6775 Freezer/Mill™ Accessories: Vial Set, https://www.fishersci.com/shop/products/spex-sampleprep-6770-freezer-mill-accessories-vial-set-9/p-2797051, (accessed October 2022).

126 Google images, https://pim-resources.coleparmer.com/item/m/spex-sampleprep-0457634-grinding-vial-set-small-vial-0-5-to-4-ml-pc-cylinder-and-end-plugs-pc-encapsulated-steel-impactor-0457634.jpg, (accessed October 2022).

127 W. K. El-Zawawy and M. M. Ibrahim, Synthesis and characterization of cellulose resins, *Polym. Adv. Technol.*, 2003, **14**, 623–631.

128 J. L. Guimarães, E. Frollini, C. G. da Silva, F. Wypych and K. G. Satyanarayana, Characterization of banana, sugarcane bagasse and sponge gourd fibers of Brazil, *Ind. Crops Prod.*, 2009, **30**, 407–415.

129 X. F. Sun, F. Xu, R. C. Sun, P. Fowler and M. S. Baird, Characteristics of degraded cellulose obtained from steam-exploded wheat straw, *Carbohydr. Res.*, 2005, **340**, 97–106.

130 B. M. Cherian, A. L. Leão, M. R. de Morais Chaves, S. F. de Souza, M. Sain and S. S. Narine, Environmental ageing studies of chemically modified micro and nanofibril phenol formaldehyde composites, *Ind. Crops Prod.*, 2013, **49**, 471–483.

131 E. Alonso, L. A. Pothan, A. Ferreira and N. Cordeiro, Surface modification of banana fibers using organosilanes: an IGC insight, *Cellulose*, 2019, **26**, 3643–3654.

132 S. Ouajai and R. A. Shanks, Composition, structure and thermal degradation of hemp cellulose after chemical treatments, *Polym. Degrad. Stab.*, 2005, **89**, 327–335.

133 W. K. El-Zawawy, Blended graft copolymer of carboxymethyl cellulose and poly(vinyl alcohol) with banana fiber, *J. Appl. Polym. Sci.*, 2006, **100**, 1842–1848.

134 L. Y. Mwaikambo and M. P. Ansell, Chemical modification of hemp, sisal, jute, and kapok fibers by alkalization, *J. Appl. Polym. Sci.*, 2002, **84**, 2222–2234.

135 T. P. Mohan and K. Kanny, Mechanical and Thermal Properties of Nanoclay-Treated Banana Fibers, *J. Nat. Fibers*, 2017, **14**, 718–726.

136 S. M. K. T, R. N, A. A, S. Siengchin, V. R. A and N. Ayrilmis, Development and Analysis of Completely Biodegradable Cellulose/Banana Peel Powder Composite Films, *J. Nat. Fibers*, 2021, **18**, 151–160.

137 B. C. Mitra, R. K. Basak and M. Sarkar, Studies on jute-reinforced composites, its limitations, and some solutions through chemical modifications of fibers, *J. Appl. Polym. Sci.*, 1998, **67**, 1093–1100.

138 A. C. Marques, presented in part at Tecnhonoly of Polymeric Materials - Continuous Processing Methods, Lisbon, October, 2021.

139 Fred W. Billmeyer, *Textbook of Polymer Science*, Wiley-Interscience, New York, 1984.

140 H. F. Giles, J. R. Wagner and E. M. Mount, *Extrusion The Definitive Processing Guide and Handbook*, William Andrew, New Yoirk, 2004.

141 C. Rauwendaal, Polymer Extrusion, Hanser, Munich, 2014.

142 How to start the extrusion, https://support.3devo.com/how-to-start-the-extrusion, (accessed October 2022).

143 Output too low or thin, https://support.3devo.com/output-too-low-or-thin, (accessed October 2022).

144 J. M. Wang, H. Wang, E. C. Chen, Y. J. Chen and T. M. Wu, Enhanced photodegradation stability in poly(Butylene adipate-co-terephthalate) composites using organically modified layered zinc phenylphosphonate, *Polymers*, 2020, **12**, 1–12.

145 P. González Seligra, L. Eloy Moura, L. Famá, J. I. Druzian and S. Goyanes, Influence of incorporation of starch nanoparticles in PBAT/TPS composite films, *Polym. Int.*, 2016, **65**, 938–945.

146 J. B. Olivato, M. V. E. Grossmann, F. Yamashita, D. Eiras and L. A. Pessan, Citric acid and maleic anhydride as compatibilizers in starch/poly(butylene adipate-co-terephthalate) blends by one-step reactive extrusion, *Carbohydr. Polym.*, 2012, **87**, 2614–2618.

147 J. Coates, Encyclopedia of Analytical Chemistry -Interpretation of Infrared Spectra, A Practical Approach, *Encycl. Anal. Chem.*, 2004, 1–23.

148 S. Mohanty and S. K. Nayak, Biodegradable nanocomposites of poly (butylene adipate-co-terephthalate) (PBAT) with organically modified nanoclays, *Int. J. Plast. Technol.*, 2010, **14**, 192–212.

149 J. H. Chen and M. C. Yang, Preparation and characterization of nanocomposite of maleated poly(butylene adipate-co-terephthalate) with organoclay, *Mater. Sci. Eng. C*, 2015, **46**, 301–308.

150 C. Badouard, F. Traon, C. Denoual, C. Mayer-Laigle, G. Paës and A. Bourmaud, Exploring mechanical properties of fully compostable flax reinforced composite filaments for 3D printing applications, *Ind. Crops Prod.*, 2019, **135**, 246–250.

151 A. Le Duigou, D. Correa, M. Ueda, R. Matsuzaki and M. Castro, A review of 3D and 4D printing of natural fibre biocomposites, *Mater. Des.*, 2020, **194**, 108911.

152 V. Mazzanti, L. Malagutti and F. Mollica, FDM 3D printing of polymers containing natural fillers: A review of their mechanical properties, *Polymers*, 2019, **11**, 1094.

153 3Devo - Filament Makers, https://www.3devo.com/filament-makers, (accessed October 2022).

Appendix A - Comprehensive list of the varied PBAT blends

Table 15 – Comprehensive list of the varied PBAT/additive composites found in the literature, along with the corresponding mechanical properties, water absorption, rheological and thermal behaviour

PBAT/additive composite	Materials	Method/ Equipment	Mechanical properties and Water absorption		Rheological properties and Thermal behavior		Ref
PBAT/PH 90/10 wt%	PH: 70-79% cellulose, 10.1% hemicelluloses	Internal Mixer	*σ	10 MPa			24
			*ε	650%			
			Lower water resistance than PBAT-g-MA/PH				
PBAT/RHS 70/30 wt%	RHS: modified with a silane coupling agent, 2.0 wt% MPS	Internal Mixer	*σ	16 MPa			27
			*ε_B	200%			
			*E	66 MPa			
			IM	28,5 kJ/m^2			
PBAT/NC 70/30 wt%	Nanochitin was prepared from chitin isolated from prawn shells	Extrusion twin screw	σ	38.5 MPa	T_g	-33.9 ºC	10
			ε_B	195.4%	T_m	132.1 ºC	
			IS	9.7 KJ/m^2	T_c	89.8 ºC	
			FS	25.2 MPa	ΔH_c	13.4 J/g	
					NC did not significantly improve the thermal stability		
PBAT/KL 94/6 wt%	Kraft lignin was obtained as a byproduct of pulp and paper manufacturing	Extrusion co-rotating twin screw	σ	17 MPa	X_c	20.7 %	30 31
					T_m	130 ºC	
			ε	545 %	T_g	-25.5 ºC	
					$T_{c\ (onset)}$	110.6 ºC	
			E	225 MPa	Increase G′ at temperatures below T_g		
PBAT/BC 95/5 and 90/10 wt%	Biochar was obtained from the pyrolysis of birch and beech wood	Extrusion twin screw	5 wt% BC	10 wt% BC	5 wt% BC	10 wt% BC	32
			*σ: 150 MPa	*σ: 90 MPa	X_c: 5.2 %	X_c: 5.1 %	
			*ε_B: 90 %	*εB: 80%	T_m: 131.2 ºC	T_m: 132.7 ºC	
			*E: 550 MPa	*E: 680 MPa	10 wt% BC had higher η*		

PBAT/ Resyflex®/fiber 80/10/10 wt% treated and untreated fibers	Munguba fibers were chemically treated by mercerization/acetylation Resyflex® was used as a plasticizer	High shear mixing	Un. fiber	T. fiber	Un. fiber	T. fiber	34
			σ_B: 10 MPa	σ_B: 9 MPa	T_m: 116 ºC	T_m: 114 ºC	
			ε_B: 349 %	ε_B: 316%	T_c: 90 ºC	T_c: 85 ºC	
			E: 87 MPa	E: 94 MPa	T_{onset}: 102 ºC	T_{onset}: 95 ºC	
PBAT/CLA 95/5 and 90/10 wt%	Cellulose acetate with a 55% degree of deacetylation	Internal Mixer	5 wt% CLA	10 wt% CLA	Thermal stability was 4–12 ºC lower than PBAT-g-MAH/CLA with higher biodegradation		33
			*σ: 11 MPa	*σ: 9 MPa			
			*ε_B: 670 %	*ε_B: 600 %			
			Has higher water absorption than PBAT-g-MAH/CLA				
PBAT/as-MCC 90/10 wt%	as-MCC: alkaline treated microcrystalline cellulose from softwood almond shells	Internal mixer	*σ	7.9 MPa	X_c	9.1 %	36
			ε_B	320 %	T_m	125 ºC	
			*E	95 MPa	Intermediate values of G′, G″ and η* when compared to pure PBAT and PBAT/as-MCC 80/20 wt%		
PBAT-g-MAH/CNC 91/9 wt %	[1]PBAT-g-MAH: percent of grafting 0.92% Cellulose nanocrystals were prepared using the sulfuric acid hydrolysis of bleached cellulose pulp	Extrusion co-rotating twin screw	$\sigma_{máx}$	18.6 MPa	X_c	8.0 %	38
					T_m	125.7 ºC	
			$\varepsilon_{máx}$	88.1 %	T_c	85.7 ºC	
					$T_{30\%}$-$T_{70\%}$	396.3 – 426.1 ºC	
			E	85.8 MPa	Better thermal stability		
					Higher G′, G″ and η*		

[1] Benzoyl peroxide was used as an initiator; *Aproximate values; σ - Tensile strength; εB - Elongation at break; E - Young's modulus; IS - Impact Strength; FS - Flexural Strength; T_g – Glass transition temperature; T_c – Crystallization temperature; T_m - Melting temperature; T_{onset} – Onset temperature; X_c – Degree of crystallinity; ΔH_c - Enthalpy of crystallization

Table 16 – Comprehensive list of the varied PBAT/TPS composites found in the literature, along with the corresponding mechanical properties, water absorption, rheological and thermal behaviour

<table>
<tr><th>PBAT/TPS composite</th><th>Materials</th><th>Method/ Equipment</th><th colspan="2">Mechanical properties and Water absorption</th><th colspan="2">Rheological properties and Thermal behavior</th><th>Ref</th></tr>
<tr><td rowspan="3">TPS/PBAT/PBAT-g-MAH
59/39/2 wt%</td><td rowspan="3">[1]PBAT-g-MAH: extent of maleation 0.55%
TPS: 20% glycerol to potato starch</td><td rowspan="3">Extrusion Single screw</td><td>σ</td><td>12.3 MPa</td><td colspan="2" rowspan="2">tan δ: decrease in magnitude of PBAT peak, amplification of the intensity of TPS peaks</td><td rowspan="3">53</td></tr>
<tr><td>ε_B</td><td>380%</td></tr>
<tr><td>E</td><td>58 MPa</td><td colspan="2">Higher values of G′ and η*</td></tr>
<tr><td rowspan="7">MTPS/PBAT
Or
MTPS/PBAT/Coated
70/30 wt%</td><td rowspan="7">Corn starch: 73% amylopectin and 27% amylose
TPS: 3:7 glycerol to corn starch
MTPS: 2.5 phr MA</td><td rowspan="7">Extrusion twin screw</td><td colspan="2">MTPS/PBAT/Coated (70/30)</td><td colspan="2">TPS/MTPS degradation 130 °C - 345 °C</td><td rowspan="7">54</td></tr>
<tr><td>*σ</td><td>6 MPa</td><td colspan="2">PBAT degradation 350ºC – 440ºC</td></tr>
<tr><td>*ε_B</td><td>25%</td><td colspan="2">TPS/MTPS – PBAT 270ºC-390ºC</td></tr>
<tr><td>*E</td><td>140 MPa</td><td colspan="2" rowspan="2">MTPS/PBAT (70/30)</td></tr>
<tr><td>*SS</td><td>4.5 MPa</td></tr>
<tr><td>WVP</td><td>reduced by 86.8%</td><td colspan="2" rowspan="2">Higher values of G′</td></tr>
<tr><td>OP</td><td>increased to 74.3%</td></tr>
<tr><td rowspan="2">PBAT/TPS-TA
30/70/0.7 w/w/w</td><td rowspan="2">TPS: corn starch/glycerol 70/30 w/w</td><td rowspan="2">Extrusion twin screw</td><td>σ</td><td>16.1 MPa</td><td colspan="2">Maximal tan δ −14.6 ºC</td><td rowspan="2">57</td></tr>
<tr><td>ε_B</td><td>1311 %</td><td colspan="2">Highest values of G′ and η*</td></tr>
<tr><td rowspan="3">PBAT/TPS/MA/GLY
40.5/49.5/1.5/8.5 wt%</td><td rowspan="3">Native cassava starch</td><td rowspan="3">Extrusion Single screw</td><td>*σ</td><td>5.5 MPa</td><td colspan="2" rowspan="3"></td><td rowspan="3">59</td></tr>
<tr><td>*ε</td><td>550%</td></tr>
<tr><td>*WVP</td><td>1.8x10^{-10} g/m.s.Pa</td></tr>
<tr><td rowspan="4">PBAT/TPS/CA/GLY
40.5/49.5/1.5/8.5 wt%</td><td rowspan="4">Native cassava starch (amylose 20.8 ± 0.6 wt%)</td><td rowspan="4">Extrusion Single screw</td><td>*σ</td><td>6.58 MPa</td><td colspan="2" rowspan="4"></td><td rowspan="4">146</td></tr>
<tr><td>*ε_B</td><td>16.39 %</td></tr>
<tr><td>*WVP</td><td>1.97 x10^{-10} g/m.s.Pa</td></tr>
<tr><td>Opacity</td><td>0.66 % μm^{-1}</td></tr>
<tr><td rowspan="3">TPS/PBAT/Sepiolite
78/19/3 wt%</td><td rowspan="3">Native cassava starch (amylose 20.8 wt%; protein 0.28 wt%; lipids 0.11 wt%; ash 0.22 wt%)</td><td rowspan="3">Internal mixer</td><td>σ</td><td>3.4 MPa</td><td colspan="2" rowspan="3">Addition of sepiolites improved thermal properties of the 80/20 TPS/PBAT blend</td><td rowspan="3">60</td></tr>
<tr><td>E</td><td>82.3 MPa</td></tr>
<tr><td>ε_B</td><td>25.4 %</td></tr>
<tr><td rowspan="4">TPS/PBAT/Sepiolite
47.6/47.6/4.8 wt%</td><td rowspan="4"></td><td rowspan="4">Internal mixer</td><td colspan="2" rowspan="2">Addition of sepiolites decreased the water adsorption rate</td><td>T_g</td><td>-31 ºC</td><td rowspan="4">52</td></tr>
<tr><td>T_m</td><td>126 ºC</td></tr>
<tr><td rowspan="2">Opacity</td><td rowspan="2">0.13 %·μm^{-1}</td><td>T_c</td><td>86 ºC</td></tr>
<tr><td>X_c</td><td>4.5 %</td></tr>
</table>

TPS/PBAT/HNTs 19/76/5 wt% HNTs	TPS: weight fraction of cassava starch:glycerol:water of 54:23:23	Internal mixer	σ	13 MPa	Higher value of G′		62
			E	595.44 MPa			
			ε_B	6.45%	tan δ −25.5 ºC		
TPS-BT/PBAT Or TPS-MMT/PBAT 40/60 wt%	TPS: ratio maize starch and glycerol 4:1	Extrusion twin screw	TPS-BT/PBAT		TPS-BT/PBAT		44
			σ	7.2 MPa	T_m	126.6 ºC	
			ε_B	411.2%	T_c	90.7 ºC	
					X_c	11%	
			E	67 MPa	$T_{10} – T_{75}$	291 – 405 ºC	
			TPS-MMT/PBAT		TPS-MMT/PBAT		
			σ	8.7 MPa	T_m	126.6 ºC	
			ε_B	262.4%	T_c	88.1 ºC	
					X_c	11.8%	
			E	94 MPa	$T_{10} – T_{75}$	268 – 407 ºC	
TPS/PBAT/C30B 29/68/3 wt%	Starch: native tapioca starch with 30-wt% amylase, 70-wt% of amylopectin TPS: 70% of starch, 20% of glycerol and 10% of water	Extrusion Co-rotating twin-screw	σ	11.20 MPa	T_g	-37.05 ºC	46
					T_m	112.29 ºC	
			E	169.65 MPa	T_c	77.53 ºC	
			ε_B	564%	X_c	11.37%	
			Tear strength	43.71 gf/µm	T_d	416 ºC	
PBAT/TPS/Babassu mesocarp 58/25/17 wt% at 190 ºC	Babassu mesocarp: cellulose (45%), hemicellulose (34%), lignin (18%) and 3% mineral ashes	Internal mixer	σ	7.15 MPa			63
			E	244.9 MPa			
			ε_B	7.15 %			
TPS/PLA/PBAT/JF 52/26/8/13 wt%	Jute fiber: moisture content of ~ 15 wt% and aspect ratio of 40–60	Extrusion twin-screw	*σ	45 MPa	Increased G′		64
			E	3800 MPa	Enhanced crystallinity		
			*ε_B	2%	Reduced Tg		
			IS	30 J/m	Reduced Tm		

[1] Benzoyl peroxide; *Aproximate values; σ - Tensile strength; εB - Elongation at break; E - Young's modulus; IS - Impact strength; FS - Flexural strength; SS – Shear Stregnth; OP - Oxygen permeability; WVP - Water vapor permeability; T_d - Degradation temperature; T_g – Glass transition temperature; T_c – Crystallization temperature; T_m - Melting temperature; X_c – Degree of crystallinity

Table 17 – Comprehensive list of the varied PBAT/PLA composites found in the literature, along with the corresponding mechanical properties, water absorption, rheological and thermal behaviour

PBAT/PLA composite	Materials	Method/ Equipment	Mechanical properties and Water absorption		Rheological properties and Thermal behavior		Ref
PLA/PBAT/DCP 80/20/0.1; 0.2; 0.5; 1.0 w/w/w	Dicumyl peroxide (DCP) is a radical initiator	Internal mixer	1 wt% - *σ: 46 MPa		0.5 wt% - Higher intensity for tan δ peak of PBAT		82
			0.1-0.2 wt% - εB 300%				
			0.5 wt% - Impact toughness: 110 J/m		1 wt% - Higher value of G′ and η*		
PLA/PBAT/BIBP 40/60/0.1 w/w/w	bis(tert-butyl dioxy isopropyl) benzene (BIBP) is a crosslinking agent	Extrusion twin screw	σ (MD)	48.7 MPa	X_c	X_{c1}: 2.9%	83
						X_{c2}: 40%	
			ε_B (MD)	364.6%	T_g	T_{g1}: −31.3 ºC	
						T_{g2}: 60.4 ºC	
			TS (MD)	159.1 kN/m	T_m	T_{m1}: 129 ºC	
						T_{m2}: 166.9 ºC	
			SS	13.6 N/15 mm	$T_{máx}$	PLA: 349 ºC	
						PBAT: 404 ºC	
PLA/PBAT/T-GMA 85.7/9.5/4.8 and 63.6/27.3/9 wt%	T-GMA is a random terpolymer of ethylene, acrylic ester and GMA	Extrusion co-rotating twin screw	PLA/PBAT/T-GMA 90/10/5 wt%		PLA/PBAT/T-GMA 70/30/10 wt%		87
			*σ	30 MPa	T_m	148.2 ºC	
			*ε_B	180%	T_c	110.6 ºC	
			*IS	18 kJ/m^2	Higher G′, G″ and η*		
PLA/PBAT/EMA-GMA 82/10/8 and 75/10/15 wt%	methylacrylic ester and glycidyl methacrylate contents were 24 wt% and 8 wt%	Extrusion Single screw	PLA/PBAT/EMA-GMA 82/10/8 wt%		PLA/PBAT/EMA-GMA 75/10/15wt%		90
			σ	44 MPa	T_g PBAT	-27.3 ºC	
			ε_B	320%			
			E	1.7 GPa	T_g PLA	66.7 ºC	
			IS	45.2 kJ/m^2			
PLA/PBAT/BETT 50/50/2 w/w/w	BETT is a reactive compatibilizer	Internal mixer	E	1022 MPa	X_c	33.5%	78
			σ	47 MPa	T_g	-24.3 ºC (PBAT)	
						61.6 ºC (PLA)	
			ε_B	462 %	$T_{m\,PLA}$	169.1 ºC	
					$T_{cc\,PLA}$	107.9 ºC	
			*IS	50 kJ/m^2	Intermediate value of G′, G″ and η*		
PLA/PBAT/MDI 49/49/2 wt%	Methylene diphenyl diisocyanate (MDI) is a chain extender	Internal mixer	σ	48.8 MPa	X_c	37.6 %	84
					$T_{m\,PLA}$	167.8 ºC	
			ε_B	663%	T_g	PLA: 62.2 ºC	
						PBAT: -24.1 ºC	
			IS	70 kJ/m^2	Higher value of G′ and η*		

PBAT/PLA/TEC /PLA-g-MAH Or PBAT/PLA/TEC/TDI 9.3/90/0.7 wt% and 15 phr TEC	[1]PLA-g-MAH: degree of grafting 1.06 wt% Triethyl citrate (TEC) is a plasticizer Toluene diisocyanate (TDI) is a compatibilizer	Extrusion co-rotating twin screw	7 wt% TDI	7 wt% PLA-g-MAH	7 wt% TDI	7 wt% PLA-g-MAH	75
			σ: 25.2 MPa	σ: 11.69 MPa	X_c: 30.1%	X_c: 32%	
			ε_B: 241%	εB: 229 %	T_g: 40.6 ºC	T_g: 36.6 ºC	
			IS: 272 kJ/m^2	IS: 506.9 kJ/m^2	T_{cc}: 91.1 ºC	T_{cc}: 80.6 ºC	
					T_m: 149.6 ºC	T_m: 148.4 ºC	
AAE-10-PLA/PBAT 35/65 wt% with 3 phr talc and 0.3 phr wax	AAE-05-PLA: 100 wt% PLA and AAE 5 phr adipic acid ester AAE-10-PLA: 100 wt% PLA and AAE 10 phr	Extrusion counter-rotating twin screw	E	MD: 1332 MPa	X_c	12.11%	92
				TD: 829 MPa			
			σ	MD: 29.32 MPa	T_g	42.55 ºC	
				TD: 17.74 MPa			
			ε_B	MD: 325%	T_m	165.83 ºC	
				TD: 275%			
			TS	MD: 8.67 N/mm	T_{cc}	89.09ºC	
				TD: 16.16 N/mm			
PLA/PBAT/TBT/GNPs 70/30 wt% 5/1 phr	MMT: modified by 15-35 wt.% octadecylamine and 0.5-5 wt.% amino-propyltriethoxysilane	Solution casting	Stress at break	27.79 MPa	T_g	53.8 ºC	97
					T_c	111.9 ºC	
			ε_B	42.44%	T_m	148.2 ºC	
						153.5 ºC	
			E	1227.67 MPa	$T_{máx}$	360.2 ºC	
OMt/EFG-PLA/PBAT 80/20 % PLA/PBAT with 3 % OMt and 5% EFG	Cloisite® 30B: montmorillonite modified with methyl tallow bis-2-hydroxyethyl ammonium Cloisite® 15A: montmorillonite modified with dimethylhydrogenated tallow ammonium	Extrusion Twin screw	C15A/EFG-PBAT/PLA	C30B/EFG-PBAT/PLA	Both C15A/EFG-PBAT/PLA and C30B/EFG-PBAT/PLA had higher values of G′ and η*		96
			E: 903.15 MPa	E: 904.5 MPa			
			ε_B: 182%	ε: 150.86%			
			$\sigma_{máx}$: 44.52 MPa	$\sigma_{máx}$: 48.82 MPa			

1Dicumyl peroxide was used as an initiator; *Aproximate values; σ - Tensile strength; εB - Elongation at break; E - Young's modulus; IS - Impact strength; TS – Tear Strength; SS - Sealing Strength; MD - Machine Direction; TD - Transverse Direction; T_{cc} – Cold-crystallization temperature; T_g – Glass transition temperature; T_c – Crystallization temperature; T_m - Melting temperature; X_c – Degree of crystallinity

Table 18 – Comprehensive list of the varied Banana fiber/LDPE composites found in the literature, along with the corresponding mechanical properties, water absorption, rheological and thermal behaviour

BaF/LDPE composite	Materials	Method	Mechanical properties and Water absorption			Rheological properties and Thermal behavior		Ref
Non-woven banana fibers from different parts of bark	^{1}IB: inner bark ^{1}MB: middle bark ^{1}OB: outer bark	Wet laid web formation	IB	σ	1.23 MPa			108
				E	67MPa			
				ε_B	3.82 %			
			MB	σ	6.33 MPa			
				E	165 MPa			
				ε_B	9.65 %			
			OB	σ	8.56 MPa			
				E	215 MPa			
				ε_B	12.56 %			
BaF/LDPE 40/60 wt%	BaF: harvested in Sri Lanka (fiber length 20 cm) LDPE: waste plastic sourced from a textile company and from IKEA	Compression molding		σ	32.8 MPa			111
				*E	3.2 GPa			
BaF/LDPE 50/50 wt%	BaF: mechanically extracted	Hydraulic hot press		σ	9.056 MPa			100
				E	155.39 MPa			
				ε_B	6.805 mm			
				FS	17.34 MPa			
				Water absorption	18.63 %			
Banana starch/LDPE 20/80 wt%		Extrusion twin screw		*σ	12 MPa	T_m	111.23 ºC	109
						T_c	100.08 ºC	
				*ε_B	100 %	X_c	15.43 ºC	
Banana starch/LDPE/LDPE-g-MAH 20/80/10 wt%	PE- g-MA: 0.5–1 wt % graft level was	Extrusion twin screw		*σ	13.5 MPa	T_m	110.76 ºC	109
						T_c	101.78 ºC	
				*ε_B	125 %	X_c	12.16 %	

BaF/LDPE-g-MAH 40/60 wt% BaF/LDPE/LDPE-g-MAH 30 wt%, 0.25/0.75 weight ratio	BaF: 43.5 wt % cellulose, 16.9 wt % lignin, 31.7 wt % hemi-cellulose, 9.9 wt% ash and 6.1 wt% wax Stearic acid was used as a compatibilizer	Extrusion twin screw And Compression molding	BaF/LDPE-g-MAH 40/60 wt%	BaF/LDPE/LDPE-g-MAH 30 wt% /0.25/0.75	BaF/LDPE-g-MAH 40/60 wt%	BaF/LDPE/LDPE-g-MAH 30 wt% /0.25/0.75	118
			*σ_B 17 MPa	*σ_B 16 MPa	T_m 111.2 ºC	T_m 120 ºC	
			*E 275 MPa	*E 175 MPa			
			*ε_B 7%	*ε_B 10%	X_c 0.45 %	X_c 0.24 %	
BaF/LDPE/LDPE-g-MAH 10/90, 15/85, 20/80, 25/75, and 30/70 wt % with 3 wt% LDPE-g-MAH BaF - acrylic acid (AA) treatment	BaF: 63–64 wt % cellulose, 5 wt % lignin and 19 wt % hemi-cellulose,10 mm LDPE-g-MAH: 0.5–0.8 % MAH	Compression molding	BaF/LDPE/LDPE-g-MAH (AA) 25 wt%		BaF/LDPE/LDPE-g-MAH (AA) 25 wt%		110
			σ	12.4 MPa	T_o	241 ºC	
			E	1119 MPa			
			ε_B	6%			
			FS	23.3 MPa	T_f	461 ºC	
			IS	13.8 kJ/m^2			

[1] Treated with 15% NaOH at 90ºC; *Aproximate values; σ - Tensile strength; σB – Stress at break; εB - Elongation at break; E - Young's modulus; IS - Impact strength; FS - Flexural strength; T_o – Onset degradation temperature; T_f – Final degradation temperature; T_c – Crystallization temperature; T_m - Melting temperature; X_c – Degree of crystallinity

Appendix B –SPEX SamplePrep 6770 Freezer/Mills apparatus and 3Devo® composer 450 desktop apparatus

SPEX SamplePrep 6770 Freezer/Mills apparatus

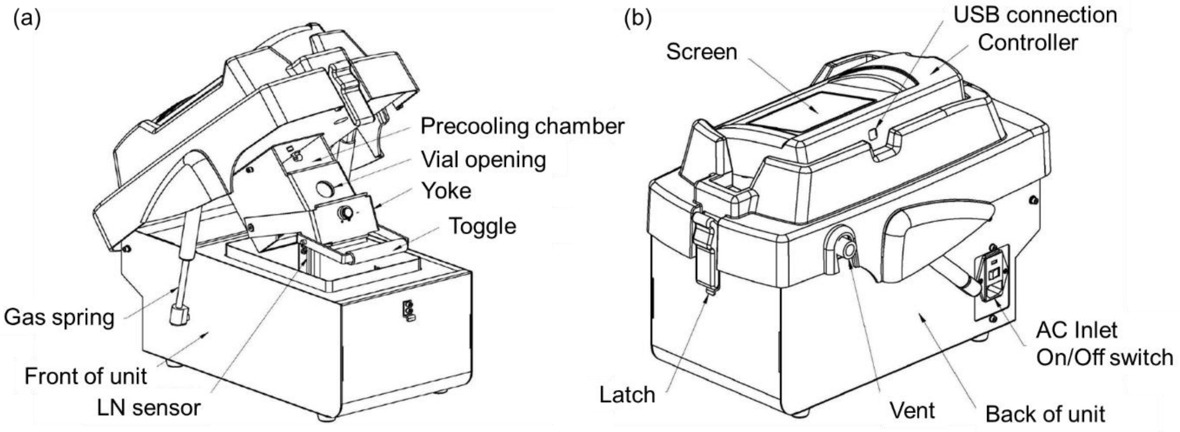

Figure 36 - SPEX SamplePrep 6770 Freezer/Mills apparatus (a) from the front (b) from the back

The equipment uses a grinding mechanism with a steel impactor driven by dual electromagnets and is cooled with liquid nitrogen. The average consumption of the latter is around 4-5 liters for initial cool-down and filling of the tub, 2-5 liters for each hour of operation.

This equipment is comprised of:

- Precooling chamber: pre-cooling one or two loaded vials;
- Vial opening: insertion of vial for grinding;
- Grinding Vials: typical biological sample weight varies according to the vials used, from around 1g to 0.5 g for metal and plastics vials, respectively;
- Yoke: handle with toggle that should move freely and properly;
- LN sensor: liquid nitrogen sensor (shutdown is automatically triggered if the level is too low);
- Gas spring: damps and controls the movement of the lid;
- Screen: control panel that programs and operates the Freezer/Mill through touch-screen;
- USB Connection: enables linkage of the Freezer/Mill to a PC or LIMS system;
- Controller: the control panel is detachable for remote operation;
- Vent: enables expulsion of a stream of condensed water vapor (“fog”).[124]

3Devo® composer 450 desktop apparatus

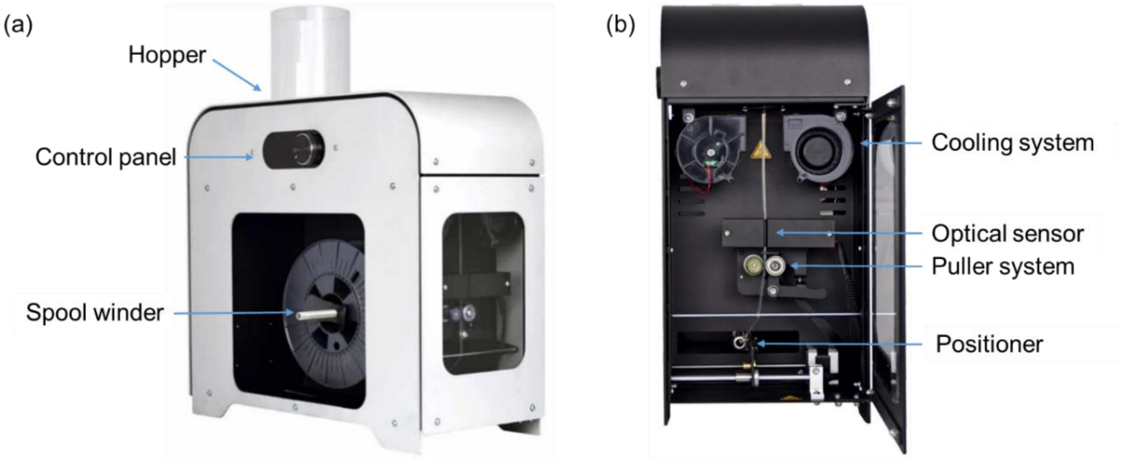

Figure 37- 3Devo® composer 450 desktop extruder and its apparatus (a) right side of the model (b) front of the extruder with open panel. Adapted from 3Devo - Filament Makers [153]

The 3Devo® composer 450 desktop extruder is comprised of:

- Control panel: has easily accessible settings with convenient standard material pre-sets and customizable material profiles for perfect results (display interface). Also allows for a simple USB connectivity with a computer/laptop (connectivity);
- Hopper: comprised of an optical sensor to check the material level, removable tube, multiple sizes support and a built-in safety grille;
- Extruder: made of nitride hardened steel extruder screw with a swappable extruder design and possesses 4 heating zones with a replaceable extruder nozzle;
- Cooling system: has dual fan system for even air distribution with an adjustable fan angles for optimal air flow and customizable, material-specific fan speeds;
- Sensor: (1) optical sensor – possesses one nozzle for all filament diameters in an ideal sensor placement to ensure filament roundness with an accurate diameter measurement between 0.5mm and 3.0mm (43 micron precision); (2) puller system – has automatic speed adjustment for accurate diameter control and changeable puller wheels to suit material temperature variations;
- Positioner: automatic spooling to user-defined size with adjustable positioner and a maximum spool width of 120mm with a retractable arm for neat, even winding of all spool sizes;
- Spool winder: fits spools with a maximum diameter of 240mm and a maximum width of 120mm. Has a user-friendly slipper clutch for spool tension adjustments and a swappable spool mount for quick changing between spools.[153]

Appendix C – Sample sizes for DMA and water absorption tests

Table 19 – Sample dimensions of DMA testing

Sample sizes (length x depth x width)			
PBAT	$20x9.50x2.05\ mm$	**2 wt% T. Middle**	$20x9.51x2.07\ mm$
2 wt% Interior	$20x9.50x2.10\ mm$	**5 wt% T. Middle**	$20x9.52x2.10\ mm$
2 wt% T. Interior	$20x9.52x2.10\ mm$	**8 wt% T. Middle**	$20x9.50x2.31\ mm$
2 wt% Middle	$20x9.40x2.20\ mm$	**2 wt% Exterior**	$20x9.55x2.12\ mm$
5 wt% Middle	$20x9.55x2.09\ mm$	**2 wt% T. Exterior**	$20x9.52x2.12\ mm$
8 wt% Middle	$20x9.55x2.10\ mm$		

Table 20 – Sample dimensions of water absorption testing

Sample sizes (length x diameter (mm))					
PBAT	$12.70\ x\ 1.69$	**2 wt% Interior**	$15.52\ x\ 1.47$	**2 wt% T. Interior**	$15.96\ x\ 1.71$
	$17.98\ x\ 1.70$		$20.95\ x\ 1.52$		$21.86\ x\ 1.60$
	$22.99\ x\ 1.74$		$26.05\ x\ 1.54$		$28.81\ x\ 1.60$
	$29.20\ x\ 1.67$		$33.65\ x\ 1.62$		$37.94\ x\ 1.67$
	$34.76\ x\ 1.72$		$40.54\ x\ 1.60$		$44.80\ x\ 1.66$
2 wt% Middle	$12.56\ x\ 1.62$	**5 wt% Middle**	$10.79\ x\ 1.54$	**8 wt% Middle**	$15.40\ x\ 1.95$
	$16.10\ x\ 1.60$		$14.79\ x\ 1.57$		$20.48\ x\ 1.68$
	$19.71\ x\ 1.62$		$18.43\ x\ 1.55$		$24.47\ x\ 1.74$
	$23.70\ x\ 1.68$		$23.39\ x\ 1.58$		$27.92\ x\ 1.69$
	$31.29\ x\ 1.74$		$27.86\ x\ 1.54$		$31.53\ x\ 1.67$
2 wt% T. Middle	$13.52\ x\ 1.85$	**5 wt% T. Middle**	$15.47\ x\ 1.65$	**8 wt% T. Middle**	$13.14\ x\ 1.76$
	$18.78\ x\ 1.70$		$23.14\ x\ 1.80$		$18.92\ x\ 1.82$
	$25.86\ x\ 1.84$		$29.35\ x\ 1.66$		$24.29\ x\ 1.78$
	$33.47\ x\ 1.89$		$35.29\ x\ 1.74$		$30.20\ x\ 1.74$
	$38.89\ x\ 1.89$		$41.56\ x\ 1.70$		$37.73\ x\ 1.75$
2 wt% Exterior	$16.74\ x\ 1.74$	**2 wt% T. Exterior**	$16.60\ x\ 1.56$		
	$22.26\ x\ 1.71$		$21.89\ x\ 1.64$		
	$29.64\ x\ 1.63$		$30.54\ x\ 1.68$		
	$36.24\ x\ 1.77$		$35.08\ x\ 1.62$		
	$43.94\ x\ 1.67$		$42.68\ x\ 1.60$		

Appendix D – FTIR spectra and Thermogravimetric analysis (TGA) and Differential thermogravimetric analysis (DTG) thermogarms

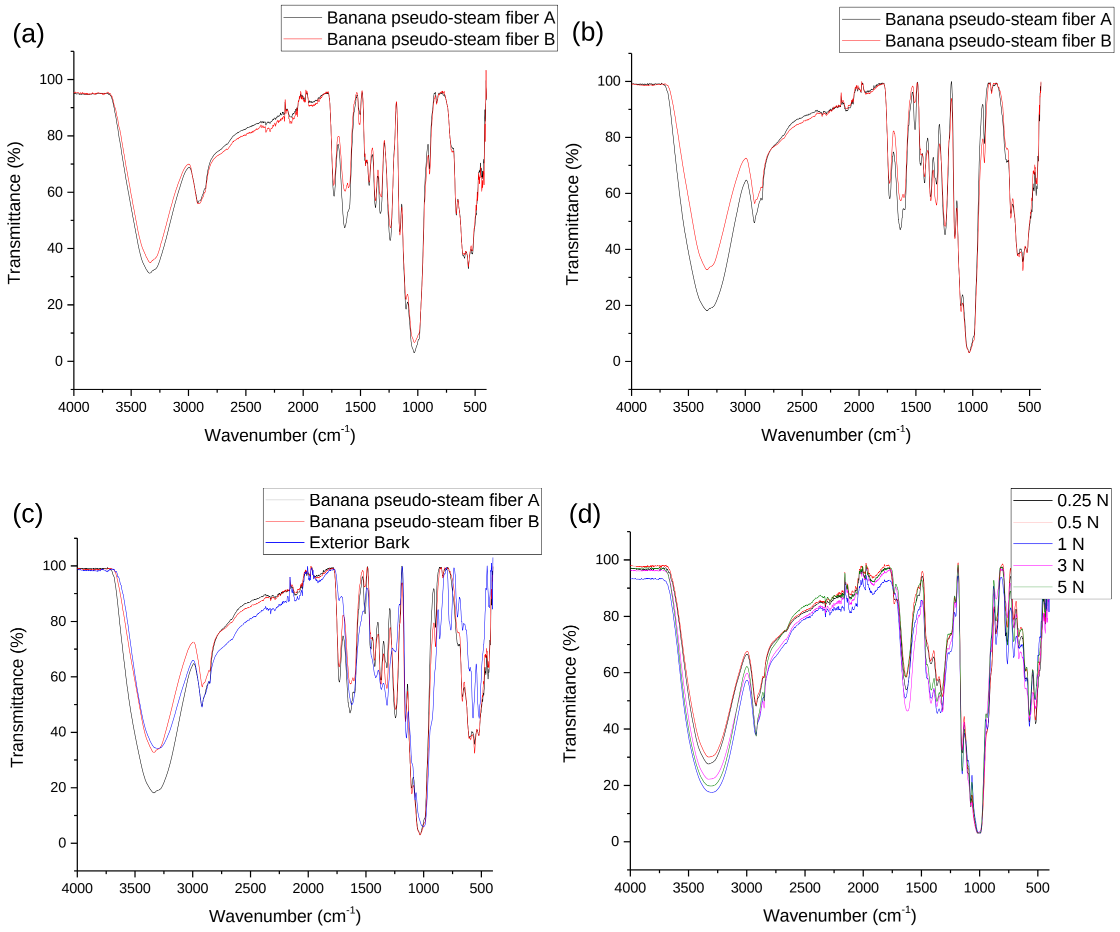

Figure 38– FTIR spectra of (a) interior fibers and (b) exterior fibers from banana pseudo-steam trunks from trees A and B from figure 14 (c) bark and exterior fiber (d) alkali treated exterior bark for concentrations of sodium hydroxide of 0.25, 0.5, 1, 3 and 5 %

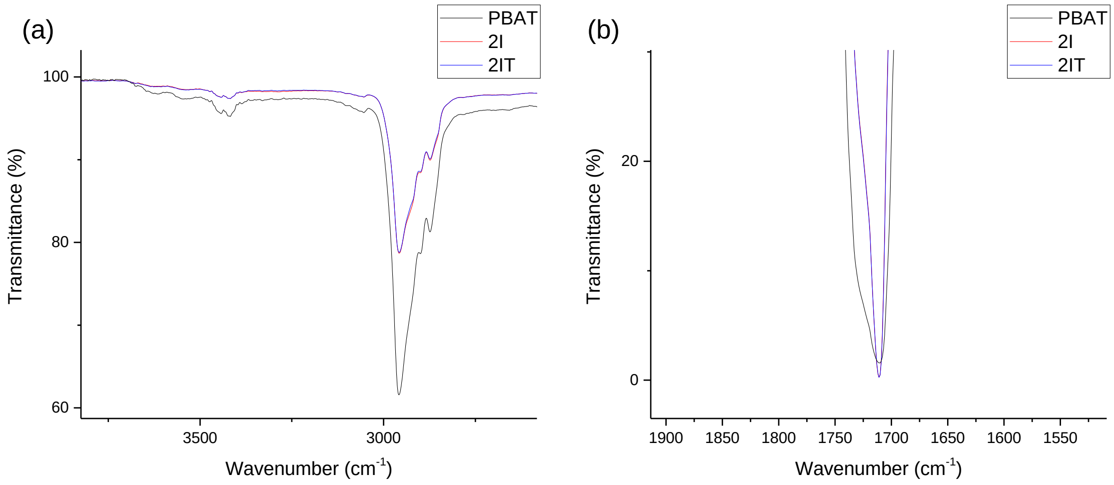

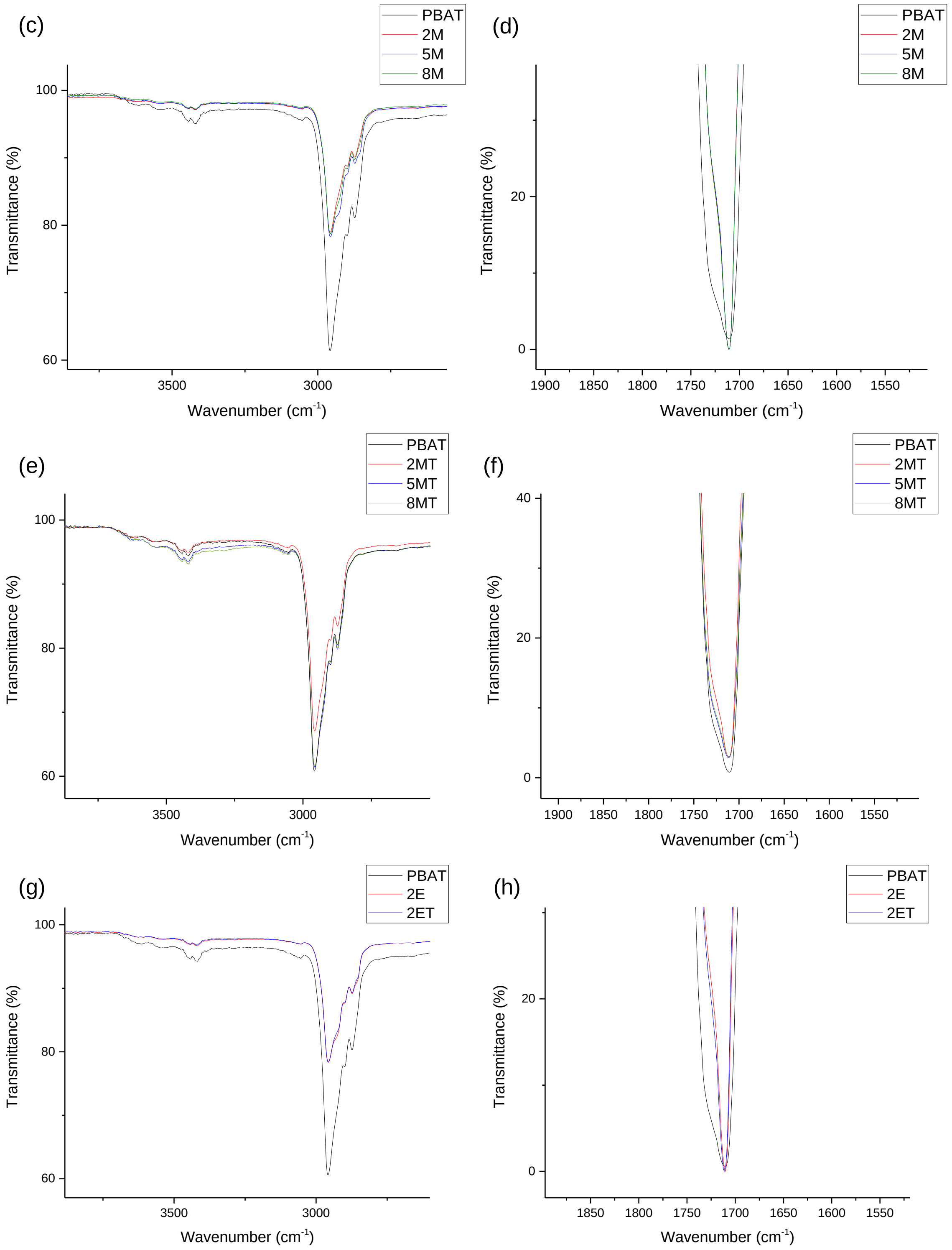

Figure 39 – FTIR spectra of respectively zoomed section between 4000 – 2000 cm^{-1} and 1710 cm^{-1} for (a –b) neat PBAT and PBAT/treated and untreated interior composites; (c - d) neat PBAT and PBAT/ untreated middle composites; (e - f) neat PBAT and PBAT/treated middle composites; (g - h) neat PBAT and PBAT/treated and untreated exterior composites

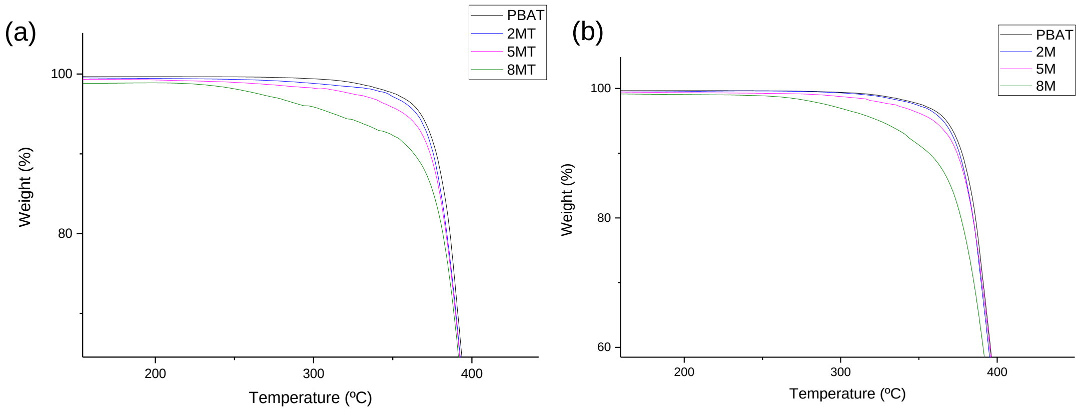

Figure 40 - Thermogravimetric analysis (TGA) zoomed at the T_{onset} for (a) neat PBAT and PBAT/treated middle composite and (b) neat PBAT and PBAT/untreated middle composite

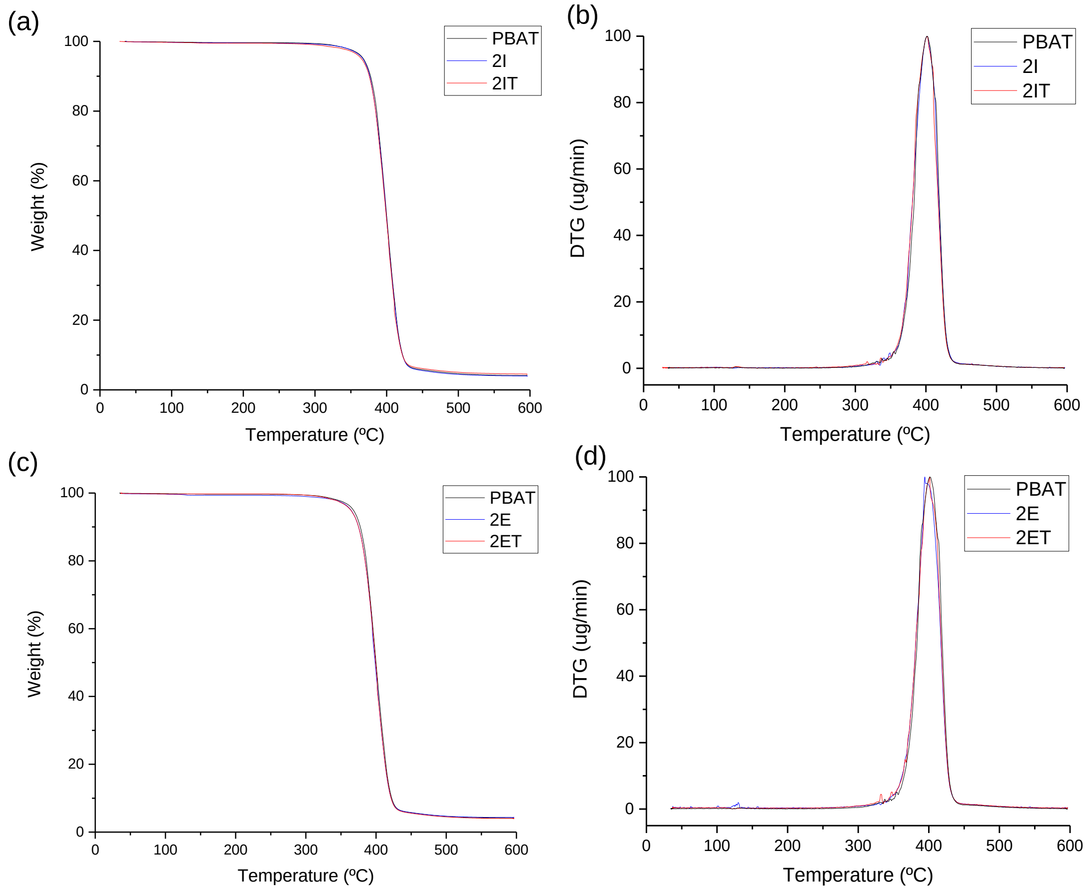

Figure 41 – Thermogravimetric analysis (TGA) of (a) neat PBAT and PBAT/treated and untreated interior composites and (c) neat PBAT and PBAT/treated and untreated exterior composites. Differential thermogravimetric analysis (DTG) of (b) neat PBAT and PBAT/treated a and untreated interior composites and (d) neat PBAT and PBAT/treated and untreated exterior composites

Appendix E - EDS data and SEM images

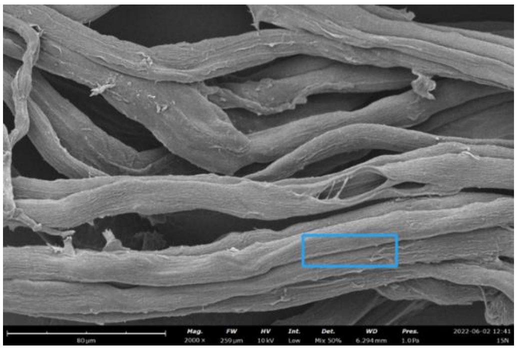

Element Number	Element Symbol	Element Name	Atomic Conc.
6	C	Carbon	53.186
8	O	Oxygen	45.515
11	Na	Sodium	0.470
79	Au	Gold	0.829

Figure 42 - SEM image (2000x, scale bar 80 µm) and EDS data for alkali treated fiber with 15% NaOH for 1 h at 90 ºC

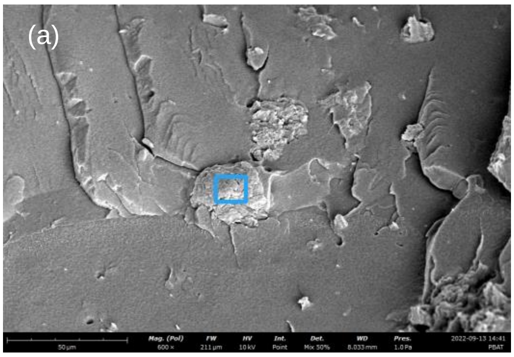

Element Number	Element Symbol	Element Name	Atomic Conc.
6	C	Carbon	59.467
8	O	Oxygen	37.097
11	Na	Sodium	3.437

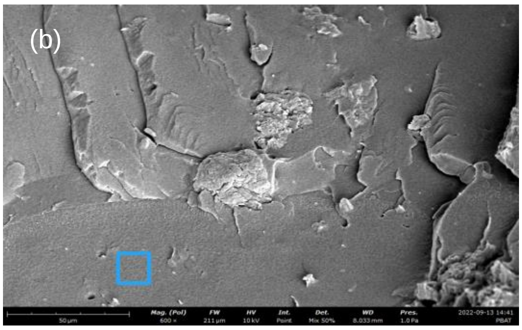

Element Number	Element Symbol	Element Name	Atomic Conc.
6	C	Carbon	67.680
8	O	Oxygen	29.649
13	Al	Aluminum	2.671

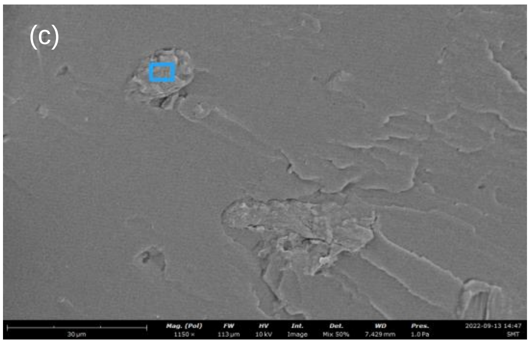

Element Number	Element Symbol	Element Name	Atomic Conc.
6	C	Carbon	64.048
8	O	Oxygen	33.525
11	Na	Sodium	2.427

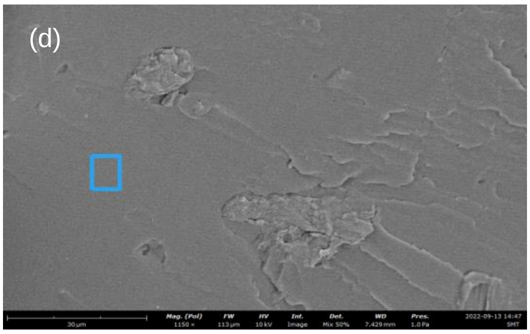

Element Number	Element Symbol	Element Name	Atomic Conc.
6	C	Carbon	72.562
8	O	Oxygen	27.438

Figure 43 - SEM image and EDS data for (a) PBAT/ 8 wt% treated middle composite (600x, scale bar 50 µm); (b) PBAT/ 8 wt% treated middle composite (600x, scale bar 50 µm); (c) PBAT/ 5 wt% treated middle composite (1150x, scale bar 30 µm); (d) PBAT/ 5 wt% treated middle composite (1150x, scale bar 30 µm)

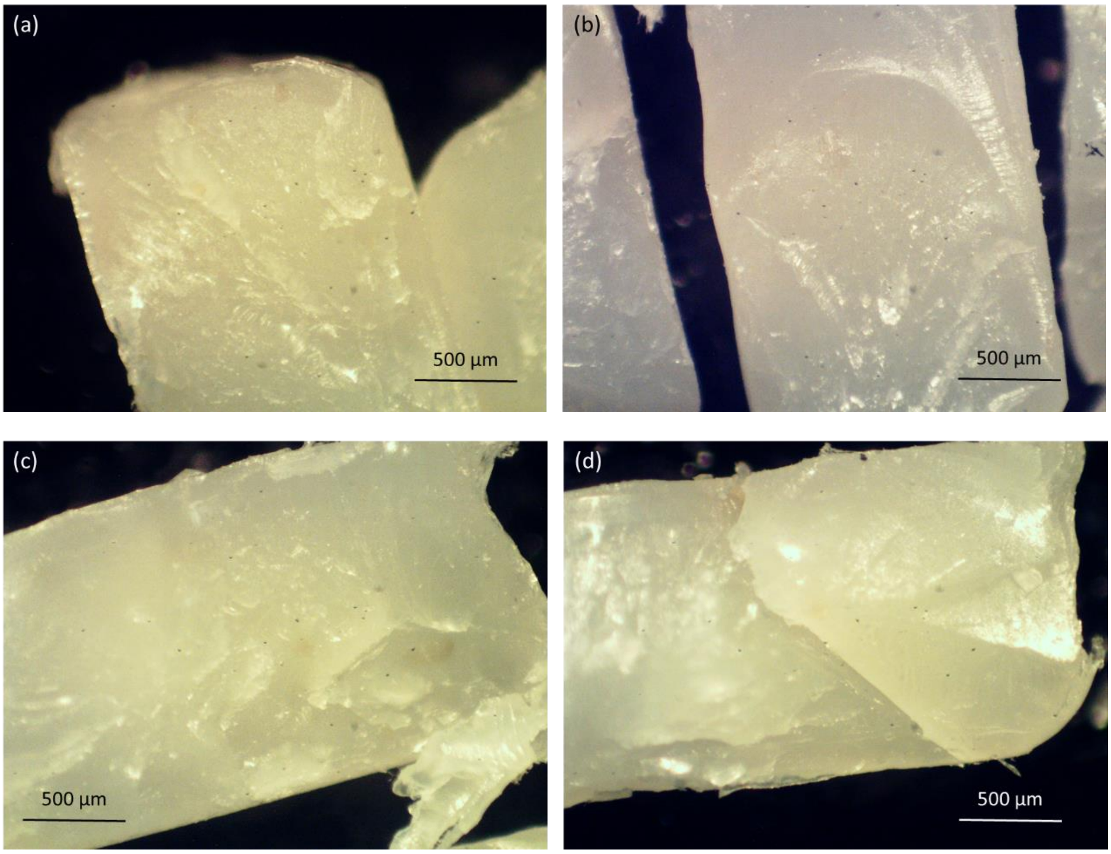

Figure 44 - Optical microscopy photographs at 4.5x for (a –b) PBAT/ 2 wt% untreated exterior composites and (c – d) PBAT/ 2 wt% treated exterior composites